

SCUOLA DI INGEGNERIA E ARCHITETTURA

Dipartimento di Ingegneria Civile, Chimica, Ambientale e dei Materiali

Ingegneria civile

TESI DI LAUREA

in

Context-Sensitive Design In Transportation Infrastructures

**“The role of paved surfaces in the Urban Heat Island
phenomenon: assessment of fundamental thermal parameters
and Finite Element Analysis for UHI mitigation”**

CANDIDATO:
David Matricardi

RELATORE:
Dott. Ing. Cesare Sangiorgi

CORRELATORI:
Dott. Ing. Valentina Di Maria
Dr. Mujib Rahman

TABLE OF CONTENTS

ABSTRACT	7
INTRODUCTION	11
1. THE UHI PHENOMENON.....	13
1.1 Surface Urban Heat Island.....	13
1.2 Atmospheric Urban Heat Island	14
1.3 Solar Reflectance	18
1.4 Solar Reflectance Index (SRI).....	19
1.5 Emissivity	20
1.6 Heat Capacity	20
1.7 Other Factors	21
1.7.1 Urban Geometry	21
1.7.2 Anthropogenic Heat.....	22
1.7.3 Weather.....	22
1.7.4 Geographic Location And Topography	23
1.8 Impacts	23
1.8.1 Energy Consumption	23
1.8.2 Air Quality	23
1.8.3 Human Health And Comfort	23
1.8.4 Water Quality.....	24
1.9 Mitigating Urban Heat Island.....	24
1.9.1 Cool Pavements	25
2. INVESTIGATION EQUIPMENT.....	29

2.1	Thermal imaging camera	29
2.1.1	Finding the emissivity.....	34
2.1.2	Measuring the temperature	36
2.2	Sunshine Pyranometer for testing.....	39
2.3	Thermocouples	41
2.4	Meteorological station	44
3. EXPERIMENTAL WORK		47
3.1	Laboratory testing.....	48
3.1.1	Tested material.....	48
3.1.2	Emissivity evaluation.....	50
3.1.3	Heat release curves	55
3.2	Outside investigation	64
3.2.1	Emissivity evaluation.....	66
3.2.2	Albedo measurements.....	71
3.2.3	Temperature readings	78
4.CASE STUDY MODELLING.....		81
4.1	ENVI-met software (version 3.1)	81
4.1.1	Software architecture	81
4.1.2	Simulation models	90
4.1.3	Surfacing materials used.....	97
4.1.4	Urban canyon simulations	105
4.1.5	Heat basin simulations	113
4.1.6	Annex 1: urban canyon simulations bar charts.....	128
4.1.7	Annex 2: urban heat basin simulations bar charts	129
CONCLUSIONS.....		131
ACKNOWLEDGEMENTS		137

BIBLIOGRAPHY.....139

ABSTRACT

This thesis work has been carried out during the Erasmus exchange period at the Nottingham Trent University's Academic School of Architecture, Design and the Built Environment in Nottingham, United Kingdom.

Nowadays the environmental issues and the climatic change play fundamental roles in the design of urban spaces. Our cities are growing in size, many times only following immediate needs without a long-term vision. Consequently, the sustainable development has become not only an ethical but also a strategic need: we can no longer afford an uncontrolled urban expansion. One serious effect of the territory industrialisation process is the increase of urban air and surfaces temperatures compared to the outlying rural surroundings. This difference in temperature is what constitutes an *urban heat island* (UHI).

The purpose of this study is to provide a clarification on the role of urban surfacing materials in the thermal dynamics of an urban space, resulting in useful indications and advices in mitigating UHI.

With this aim, 4 coloured concrete bricks were tested, measuring their emissivity and building up their heat release curves using infrared thermography. Two emissivity evaluation procedures were carried out and subsequently put in comparison. Samples performances were assessed, and the influence of the colour on the thermal behaviour was investigated.

In addition, some external pavements were analysed. Albedo and emissivity parameters were evaluated in order to understand their thermal behaviour in different conditions. Surfaces temperatures were recorded in a one-day measurements campaign.

ENVI-met software was used to simulate how the tested materials would behave in two typical urban scenarios: a *urban canyon* and a *urban heat basin*. Improvements they can carry to the urban microclimate were investigated.

Emissivities obtained for the bricks ranged between 0.92 and 0.97, suggesting a limited influence of the colour on this parameter. Nonetheless, white concrete brick showed the best thermal performance, whilst the black one the worst; red and yellow ones

performed pretty identical intermediate trends. De facto, colours affected the overall thermal behaviour.

Emissivity parameter was measured in the outdoor work, getting (as expected) high values for the asphalts. Albedo measurements, conducted with a sunshine pyranometer, proved the improving effect given by the yellow paint in terms of solar reflection, and the bad influence of haze on the measurement accuracy.

ENVI-met simulations gave a demonstration on the effectiveness in thermal improving of some tested materials. In particular, results showed good performances for white bricks and granite in the heat basin scenario, and painted concrete and macadam in the urban canyon scenario. These materials can be considered valuable solutions in UHI mitigation.

KEYWORDS:

Urban Heat Island, thermal imaging, emissivity, urban canyon, painted materials

Questo elaborato di tesi è stato realizzato durante il periodo di scambio Erasmus presso l'Academic School of Architecture, Design and the Built Environment della Nottingham Trent University, Nottingham, Regno Unito.

Al giorno d'oggi le questioni ambientali e il cambiamento climatico rivestono un ruolo fondamentale nella progettazione degli spazi urbani. Le nostre città crescono in dimensione, molte volte solamente seguendo immediate necessità senza una visione di lungo termine. Conseguentemente, lo sviluppo sostenibile è diventato non solo una questione di etica, ma anche una necessità strategica: non possiamo più permetterci un'espansione urbana incontrollata. Un grave effetto del processo di industrializzazione territorio è l'aumento della temperatura dell'aria e delle superfici urbane rispetto alle zone rurali periferiche. Questa differenza di temperatura è ciò che costituisce un' isola di calore urbana (UHI).

Lo scopo di questo studio è quello di chiarire il ruolo dei materiali da pavimentazione urbani nelle dinamiche termiche di uno spazio urbano, con conseguenti indicazioni e consigli utili a mitigare l'UHI.

A tal fine sono stati testati 4 mattoni in calcestruzzo colorato misurando la loro emissività e costruendo le curve di rilascio del calore, tramite l'utilizzo della termografia a infrarossi. Sono state testate due procedure di valutazione dell'emissività e successivamente messe a confronto.

Sono quindi state valutate le performance dei campioni ed è stata studiata l'influenza del colore sul comportamento termico.

Sono state inoltre analizzate alcune pavimentazioni esterne. Per capire il loro comportamento termico in differenti condizioni, sono stati valutati i parametri di albedo ed emissività. È stata effettuata una campagna di misure giornaliera al fine di raccogliere le temperature superficiali.

Il software ENVI-met è stato utilizzato per simulare il comportamento dei materiali testati in due tipici scenari urbani: un canyon urbano e un bacino di calore urbano. Quindi sono stati studiati i miglioramenti che tali materiali potrebbero portare al microclima urbano.

Le emissività ottenute per i mattoni si sono attestate tra 0.92 e 0.97, suggerendo una limitata influenza del colore su questo parametro. Tuttavia, il mattone bianco ha mostrato la miglior prestazione termica, mentre il nero quella peggiore; il rosso e il giallo hanno avuto prestazioni quasi identiche. De facto, i colori influenzano il comportamento termico complessivo.

Il parametro di emissività è stato misurato nella fase esterna di ricerca, ottenendo (come previsto) valori elevati per gli asfalti. Le misure dell'albedo, condotte con un piranometro, hanno dimostrato l'effetto migliorativo della vernice gialla in termini di riflessione solare, e la cattiva influenza della foschia nella precisione di misura.

Le simulazioni con ENVI-met hanno dato dimostrazione sull'efficacia nel miglioramento termico di alcuni materiali testati. In particolare, i risultati hanno mostrato buone prestazioni per i mattoni bianchi e per il granito nello scenario del bacino di calore, e per il cemento e il macadam dipinti nello scenario del canyon urbano. Tali materiali possono essere considerati valide soluzioni nella mitigazione dell'UHI.

INTRODUCTION

Nowadays the environmental issues and the climatic change play fundamental roles in the design of urban spaces. In fact, the 80% of the world population will live in cities until 2030 [1], worsening the overpopulation problem and so the quality of life. Consequently, the sustainable development has become not only an ethical but also a strategic need: we can no longer afford an uncontrolled urban expansion.

Two serious linked effects of this matter are the raise of the micro-scale environmental temperature and the increase of the heat waves frequency and duration, carrying dangerous repercussions such a bigger electric power consumption, more health problems for sensitive subjects (children and elderly people), increasing of atmospheric pollution and greenhouse gases, deterioration of water quality. In particular, many urban and suburban areas experience elevated temperatures compared to the outlying rural surroundings; this difference in temperature is what constitutes an *urban heat island* (UHI) (fig.1) [2]. As already determined in previous researches, the temperature difference between urban and suburban areas, in a large one-million-people city, can range between 1 and 3°C during the day, and reach up to 12°C in the night time [3,4].

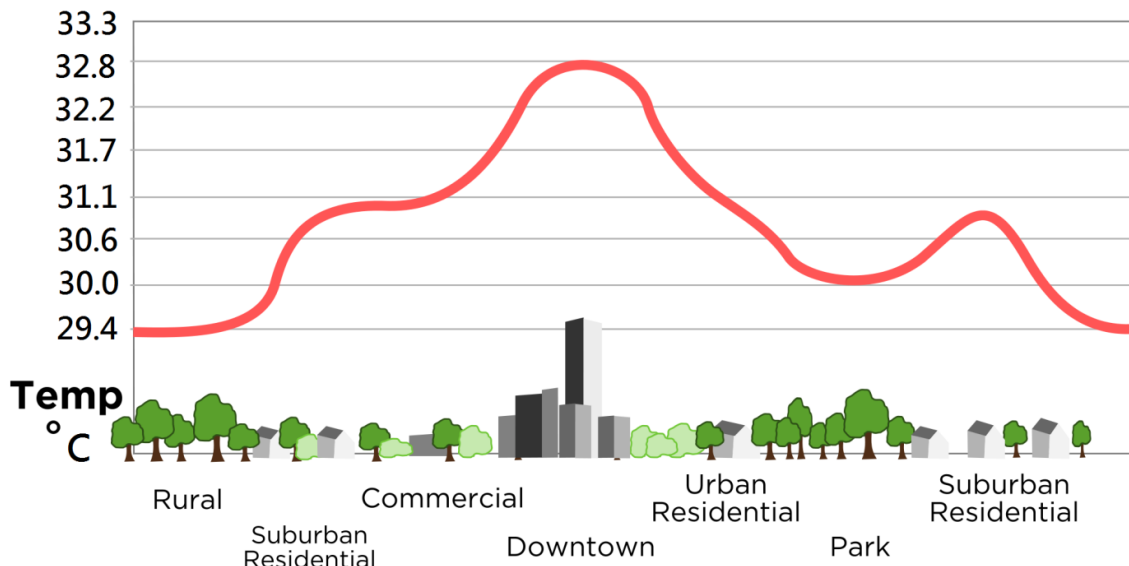


Fig. 1: UHI temperature profile [5]

It is possible to recognize different causes leading to such phenomenon, but basically the main reason is the territory industrialisation process. In fact, the expansion of metropolitan areas results in an increase in the “grey surfaces” (mainly asphalt and

concrete) with a consequent loss of green areas. Urban surfacing materials, also due to their low reflectivity, tend to store short-wave radiation in the day time, and to release it during the night. So the air does not cool down, causing an overheating of low atmospheric layers through the convection process. Moreover these surfaces become impermeable and dry, abating the cooling effect of evapotranspiration. Also the urban geometry has its own effects: buildings prevent the cooling effect of wind, hindering the natural air recirculation. The UHI presence is particularly noticeable in larger towns but it is quite evident even in the smaller ones, although the effect decreases as the urban size decreases [6].

The main purpose of the research is to test some paving materials able to mitigate the UHI phenomenon and to provide a general improvement to the micro-scale climate. Basically the experimentation had three phases. The first one, conducted at the Architecture, Design and Built Environment Academic School's laboratory of the Nottingham Trent University (Maudslay building, City Campus), consisted in testing four concrete coloured interblocks in order to evaluate their thermal behaviour. The second one, carried out in the external areas of the Nottingham Trent University's City Campus, consisted in measuring the thermal parameters of different paving surfaces. The last one was the simulative phase: using a CFD software called "*Envi-met*", the geometric model of the area and different improving scenarios have been developed.

In CHAPTER 1 a background on the Urban Heat Island phenomenon is provided, focusing on the factors affecting it and the impacts that it causes.

A description of the technical equipment used in the research is contained in CHAPTER 2, this section gives an explanation of the fundamental operating principles of the instruments.

CHAPTER 3 describes two fundamentals phase: the laboratory part, where the experimentation on some coloured bricks was carried out; the external part, where different surfacing materials were analysed.

All the simulations and the results worked out are contained in CHAPTER 4. Here the thermal performances of different paving materials were assessed.

The final analysis, deductions and recommendations are enclosed in the CONCLUSION.

CHAPTER 1:

THE UHI PHENOMENON

Many studies have been carried out in order to investigate the heat island effect providing full documentation of the problem [7,8,9,10,11]. In particular it is possible to recognize two different types of urban heat island, respectively the *surface* one and the *atmospheric* one [2]. To make a distinction between the two categories is important for getting a proper understanding of the causes and the effects so to identify the most adequate mitigation method. As established by different researches [3,4,12,13], they differ in the time they occur, in the intensity they affect the urban environment, in their identification techniques, in their representation (tab.1).

Feature	Surface UHI	Atmospheric UHI
Temporal Development	<ul style="list-style-type: none"> • Present at all times of the day and night • Most intense during the day and in the summer 	<ul style="list-style-type: none"> • May be small or non-existent during the day • Most intense at night or predawn and in the winter
Peak Intensity (Most intense UHI conditions)	<ul style="list-style-type: none"> • More spatial and temporal variation: <ul style="list-style-type: none"> ▪ Day: 18 to 27°F (10 to 15°C) ▪ Night: 9 to 18°F (5 to 10°C) 	<ul style="list-style-type: none"> • Less variation: <ul style="list-style-type: none"> ▪ Day: -1.8 to 5.4°F (-1 to 3°C) ▪ Night: 12.6 to 21.6°F (7 to 12°C)
Typical Identification Method	<ul style="list-style-type: none"> • Indirect measurement: <ul style="list-style-type: none"> ▪ Remote sensing 	<ul style="list-style-type: none"> • Direct measurement: <ul style="list-style-type: none"> ▪ Fixed weather stations ▪ Mobile traverses
Typical Depiction	<ul style="list-style-type: none"> • Thermal image 	<ul style="list-style-type: none"> • Isotherm map • Temperature graph

Table 1: features of surface and atmospheric UHI [2]

1.1 Surface Urban Heat Island

It refers to the difference in temperature between dry and exposed urban surfaces (such as roofs and pavements) and shaded and moist surfaces (as natural vegetated ground in the rural surroundings). The first ones can reach temperatures 27 to 50°C hotter than the air, whilst the second ones tend to remain close to the atmospheric temperature [14]. Typically the effect is more accentuated during the day, when the temperature difference can range between 10 and 15°C. During the night the difference is less intense (5 to 10°C) [12]. The detection and measure of the UHI are conducted using both direct and indirect methods, for instance with thermographic measurement techniques or remote sensing. Besides researchers often use numerical models or estimates based on

empirical models. Usually all the data collected contribute to work out thermal images of the analyzed area (fig.2).

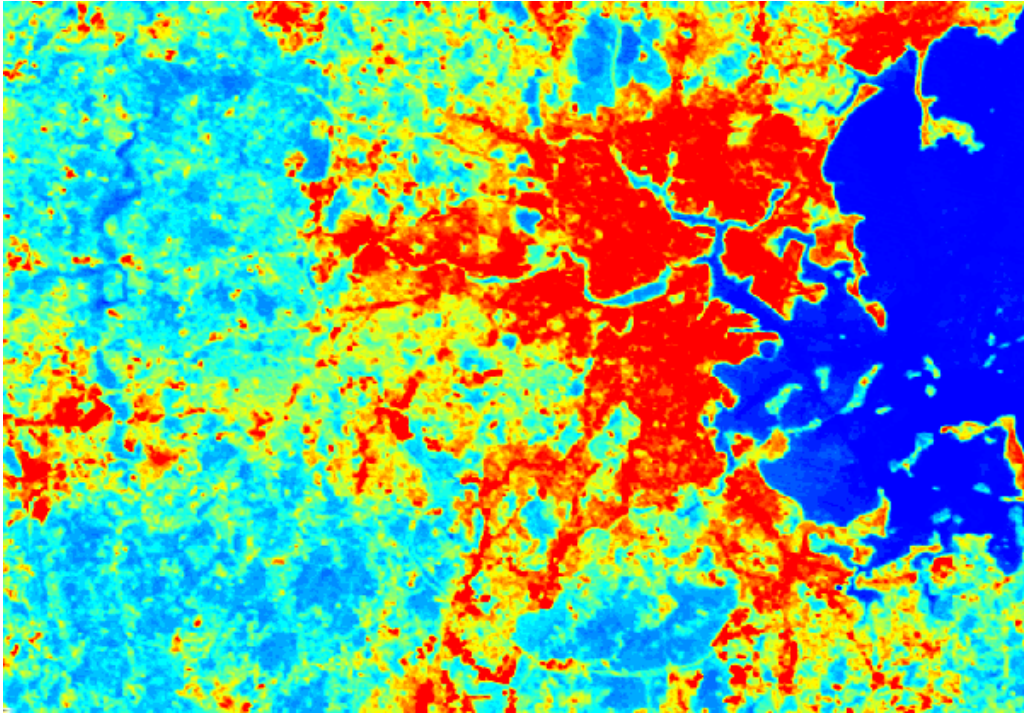


Figure 2: surface temperature in Boston, Massachusetts [15]

1.2 Atmospheric Urban Heat Island

It is characterized by the temperature air difference between the urban area and the rural surroundings. Its variation is less significant than the surface UHI: it has been suggested that, on an annual mean basis, air temperature in large cities can be 1 to 3°C warmer than those of their rural surroundings [2]. The effect is more significant after sunset whereas during the day it manifests itself weakly, due to the thermal inertia of surfacing materials and their consequent slow heat release. With reference to different space volumes in city, this UHI type can be further divided in two sub-categories: *Canopy Layer UHI* and *Boundary Layer UHI*. The first one occurs in the space volume where people live, namely from the ground to the top of buildings and trees. The second one extends from the rooftops to the height where the built-up area no longer affects the atmosphere (typically no more than 1.5 km from the surface) [6]. The canopy UHI is usually the category to which UHI studies refer, and so does this research.

The surface UHI affects the atmospheric one through the thermal exchange between surfaces and air, especially in the canopy layer (closer to the ground). In fact, the convection process cools down the air in a vegetated area (due to the moisture and to the

consequent evapotranspiration) and warms up in a dense built-up area, where the impervious materials make possible to collect water and to brought it away. Thanks to the continuous mixing within the atmosphere, the air temperature tends to remain more constant than the surface temperature. In particular, the larger variations between the two trends occur during the day, whilst they both are fairly similar at night. The presence of bodies of water, due to the high heat capacity, abates the temperature changes between daytime and nighttime (fig.3).

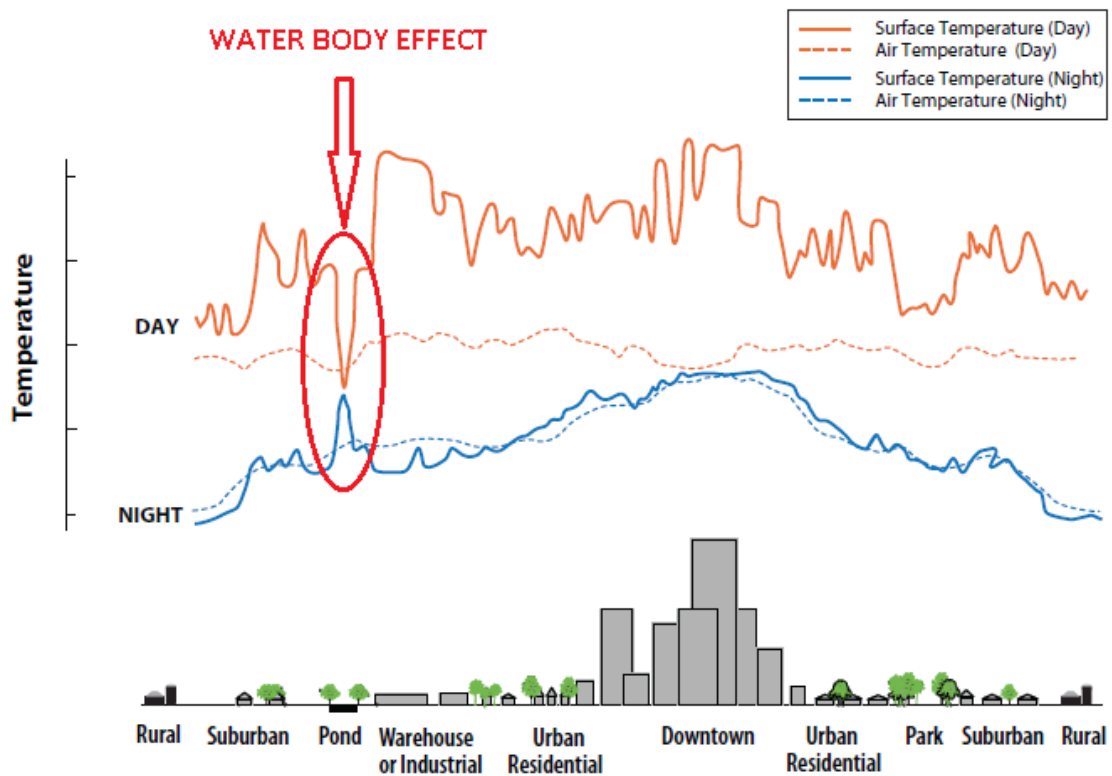


Figure 3: comparison between air and surface temperature trends [2]

Regarding the measurement techniques adopted by the researchers, the direct ones occupy a primary importance. The easiest and most reliable method is to determine the air temperatures through a dense network of sampling points from fixed or mobile stations [2]. Data are then graphically represented in order to give an immediate and clear understanding of the real condition. For instance, to draw an isotherm map could give a good idea of the situation (fig.4).

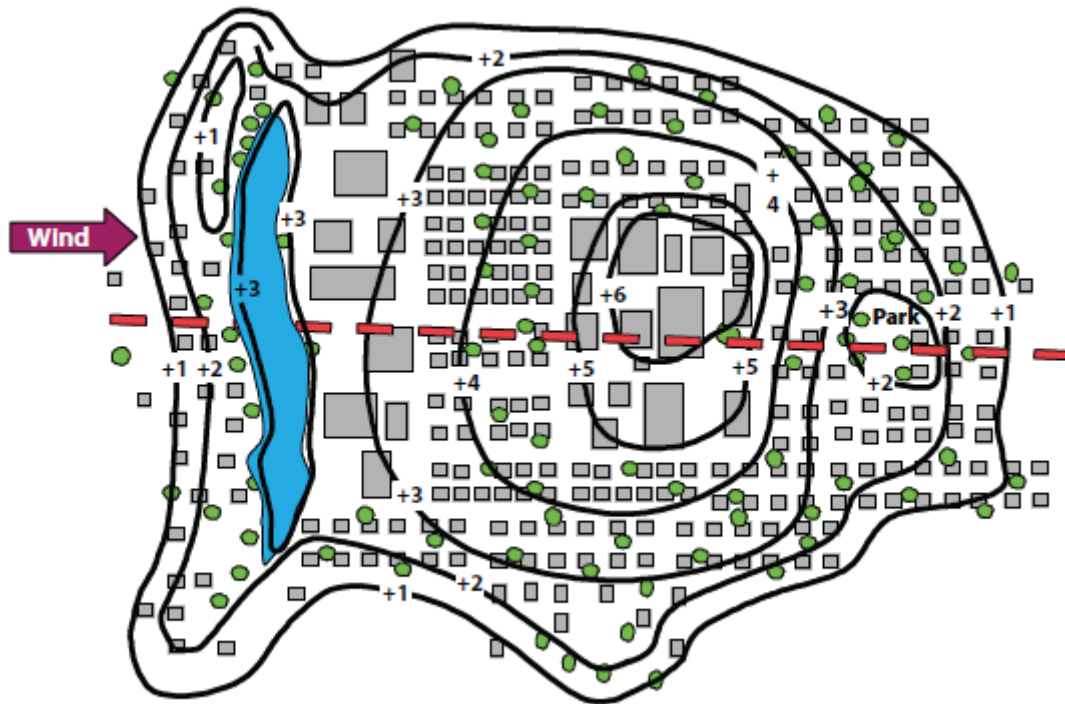


Figure 4: conceptual map with overlaid isotherms [2]

The formation of UHI involves many factors. The most important are the vegetation reduction, the urban materials thermal and radiative properties, the urban geometry, the anthropogenic heat emissions, the weather, the geographic location (tab.2).

Factors Communities are Focusing On
<ul style="list-style-type: none"> • Reduced vegetation in urban regions: Reduces the natural cooling effect from shade and evapotranspiration. • Properties of urban materials: Contribute to absorption of solar energy, causing surfaces, and the air above them, to be warmer in urban areas than those in rural surroundings.
Future Factors to Consider
<ul style="list-style-type: none"> • Urban geometry: The height and spacing of buildings affects the amount of radiation received and emitted by urban infrastructure. • Anthropogenic heat emissions: Contribute additional warmth to the air.
Additional Factors
<ul style="list-style-type: none"> • Weather: Certain conditions, such as clear skies and calm winds, can foster urban heat island formation. • Geographic location: Proximity to large water bodies and mountainous terrain can influence local wind patterns and urban heat island formation.

Table 2: factors that produce UHI [2]

The lack of green area in cities has a significant impact on UHI problem. Trees provide shades able to keep surfaces cooler, protecting them from the solar radiation. Vegetation also helps to reduce the air temperature thanks to the evapotranspiration, that

is the process of dissipation of the latent energy of water turning it from its liquid to its vapour form. This phase change cools down the air surrounding. Built-up surfaces (paved surfaces, roofs, sidewalks, parking lots, roads) have a much more little ability to evaporate water (fig.5).

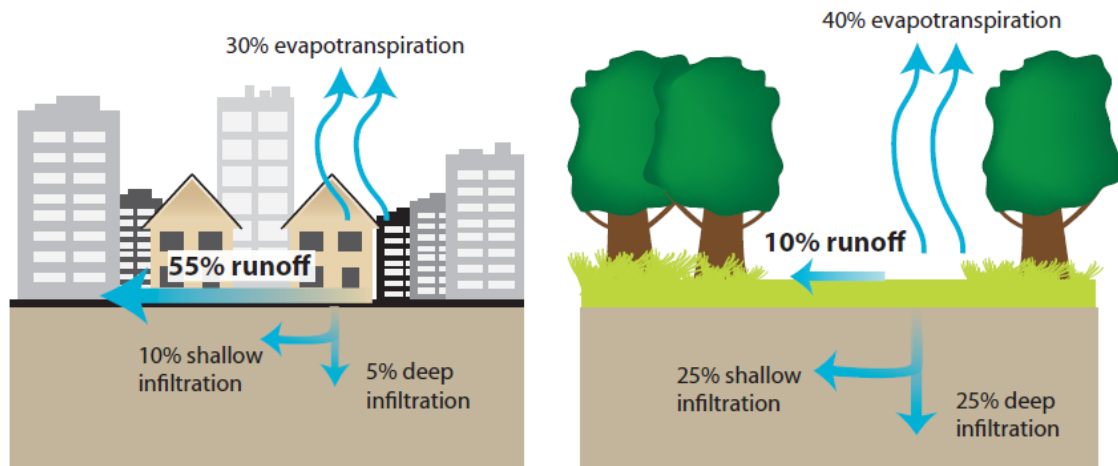


Figure 5: evapotranspiration in urban (left) and rural (right) areas [2]

Urban materials play a fundamental role in the UHI development. In particular their thermal performance influences the formation and the intensity of the phenomenon. The most important factors in this case are the *solar reflectance*, the *thermal emissivity* and the *heat capacity*. Sunlight reaches the Earth with a specific band of wavelength, the *solar spectrum*. It is composed of ultraviolet (UV) rays, visible (Vis) light, infrared energy (IR), and they reach the Earth respectively in 5% (including the part responsible for sunburns), 40% (with the visible colours wavelengths) and 55% (responsible for the heat sensation) of the total amount (fig.6).

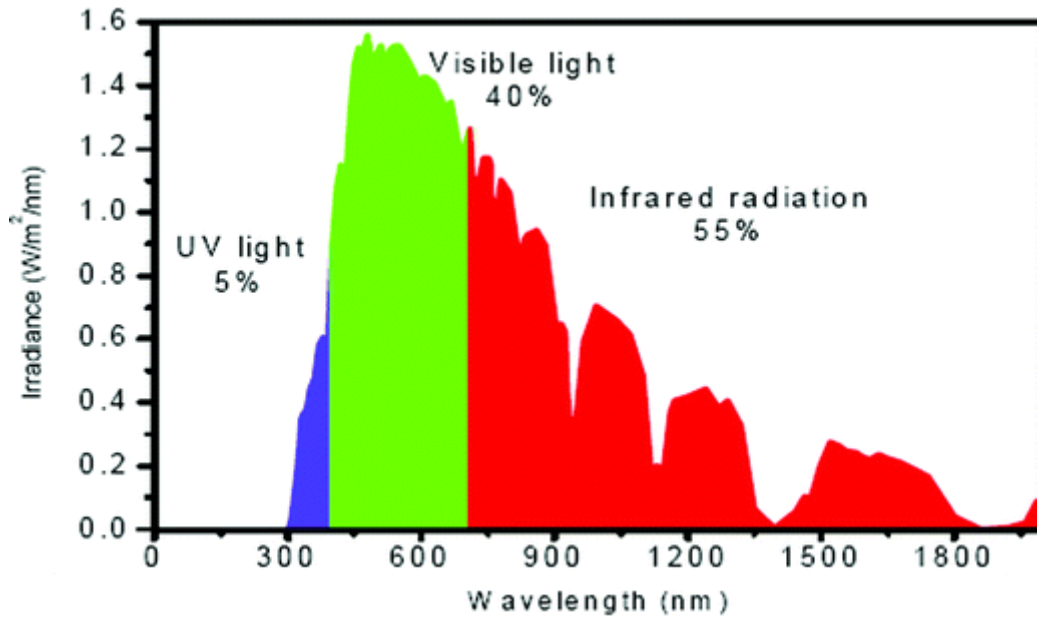


Figure 6: solar energy composition [16]

1.3 Solar Reflectance

Also called Albedo, it is the ratio of solar radiation reflected by a surface to the total radiation reaching that surface. The albedo of an object is expressed in percentage, so it can range between 0 (0%) and 1 (100%). The first case refers to a situation of no reflection, typical of a black body (an object able to capture the total amount of the incoming radiation), while the second case means that the surface reflects the whole quantity of incoming radiation. For example, the planet Earth has an average albedo of 0.3 [17]. Darker surfaces present lower reflectivity values, so does the bigger part of urban surfacing materials (asphalt, concrete), increasing surfaces and air temperatures and worsening the UHI problem (fig.7). In fact, the material's colour affects albedo, because much of the solar radiation occupies the visible part of the spectrum. Generally solar reflectance is measured with a solar reflectometer (ASTM C1549), a sunshine pyranometer (ASTM E1918) or using spectrophotometric measurements (ASTM E903 and E892).

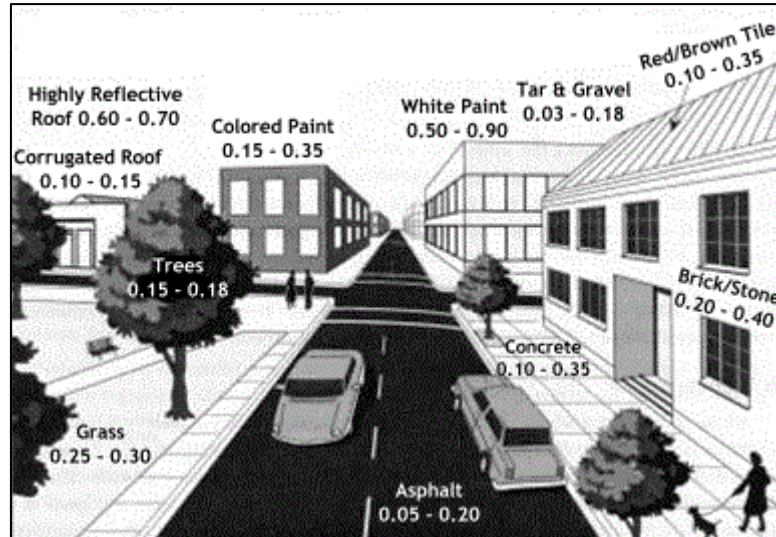


Figure 7: urban albedos [18]

1.4 Solar Reflectance Index (SRI)

A good way to assess the thermal performance of a material is to calculate its SRI. According to ASTM E1980-01, SRI quantifies how hot a flat surface would get relative to a standard black (reflectivity 5%, emissivity 90%) and a standard white surface (reflectivity 80%, emissivity 90%). It ranges between 0 (standard black surface) and 100 (standard white surface) and is calculated as follows:

$$SRI = \frac{(T_{black} - T_{surface})}{(T_{black} - T_{white})} \cdot 100$$

where T_{black} , T_{white} and $T_{surface}$ are the steady state of temperatures of the standard black, white and material surface respectively [19]. For example, the standard black has a temperature rise of 50 °C in full sun, and the standard white has a temperature rise of 8.1 °C. Once the maximum temperature rise of a given material has been computed, the SRI can be computed by interpolating between the values for white and black. It is expected to obtain high SRI values for materials with good thermal performances (“cool”) and low values for materials with bad performances (“warm”). For very bad thermal behaviour SRI can reach negative values and for very good behaviour it can have values greater than 100.

1.5 Emissivity

Emissivity, or thermal emittance, is a measure of how much long-wave radiation (infrared) is emitted from an object, compared to that from a perfect black body of the same temperature [20]. This parameter can assume values between 0 (perfect reflector-mirror) and 1 (perfect emitter-black body), and is dependent on temperature, wavelength and surface condition. Typically a highly polished surface falls below 0.1, while an oxidized or painted surface has a higher emissivity. Oil-based paint, regardless of colour in the visible spectrum, has an emissivity over 0.9 in the infrared. Human skin exhibits an emissivity 0.97 to 0.98 (tab.3). In general metals tend to have low values, increasing with temperature, while non-metals show high values, decreasing with temperature [20]. As a matter of facts, surfaces with high emissivity values will stay cooler, thanks to their fast heat release.

1.6 Heat Capacity

Another important parameter is the material's heat capacity, that is its ability to capture and store heat. Typically construction materials (asphalt, concrete, brick) have higher values of heat capacity respect to natural materials (soil, sand), so the urban environment works as a big heat-storage, increasing the UHI. Despite urban materials generally have high emissivity values (so they dissipate heat quickly), they also have high heat capacity and low reflectivity, resulting in an overall bad thermal behaviour.

Material	Emissivity Values			
	1.0 μm	5.0 μm	7.9 μm	8-14 μm
Asbestos	0.9	0.9	0.95	0.95
Asphalt	n.r.	0.9	0.95	0.95
Basalt	n.r.	0.7	0.7	0.7
Carbon				
Unoxidized	0.8-0.95	0.8-0.9	0.8-0.9	0.8-0.9
Graphite	0.8-0.9	0.7-0.9	0.7-0.8	0.7-0.8
Carborundum	n.r.	0.9	0.9	0.9
Ceramic	0.4	0.85-0.95	0.95	0.95
Clay	n.r.	0.85-0.95	0.95	0.95
Concrete	0.65	0.9	0.95	0.95
Cloth	n.r.	0.95	0.95	0.95
Glass				
Plate	n.r.	0.98	0.85	0.85
Gob	n.r.	0.9	n.r.	n.r.
Gravel	n.r.	0.95	0.95	0.95
Gypsum	n.r.	0.4-0.97	0.8-0.95	0.8-0.95
Ice	n.r.		0.98	0.98
Limestone	n.r.	0.4-0.98	0.98	0.98
Paint (non-Al.)		0.9-0.95	0.9-0.95	
Paper (any color)	n.r.	0.95	0.95	0.95
Plastic				
Opaque	n.r.	0.95	0.95	0.95
Over 20 mils	n.r.			
Rubber	n.r.	0.9	0.95	0.95
Sand	n.r.	0.9	0.9	0.9
Snow	n.r.		0.9	0.9
Soil	n.r.		0.9-0.98	0.9-0.98
Water	n.r.		0.93	0.93
Wood (natural)	n.r.	0.9-0.95	0.9-0.95	0.9-0.95

n.r. = not recommended

Table 3: Emissivity Values for Common Materials & Non-Metals [21]

1.7 Other Factors

1.7.1 Urban Geometry

Urban geometry produces different effects in thermal behaviour of built-up spaces. Buildings act like a shade for the solar radiation incoming, providing shadows that help surfaces to stay cooler. At the same time buildings obstruct the natural wind course, decreasing its cooling effect. Large and tall constructions prevent a ready heat release from surfaces, on the contrary they absorb this energy. This effect is noticeable especially during night time, when the air remains considerable warmer than the air over rural areas. Researchers usually refer to this with “*urban canyon*” effect. In fact, tall buildings lining narrow roads create corridors, providing shadows but absorbing energy irradiated from the surfaces (fig.8). In addition there is a reduction of city’s overall albedo. The effects of urban geometry on UHI are often described through the “*sky view factor*” (SVF), which is the visible area of the sky from a given point on a surface [2].

This parameter assumes values close to 1 if the area has few obstructions (so large part of the sky is visible), and approaches 0 when several objects (e.g. buildings) prevent the sky view.



Figure 8: urban canyons trap heat [22]

1.7.2 Anthropogenic Heat

Anthropogenic heat refers to the heat dissipated by the human activities. It includes several sources such as heating/cooling systems, running appliances, transportation and traffic, industrial processes, biological processes. In addition the exhaust gases, besides raising greenhouse layer, also increase localised temperature [2].

1.7.3 Weather

Atmospheric conditions play an important role in UHI development. In particular wind and cloud cover are the two main factors. In fact, UHI finds its most favourable condition with calm winds and clear skies as they maximize the amount of solar energy reaching urban surfaces and minimize the heat that can be convected away. On the contrary, strong winds and cloud cover penalize UHI. Nevertheless during winter it is possible to get benefits from the warming effect of UHI. For instance, higher temperatures prevent the formation of ice on the road, increasing safety.

1.7.4 Geographic Location And Topography

Geographic location determines topography and climate. Obviously latitude influences the amount of radiation reaching a location. As a matter of facts, large bodies of water (e.g. lakes, rivers) can moderate temperature and generate winds that take the heat away. Also mountains have their effects, blocking wind or generating patterns that pass through a city.

1.8 Impacts

1.8.1 Energy Consumption

High temperatures, due to the cooling need, lead to the increase of energy consumption, especially during the hot summer periods. This peak urban electric demand increases 1.5 to 2 percent for every 0.9 °C increase in summertime temperature [2]. UHIs tend to exacerbate the consequences of extreme heat waves, enhancing the risk of power outages and blackouts.

1.8.2 Air Quality

The increase of energy demand also results in worsening air pollution. Indeed, the most part of the electric power is produced in fossil-fuel-burning big plants, that release harmful substances in the atmosphere. These pollutants, dangerous for the health and cause of acid rains, include sulphur dioxide (SO₂), nitrogen oxides (NO_x), particulate matter (PM), carbon monoxide (CO) and mercury (Hg). These plants also produce greenhouse gases, particularly carbon dioxide (CO₂), which contribute to global warming. Another result of overheating is the increasing of ground-level ozone (O₃) formation, that is toxic for man. This molecule is produced when NO_x and volatile organic compounds (VOC_s) react in the presence of sunlight [2].

1.8.3 Human Health And Comfort

UHIs can bring different health problems and discomforts. In particular, increased daytime temperatures, reduced night-time cooling and higher air pollution levels can lead to health harms like respiratory difficulties, heat cramps and exhaustion, non-fatal heat stroke and heat-related mortality [2]. Furthermore, the phenomenon enhance the effect of heat waves on sensitive population, such as children, elderly people, people affected by heart diseases, increasing the risk from these extremely hot and wet events.

1.8.4 Water Quality

The overheating of urban surfaces due to UHI causes the transfer of the stored heat to the runoff water. This effect, called thermal pollution, degrades the water quality and brings the overheated water into storm sewers (fig.5). Then the water drains into streams, rivers, ponds and lakes, increasing the temperature of these ecosystems and altering the natural equilibrium. All the aspects of aquatic life are affected, especially the metabolism and reproduction of many aquatic species.

1.9 Mitigating Urban Heat Island

Urban climatologists are all agreed that three strategies can help to reduce the UHI effects: trees and vegetation, cool roofs and cool pavements. The benefits of *trees and vegetation* are quite obvious. Besides the fact that they provide shadow, they also have a cooling effect on the atmosphere, thanks to the evapotranspiration. Foliage also increases the overall albedo, reflecting a bigger part of solar radiation. *Cool roof* is a roofing system able to reflect the solar radiation keeping the exposed surfaces cool (fig.9). The method consists in the use of high reflective and high emissive materials, improving the building comfort and decreasing the energy consumption. *Cool pavements* is a compendium of techniques with the objective of improving of the urban climate. The aim of this research falling under this argument, so it is provided a focus on this specific subject.

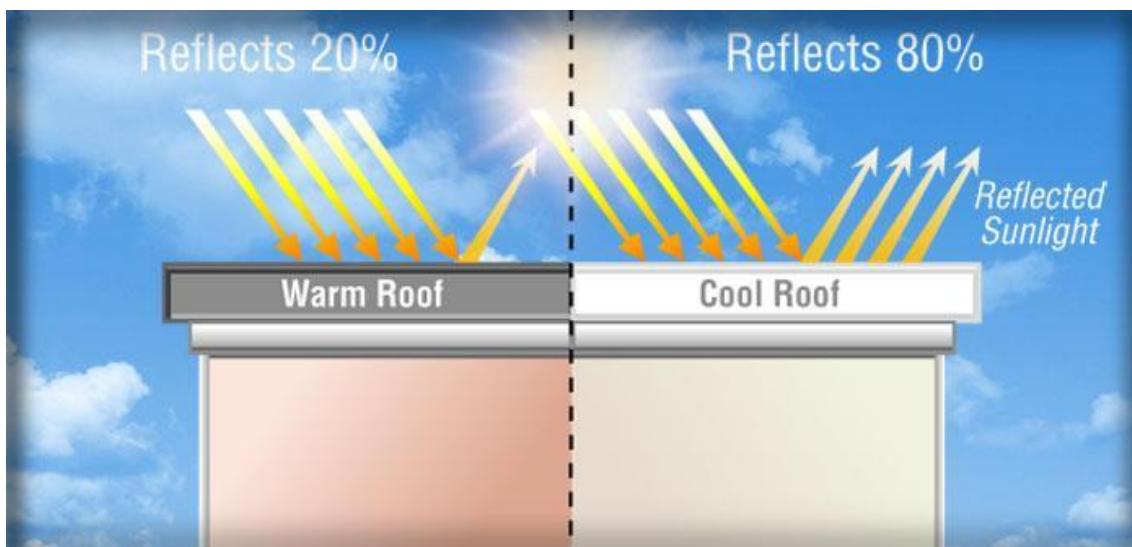


Figure 9: reflective roof [23]

1.9.1 Cool Pavements

“Cool pavements refer to a range of established and emerging materials. These pavement technologies tend to store less heat and may have lower surface temperatures compared with conventional products. They can help address the problem of urban heat islands, which result in part from the increased temperatures of paved surfaces in a city or suburb. Communities are exploring these pavements as part of their heat island reduction efforts” [25].

There are different possibilities to keep the pavement cool:

➤ *Increase pavement surface reflectance*

Albedo is one of the most important thermal parameters of a material. High albedo keeps the pavement cool as well as it reduces the temperature below the surface. In fact, less heat is available at the surface, so the conduction process brings less heat into the pavement layer.

➤ *Increase pavement emissivity*

Emissivity, as well as albedo, plays a fundamental role in the thermal performance of a pavement, as it determines how readily the surface sheds heat. Improving this parameter is an important factor in mitigating UHI; nevertheless there are only limited options to adopt cool pavement practices that modify it, as most of the paving materials are innately characterized by high emissivity values [26].

➤ *Increase pavement surface convection*

Convection is a process that transfers heat from the surface to the moving air on top of it. It depends on the speed and temperature of the air passing over the surface, pavement roughness, and the total surface area of the pavement exposed to air.

➤ *Reduce pavement thermal conductivity*

Conduction is a process that transmit heat from the pavement surface to the underlying layers. Having a low conductivity value helps to restrict the heat to the first pavement layer, avoiding to store it.

➤ *Reduce pavement heat capacity*

Heat capacity determines how much energy can be absorbed and stored in the pavement at certain temperature. Built-up areas capture more solar energy than rural surroundings because urban materials have a bigger heat capacity respect of natural soils and vegetation. As a result, this heat is released during the night, worsening the UHI.

➤ *Evaporation cooling*

The evaporation process needs energy in changing water phase from liquid to gas, cooling down a surface. Enhancing this phenomenon is a good strategy to contrast UHI.

➤ *Shading pavements*

This practice is useful to protect the pavement from the sun radiation, decreasing the surfaces heating-up.

➤ *External active mechanical cooling*

Other cooling options can be to incorporate pipes carrying water in the pavement, providing a cooling effect, or cooling through thermoelectric devices embedded in pavements.

There are different potential cool pavement types:

➤ *Conventional asphalt pavement*

Typically conventional asphalt is not a virtuous thermal material in terms of UHI. It is possible to modify it with high albedo materials such as light-colored aggregate, colored asphalt by pigments, use of tree resin in place of bitumen. If the asphalt is already installed, it is possible to treat it in order to improve its thermal performance (e.g. raise albedo) applying light-colored coating, or chip seals, whitetopping (fig.10), ultra-thin whitetopping and microsurfacing with light-colored aggregate and/or emulsified polymer resin for maintenance [27].

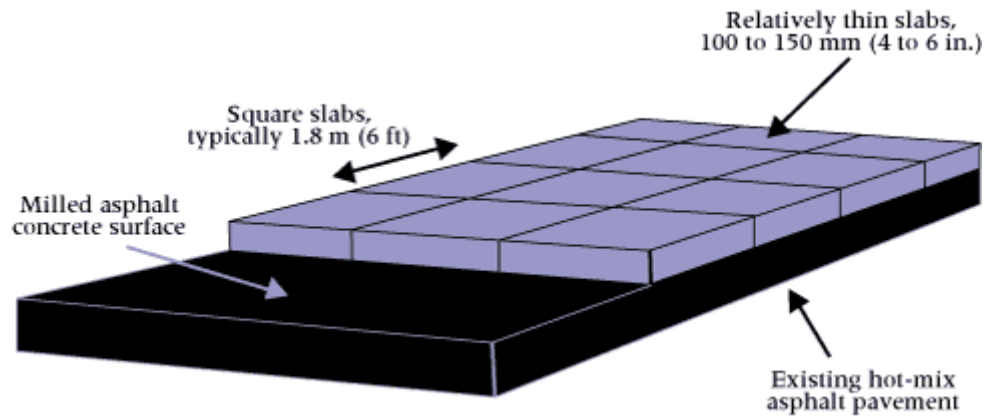


Figure 10: whitetopping [28]

➤ *Conventional concrete pavement*

Normally concrete pavement has a higher albedo than asphalt pavement. Nevertheless the parameter can be increased by using white cement, or cement blended with light color slag.

➤ *Permeable pavement*

A permeable pavement is a layer with a high number of voids. Meteoric water, instead of staying on the surface, drains through the surface where is collected and carried away (fig.11). Permeable pavements include porous asphalt pavement, pervious concrete pavement, and bricks or block pavers (e.g. interblocks). In addition to the evaporation cooling effect, permeable pavements, thanks to the increased exposed surface (given by the voids and the roughness), create air turbulence over the surface able to facilitate the convection process.

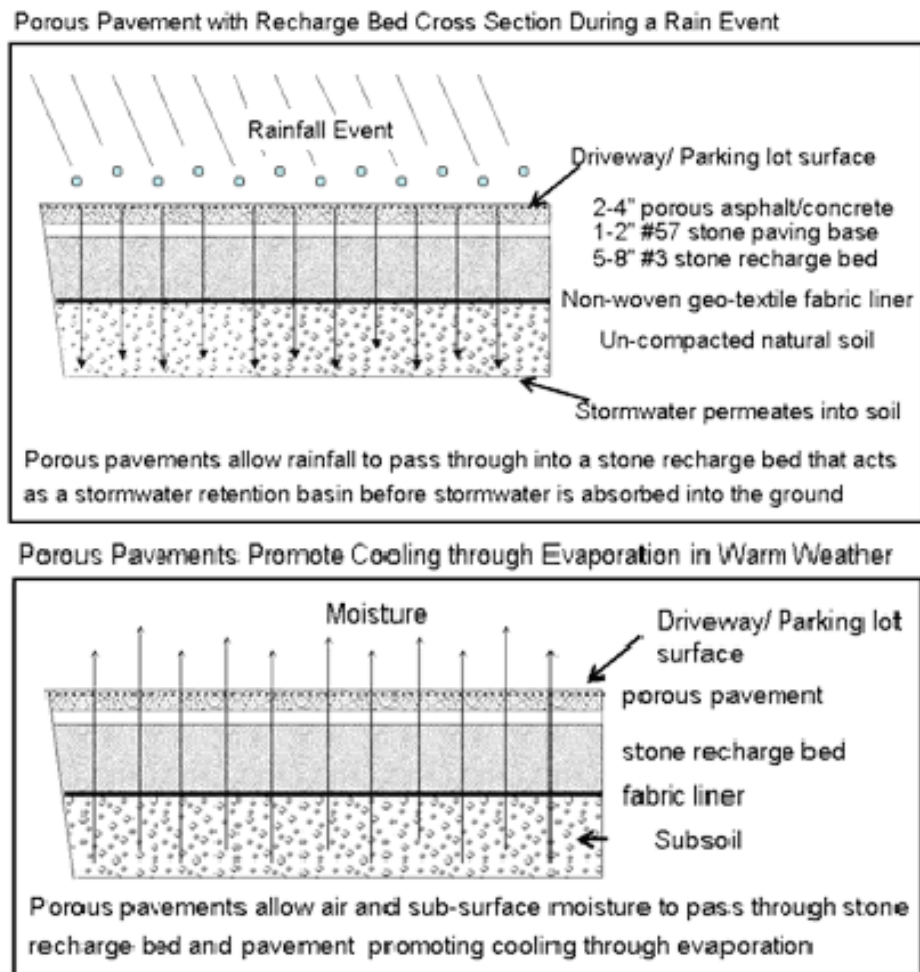


Figure 11: permeable pavement [29]

With a cool pavement technique is possible to achieve several benefits [29]:

- Mitigate urban heat island(UHI) effect;
- Reduce energy use and greenhouse emission;
- Improve water quality and reduce stormwater runoff (for permeable pavement);
- Increase pavement life/durability and waste reduction;
- Reduces pavement maintenance costs;
- Enhance night-time illumination;
- Comfort improvements;
- Improve driving safety (for permeable pavement);
- Noise reduction.

CHAPTER 2:

INVESTIGATION EQUIPMENT

This section aims to provide a description of the instrumentation used to carry out the experimentation and a basic understanding of the theoretical rudiments behind the operating principles of these instruments.

2.1 Thermal imaging camera

A thermal imaging camera is a device able to read the objects temperatures. It works detecting the infrared radiation emitted by a surface and it forms a thermal image that represents a temperature map of the object. The working principle is the same of a common camera that forms an image using the visible light.

The instrument focuses the infrared heat energy and converts it into data which then can be displayed as visible images on a screen:

- Infrared energy is emitted by an object (A).
- Optics in the thermal imaging camera focus this energy on to its infrared detector where it is converted into data (B-C).
- The thermal imaging camera's detector sends the data to its sensor electronics which process images (D).
- These images can then be viewed on a video monitor, LCD screen or a network-enabled computer (E) (fig.12).

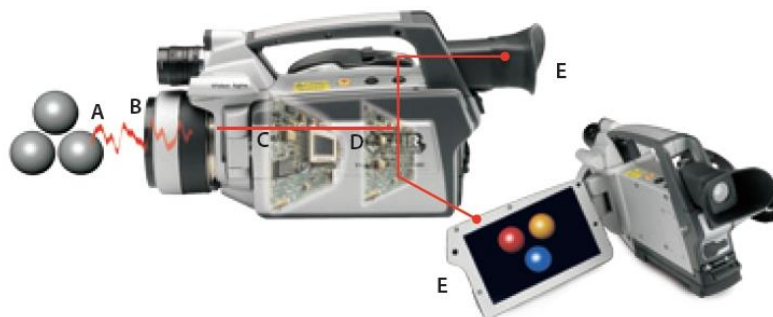


Figure 12: image processing [31]

This complex process takes a thermal imaging camera just fractions of a second [32].

Thermal imaging cameras are very useful in several applications, from buildings to military. They can save money and even save lives. Typical uses are:

- *Industrial*: identify malfunctions in electrical and mechanical systems. Inspect hot spots in engines, plants, avoiding production delays and saving money.
- *Buildings*: identify heat losses and construction defects, achieving energy savings.
- *Boundaries security*: provides adequate support to the surveillance personnel, helping in the fight against intrusions and contraband.
- *Security sector*: protection of sensible areas like ports, airports, nuclear plants, storehouses, factories, properties.
- *Research and development*: specific thermic devices to provide accurate and reliable means in the experimental field.
- *Nautical night view*: uses in night-time navigation, rescue, fight against piracy.
- *Vehicle night view*: installation as drive assistance on cars, improving road safety. Also utilized by firemen, in mines and military vehicles.
- *Automation*: continuous control of automatic industrial process.
- *Security force*: incognito watching operation.
- *Gas losses*: searching for potential gas loss dangers.
- *Fauna observation*: hunting or watching of animals in the night-time.
- *Fire safety*: firemen are able to look for people to rescue through the smoke.
- *Medical applications*: diagnostic of diseases and other general health problems [33].

Testing was conducted using a *FLIR B200* (figg.13,14). The device was used to get the emissivity parameter and the temperature of the samples and surfaces analysed.



Figure 13: FLIR B200 [20]

The camera is able to calculate the temperature of the object catching the emitted infrared radiation from it. However, the radiation measured by the instrument is not only function of the temperature, but also of the emissivity of the material. In addition, there is a contribute deriving from the reflected quote of radiation in the surroundings that hits the object. Both these two factors are influenced by the absorption of the atmosphere. Consequently, to get a correct value of temperature, is necessary to consider the effects of different radiation sources. The camera is able to automatically compensate such factors, but it needs the following parameters:

- The emissivity of the object
- The reflected apparent temperature
- The distance between the object and the camera
- The relative humidity
- Temperature of the atmosphere [20]

Imaging Performance	
Field of View (FOV) / Close Focus Limit	25° x 19° / 0.4 m (1.31 ft.)
Thermal sensitivity (NETD)	0.08°C @ +30° (+86°F) / 80mK
Detector Type	Focal Plane Array (FPA) microbolometer
IR resolution	200 x 150
Spectral range	7.5 to 13 µm
Digital zoom and pan/focus	1x - 2x continuous/auto and manual focus
IFOV (with 25° lens)	2.18 mRad
Image Presentation	
Image modes	Thermal, Visual, Thermal Fusion
FLIR Fusion	Picture in Picture (PIP) - scalable IR image in visible light image
Display	Built-in touch-screen LCD display, 3.5 in.
Video lamp	1000 cd
Visible light camera resolution	1280 x 1024 (1.3 megapixels)
Measurement	
Object temperature range	-20°C to +120°C (-4°F to +248°F), optional up to +350°C
Accuracy	±2°C (±3.6°F) or ±2% of reading
Measurement modes	5 Spotmeters, 5 Box areas, Isotherm, Auto hot/cold spot
Alarms	Humidity alarm (includes dew point alarm), Insulation alarm
Set-up controls	Mode selector, color palettes (BW, BW irr, Iron, Rain), configure info to be shown in image, local adaptation of units, language, date and time formats, and image gallery
Measurement corrections	Reflected ambient temperature and emissivity correction
Image Storage	
Digital storage/capacity	Removable SD Memory Card/1000 + JPEGs
Image storage mode & formats	IR/ visible light, simultaneous storage of IR/ visible images, all standard JPEG
Laser LocatIR™	
Classification/Type	Class 2/Semiconductor AlGaInP Diode Laser: 1mW/635 nm (red)
Power Source	
Battery type	Rechargeable Lithium-Ion battery
Battery operating time	4 hours +
Battery charging	2 bay charging system, 10-16 V input. Charging status indicated by LED's
AC operation	AC adapter, 90-260 WAC input. 12 V output to camera
Voltage	11-16 VDC
Power management	Automatic shut down and sleep mode after settable time
Environmental	
Operating temperature range	-15°C to +50°C (5°F to 122°F)
Storage temperature range	-40°C to +70°C (-40°F to +158°F)
Humidity	95% relative humidity +25°C to +40°C (+77°F to +104°F) non condensing
Water and dust resistant (encapsulation)	IP 54, IEC 360
Shock	25G, IEC 68-2-29
Vibration	2G, IEC 68-2-7
Physical Characteristics	
Weight	0.88 kg (1.94 lbs.)
Size (L x W x H)	106 x 201 x 125 mm (4.2 x 7.9 x 4.9 in.), with lens pointing forward
Tripod mounting	1/4" - 20
Interfaces	
USB (cable included)	Image transfer to PC
Video output	NTSC Video
Software	
QuickReport™	Included
Reporter™ 8 (Microsoft® Word based)	Optional

Camera includes:	
IR camera with F 1.3 25° lens, image frequency 9Hz	
Integral visible light camera with lamp	
Transport case	
Camera Lens Cap	
Battery	
2-bay battery charger	
Video Cable	
USB cable Std A <-> Mini B, 2 m/6.6 ft.	
SD Memory Card	
Sun Shield	
Stylus Pen	
User documentation CD-ROM, 21 languages	
Power supply	
Getting Started guide	
Interchangeable lenses/options/accessories	
Optional Add-on optics, Telephoto lens, 15°	
Optional Add-on optics, Wide angle lens, 45°	
High temperature option (up to +1200°C (2192°F))	
12 volt auto adapter	
Hip/Belt mounted camera holster	
Neckstrap	
USB-A for memory stick	

Figure 14: FLIR B200 technical specification [20]

It is possible to recognize three radiation contributions collected by the camera: the direct infrared radiation from the object, the radiation from the surroundings reflected via the object surface and the atmosphere contribution. In fact, the atmosphere absorbs part of the infrared emitted by the object and reflected by the object, attenuating them in the measurement path. This process is converted into a mathematic formula, used by the camera to correctly measure temperatures (fig.15).

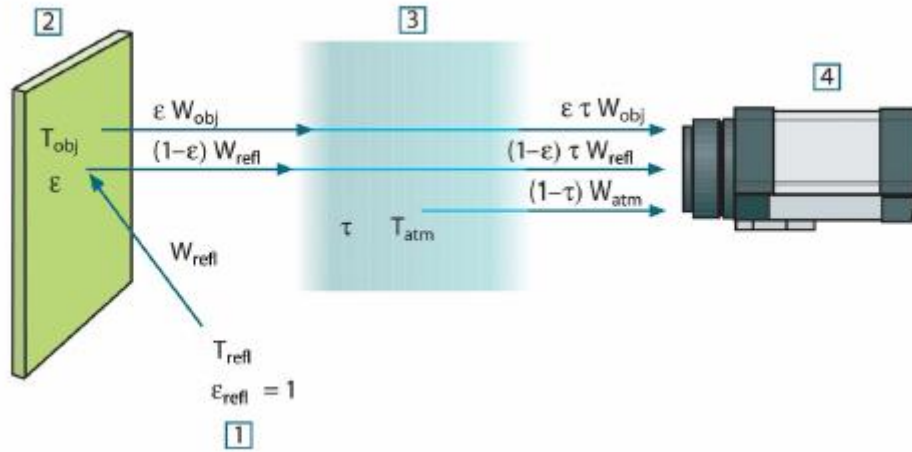


Figure 15: radiation contribute: 1-surroundings; 2-object; 3-atmosphere; 4-camera [20]

Considering the blackbody theory, it is possible to write *equation 1*:

$$U_{source} = CW(T_{source}) \quad (1)$$

where

U_{source} = camera output signal

C = constant

W = received radiation power from a blackbody source

T_{source} = blackbody temperature

Typically the source is a graybody source with emissance ϵ , so the received radiation is ϵW_{source} . The three collected radiation power terms are:

1. Emission from the object = $\epsilon \tau W_{obj}$, where ϵ is the emissance of the object and τ is the transmittance of the atmosphere. T_{obj} is the object temperature.
2. Reflected emission from the ambient sources = $(1 - \epsilon) \tau W_{refl}$, where $(1 - \epsilon)$ is the reflectance of the object. T_{refl} is the ambient temperature.
3. Emission from the atmosphere = $(1 - \tau) \tau W_{atm}$, where $(1 - \tau)$ is the emissance of the atmosphere. T_{atm} is the atmosphere temperature.

It is now possible to write the total received radiation power (*equation 2*):

$$W_{tot} = \epsilon \tau W_{obj} + (1 - \epsilon) \tau W_{refl} + (1 - \tau) W_{atm} \quad (2)$$

It can be obtained *equation 3* multiplying each term of *equation 2* by the constant C of *equation 1* and replacing the CW products by the corresponding U according to the same equation:

$$U_{tot} = \varepsilon\tau U_{obj} + (1 - \varepsilon)\tau U_{refl} + (1 - \tau)U_{atm} \quad (3)$$

Solving *equation 3* for U_{obj} (*equation 4*):

$$U_{obj} = \frac{1}{\varepsilon\tau} U_{tot} - \frac{1 - \varepsilon}{\varepsilon} U_{refl} - \frac{1 - \tau}{\varepsilon\tau} U_{atm} \quad (4)$$

This is the general measurement formula used in all the FLIR thermographic devices [19].

2.1.1 Finding the emissivity

In order to obtain the correct emissivity value is necessary to determine the *reflected apparent temperature*. This parameter is used to compensate for the radiation reflected in the object. According to the FLIR B200 manual (fig.16), the “Reflector method” was used (fig.17).

1	Crumble up a large piece of aluminum foil.
2	Uncrumble the aluminum foil and attach it to a piece of cardboard of the same size.
3	Put the piece of cardboard in front of the object you want to measure. Make sure that the side with aluminum foil points to the camera.
4	Set the emissivity to 1.0.
5	Measure the apparent temperature of the aluminum foil and write it down.

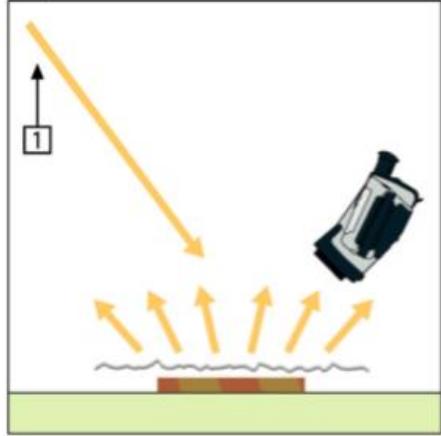


Figure 31.4 Measuring the apparent temperature of the aluminum foil

Figure 16: FLIR B200 reflector method for apparent temperature determination [20]

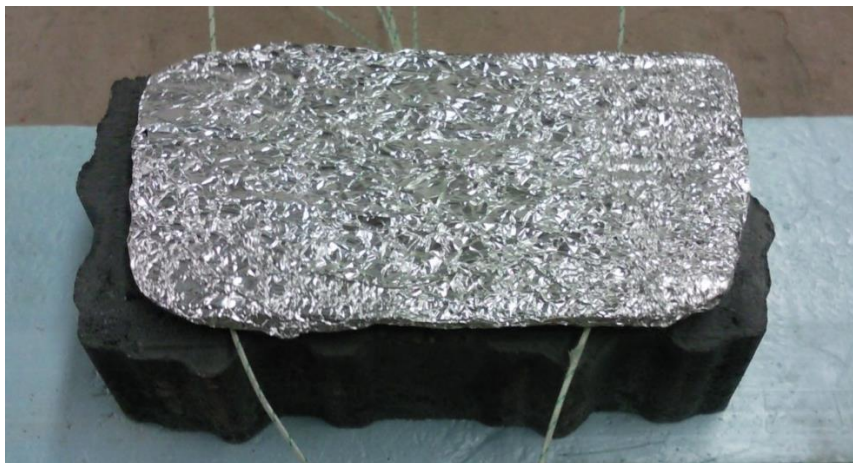


Figure 17: aluminum foil on the sample

Once determined the reflected temperature, the manual sets the steps showed in fig.18 to find the emissivity value.

1	Select a place to put the sample.
2	Determine and set reflected apparent temperature according to the previous procedure.
3	Put a piece of electrical tape with known high emissivity on the sample.
4	Heat the sample at least 20 K above room temperature. Heating must be reasonably even.
5	Focus and auto-adjust the camera, and freeze the image.
6	Adjust Level and Span for best image brightness and contrast.
7	Set emissivity to that of the tape (usually 0.97).
8	Measure the temperature of the tape using one of the following measurement functions: <ul style="list-style-type: none"> ■ Isotherm (helps you to determine both the temperature and how evenly you have heated the sample) ■ Spot (simpler) ■ Box Avg (good for surfaces with varying emissivity).
9	Write down the temperature.
10	Move your measurement function to the sample surface.
11	Change the emissivity setting until you read the same temperature as your previous measurement.
12	Write down the emissivity.

Figure 18: steps to determine emissivity [20]

The manual also gives some advices useful to correctly determine the emissivity:

- Avoid forced convection
- Look for a thermally stable surrounding that will not generate spot reflections
- Use high quality tape that you know is not transparent, and has a high emissivity you are certain of
- This method assumes that the temperature of your tape and the sample surface are the same. If they are not, your emissivity measurement will be wrong.

2.1.2 *Measuring the temperature*

To measure objects temperature is the main purpose of the thermal camera. In order to do that, the correct emissivity of the material must be set in the device. Besides, the distance from the analysed surface, the air humidity, the apparent reflected temperature must be provided to the camera (fig.19). Once all these parameters are set up, a photo from the correct distance from the object can be taken.



Figure 19: setting options [34]

On the LCD screen the correct temperature of a spot on the surface is already visualized, even before shooting. This feature is useful to have a preliminary idea. Subsequently, it is possible to analyse the photos with FLIR QUICK REPORTER, a specific software provided by FLIR (fig.20), and get the average temperature of the surface. In this way, it is also possible to obtain the emissivity value, by knowing the temperature of the piece of tape (emissivity set at 0.97) and changing the emissivity until getting the same temperature on the sample surface (see § 2.2.1) The software allows to change the setting parameters even after the photo has been taken.

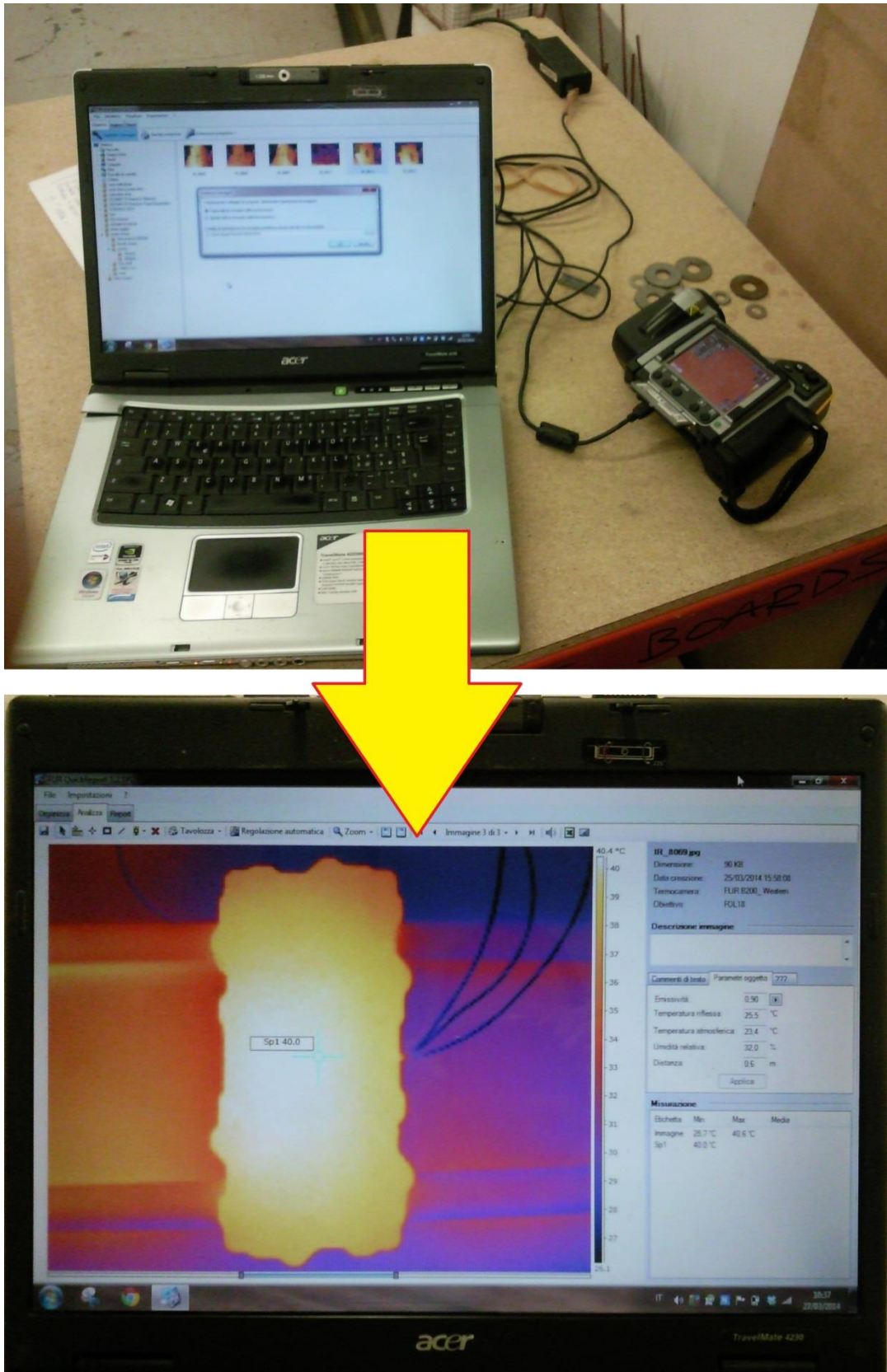


Figure 20: analyzing photos with FLIR QUICK REPORTER

2.2 Sunshine Pyranometer for testing

A pyranometer is a type of actinometer used to measure broadband solar irradiance on a planar surface and is a sensor that is designed to measure the solar radiation flux density (W/m^2) from a field of view of 180 degrees [35]. Testing was conducted using a *SPN1 Delta-T Sunshine Pyranometer* (fig.21). The device was used to get the solar reflectivity (albedo) of the external surfaces analysed.

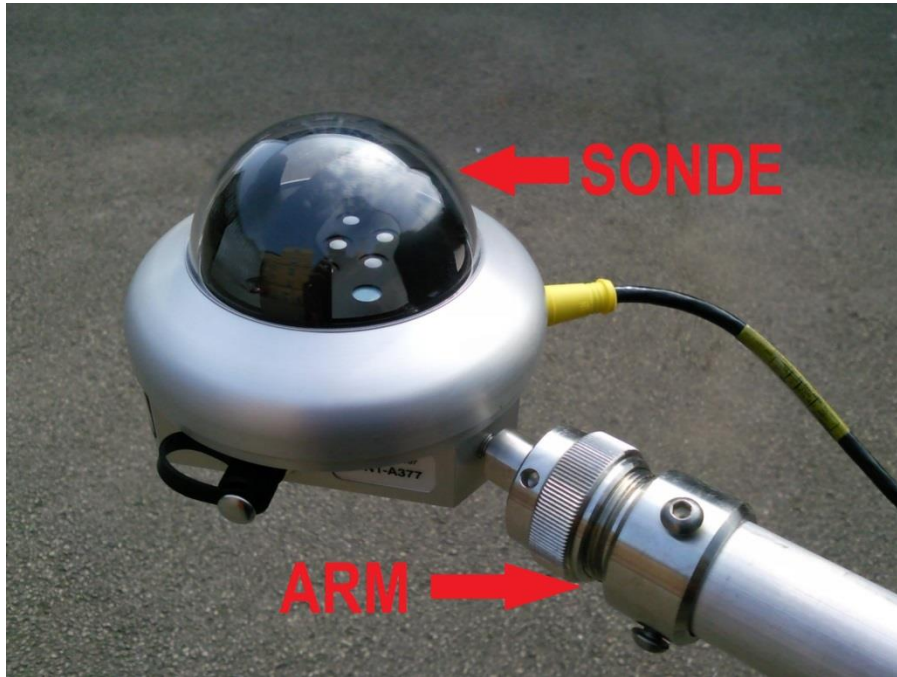


Figure 21: SPN1 Delta-T Sunshine Pyranometer

The SPN1 Sunshine Pyranometer uses an array of seven miniature thermopile sensors and a computer-generated shading pattern to measure the direct and diffuse components of incident solar radiation. The SPN1 Pyranometer computes direct radiation by subtracting the diffuse from the global (total) radiation [36]. The device has got one sensore with three output channels, designated to respectively assess the total solar radiation, the diffuse radiation and the sunshine status.

The measuring procedure, following the standard ASTM E1918-06, consists of:

- The probe shall be fixed on an support (fig.22), that places the sonde sensor at a height of 50 cm above the surface. The arm shall be aligned such that it points toward the sun (this eliminates the shadows of the people conducting the test and minimizes the effect of the shadow from equipment). The pyranometer shall be parallel to the surface where measurement in conducted.

- The pyranometer shall be faced upward (that is, looking directly away from the surface) to read incoming solar radiation.
- After that it shall be flipped downward to read the reflected solar radiation.
- The readings have to be kept constant at least for 10 seconds. The measurements of incoming and reflected radiation shall be performed in a time interval not to exceed 2 minutes.
- Solar reflectance is the ratio of the reflected radiation to incoming radiation.
- The pairs of incoming and reflected radiation shall be repeated at least three times.
- The calculated solar reflectance from all the measurements shall agree within 0.01 in a reflectivity scale of 0.00 to 1.00.
- Furthermore, the standard provides some recommendations:
- Be sure that the investigated surface is large (circles, with at least four meters in diameter or squares four meters on a side), homogeneous, low-sloped, such as roofs, streets and parking lots. The measurements shall be performed on dry surfaces.

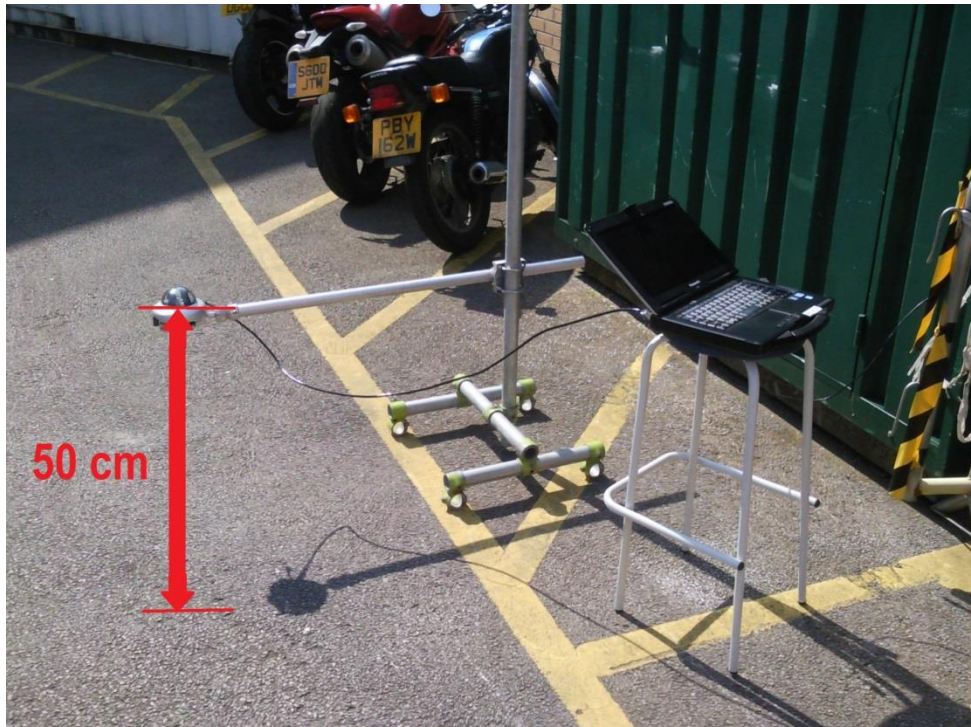


Figure 22: pyranometer support

- Cloud cover and haze significantly affect the measurements. The tests shall be conducted on a clear sunny day with no cloud cover or haze during the

individual measurements. To decide if the weather conditions are acceptable, the standard provides some additional information in the Annex section.

- The test shall be done in conditions where the angle of the sun to the normal from the surface of interest is less than 45° .

In order to visualize and elaborate the data collected by the pyranometer, the device is provided with *SunRead* software (fig.23), able to read the SPN1 output values and status information via the PC RS232 serial port.

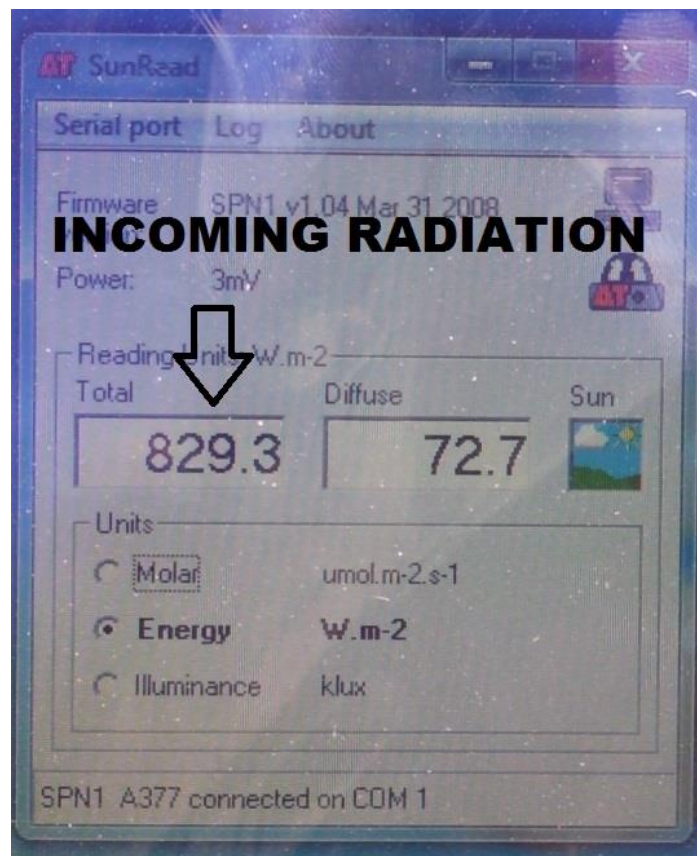


Figure 23: SunRead software

2.3 Thermocouples

A thermocouple is a temperature-measuring sensor composed by two dissimilar conductors that contact each other at one or more spots, where a temperature differential is measured by the different conductors. When the temperature of one spot differs from the reference temperature set in the device, it produces a voltage (proportional to temperature) called E.M.F. (electromotive force), displayed converted in a heat unit of measure (typically Celsius or Fahrenheit degrees). It is possible to represent the E.M.F. as follows:

$$e = \alpha(T_1 - T_2) + \beta(T_1^2 - T_2^2) \quad (5)$$

Where e is the E.M.F., α and β are constants of the thermocouple, T_1 and T_2 are the temperatures.

A thermocouple requires a reference junction, placed in series with the sensing junction. As the two junctions are at different temperatures a thermal E.M.F. is generated. The reference junction is used to correct the sensing junction measurement (fig.24).

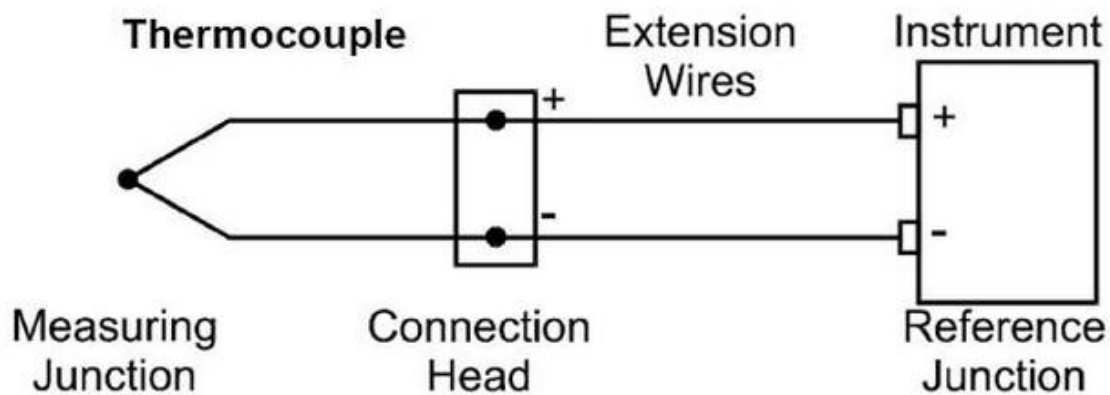


Figure 24: schematic for a thermocouple/instrument connection [37]

The resulting voltage is proportional to the temperature difference between the two junction. This phenomenon is called Seebeck effect. It generates small voltages in the wire connecting the junctions, as great as the temperature gradient is. In practice the Seebeck voltage is made up of two components: the Peltier voltage generated at the junctions, plus the Thomson voltage generated in the wires by the temperature gradient. The Peltier voltage is proportional to the temperature of each junction while the Thomson voltage is proportional to the square of the temperature difference between the two junctions. Each thermocouple has its characteristic Seebeck voltage curve, depending on the component metals, their purity, their homogeneity and their crystal structure [34].

In this research the thermocouples were installed inside the samples and on their surfaces. The resulting temperature were collected by a data logger (fig.25). Moreover, a portable thermocouple was used in the external activity (fig.26).



Figure 25: thermocouples and data logger



Figure 26: portable thermocouple

2.4 Meteorological station

Two different typologies of meteorological stations were used in this research: a portable hygro-thermometer humidity alert and a meteorological station.

The portable station model used is an *Extech Hygro-Thermometer Humidity Alert w/Dew Point* (fig.27,28). It measures the moisture and the temperature in both external and internal environments.

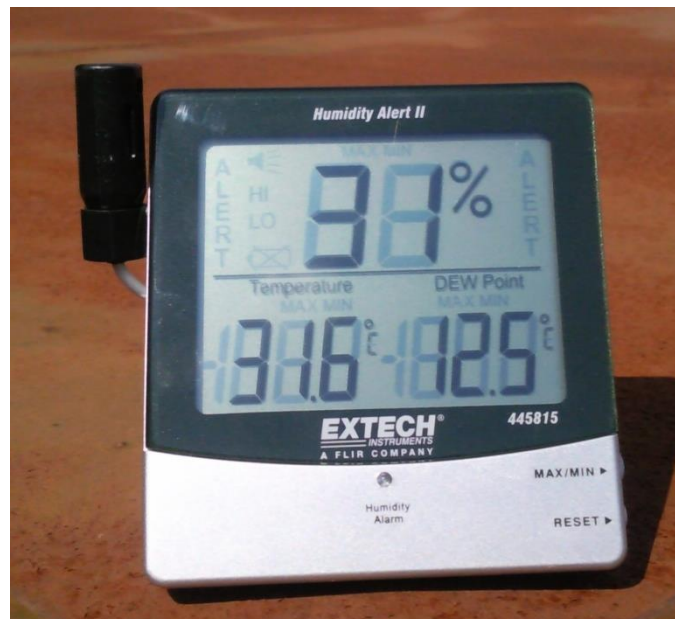


Figure 27: Extech Hygro-Thermometer Humidity Alert

Specifications	
Humidity	10 to 99%
Temperature	14 to 140°F (-10 to 60°C)
Basic Accuracy	±4%RH; ±1.8°F/1°C
Dimensions	4.3 x 3.9 x 0.78" (109 x 99 x 20mm)
Weight	6oz (169g)

Figure 28: portable station technical specifications [38]

Other temperature data were collected from the meteorological station placed at the Nottingham High School, in Nottingham (fig.29). The Geography Academic Department has joined the Weather Underground global network, so a significant amount of data are available for free on the Weather Underground website, such as the temperature, the humidity, the wind direction and speed, the pressure [39].

July 21, 2014

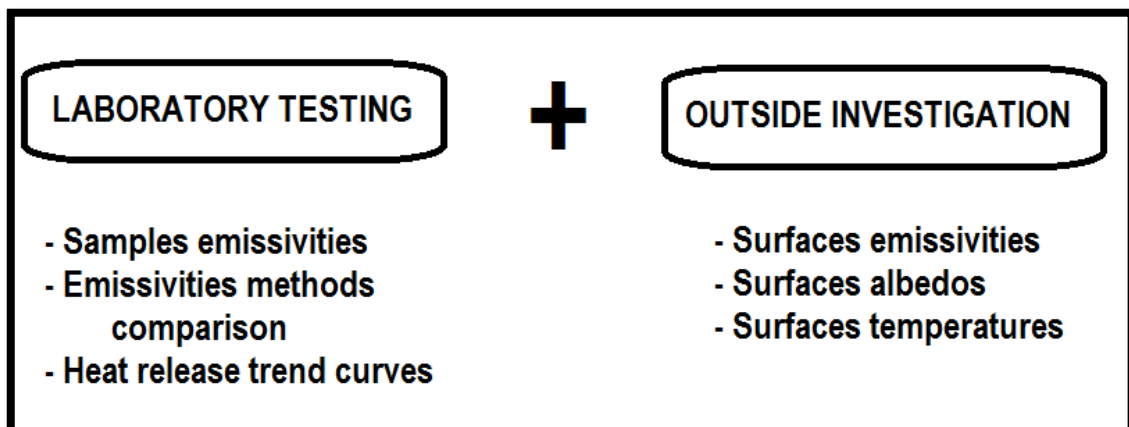
Time	Temperature	Dew Point	Humidity	Wind	Speed	Gust	Pressure	Precip. Rate.	Precip. Accum.
12:05 AM	17.2 °C	15.1 °C	87 %	NW	12.9 kph	20.9 kph	1017.2 hPa	0 mm	0 mm
12:10 AM	17.2 °C	15.2 °C	88 %	NW	12.9 kph	20.9 kph	1017.5 hPa	0 mm	0 mm
12:17 AM	17.2 °C	15.2 °C	88 %	NW	12.9 kph	20.9 kph	1017.5 hPa	0 mm	0 mm
12:25 AM	17.2 °C	15.4 °C	89 %	NW	11.3 kph	20.9 kph	1017.5 hPa	0 mm	0 mm
12:35 AM	16.7 °C	14.8 °C	89 %	NW	11.3 kph	20.9 kph	1017.5 hPa	0 mm	0 mm
12:40					9.7	20.9	1017.5		

Figure 29: weather data from Weather Underground [39]

CHAPTER 3: EXPERIMENTAL WORK

The experimental part of this research was organized in two phases:

1. **LABORATORY TESTING:** the thermal performances of a paving material were investigated, with the purpose of determining if it is a good material in terms of UHI mitigation. All the experimentations were carried out at the Maudslay Building Workshop of Nottingham Trent University's Architecture, Design and the Built Environment Academic School, in Nottingham. The samples were tested using the FLIRB200 thermal camera and FLIR Quick Reporter software. The procedure of the test took place from March to May 2014.
2. **OUTSIDE INVESTIGATION:** the thermal performances of different urban surfaces were measured, in order to understand if the materials in which existing pavements are made of have a good thermal behaviour. All the measurements were collected near the Maudslay Building, on the Nottingham Trent University's properties. The surfaces were tested using the FLIRB200 thermal camera and FLIR Quick Reporter software, the SPN1 Delta-T Sunshine Pyranometer, a portable thermocouple, the Extech Hygro-Thermometer Humidity Alert. The procedure of the test took place from May to July 2014.



3.1 Laboratory testing

Permeable paving bricks were tested. The samples were heated by an infrared lamp, and subsequently their thermal parameters were collected. Emissivity was measured, a significant thermal parameter of a material, able to represent its thermal performance. Two different emissivity evaluation procedures were compared: the thermal camera's manual method and the thermocouples method. Then emissivity was used to measure the temperature of the specimens with the thermal camera, in order to build the heat release trends of the bricks.

3.1.1 Tested material

The material used for testing was the “MARSHALL PRIORA PERMEABLE BRICK”, concrete interblocks with the following dimensions:

- Length 200 mm
- Width 100 mm
- Height 60 mm.

Four different colours of bricks were selected for testing, charcoal (black), red, white and yellow (fig.30). All samples were made of the same concrete mix, and were identical apart from colour. The white brick paint, unlike the others, was a shiny type (fig.31).

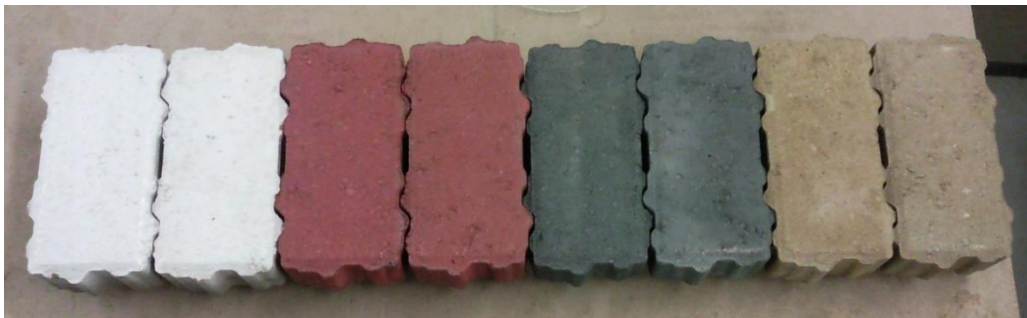


Figure 30: Marshall Piora Permeable bricks



Figure 31: white sample shiny paint

The sample were instrumented with thermocouples sensor, three inside the bulk and five on the surface, all fixed with a thermo-stable glue (fig.32). The sensors were connected to a data logger that was automatically storing results at 10-minute intervals (fig.33). It was therefore possible to monitor and record the temperature variations inside the specimens and on their surfaces.

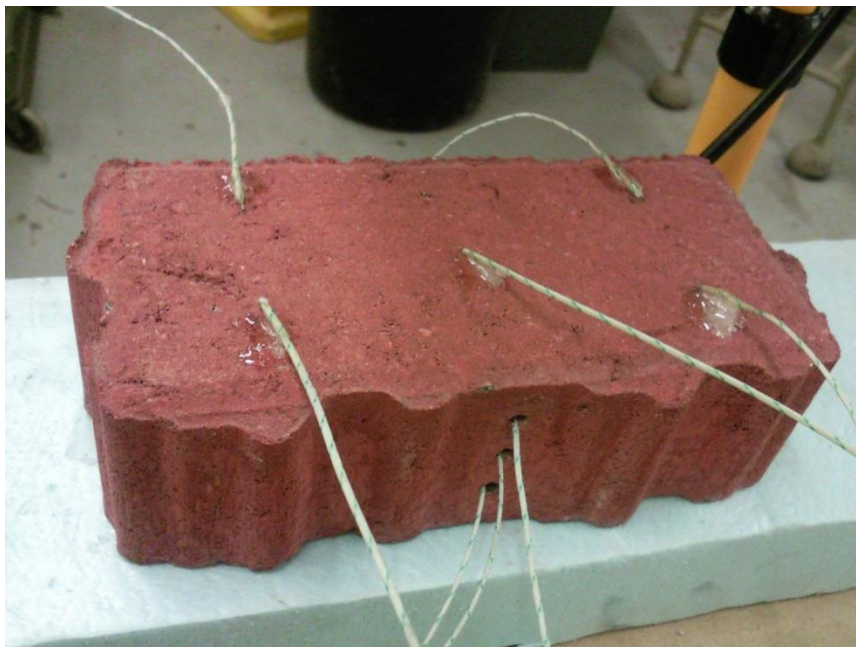


Figure 32: thermocouples positions

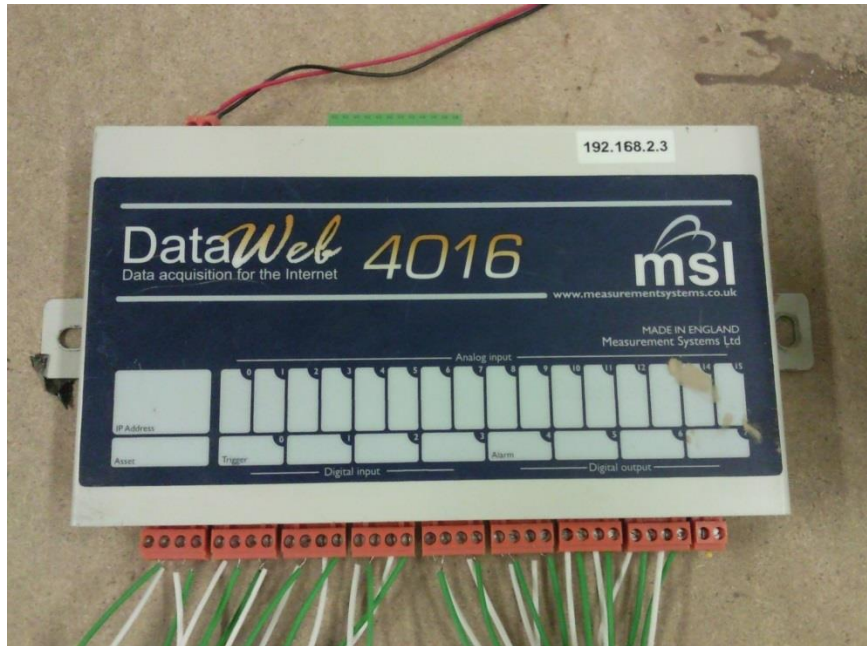


Figure 33: data logger

3.1.2 Emissivity evaluation

Two different emissivity measuring procedures were performed, aiming to understand if there is another effective method to get this fundamental thermal parameter. In fact, especially outside, it happens that the thermal camera's manual procedure (see § 2.2.1) can be difficult to execute, for a number of reasons. First of all, it is not always possible and practical to put a piece of electrical tape on the investigated surface. Besides, it takes a non-negligible amount of time, as the operator has to wait until the tape reaches the same temperature of the surface (if not, the method does not work properly). In addition there is an approximation given by the tape, as none can be sure about its emissivity. Finally, it could be useful to have another way to assess the parameter and so to have a comparison result. For these reasons, the *thermocouples method* was set up, using the surface thermocouples instead of the electrical tape.

- THERMAL CAMERA'S MANUAL METHOD (see § 2.2.1)

Once all brick samples had been prepared they were placed on a table in the testing area. The testing area was environmentally monitored throughout the experiment for air temperature, reflective temperature and humidity; the bricks were elevated off the table surface using wooden blocks. The heat lamps were placed above the samples at a 30° angle. The lights were placed 600 mm above the top of the brick, allowing for localised heating onto the brick.

Following the manual, it was determined the apparent temperature with the *reflector method* and set it in the thermal camera. Two squares of a common black electrical tape were put on the surfaces of each brick. With the infrared lamp, the specimens were heated up for two hours, until reaching a temperature 20°C hotter than the room one (fig.34). Then the lamp was turned off.

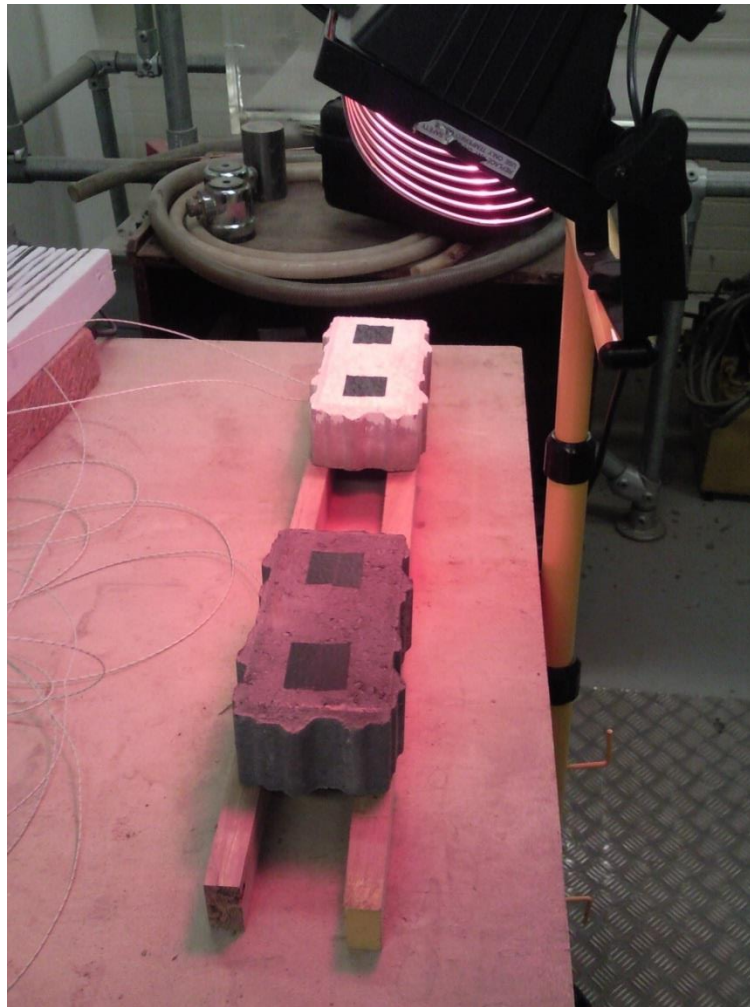


Figure 34: heating up the bricks

Subsequently, the emissivity was set to 0.97 and a photo for each brick was taken. At this point, the correct value of temperature was calculated on the tape's surface. FLIR Quick Reporter software was used to change the emissivity value until getting the same temperature recorded on the tape. The emissivity got is the correct value for the brick (fig.35).

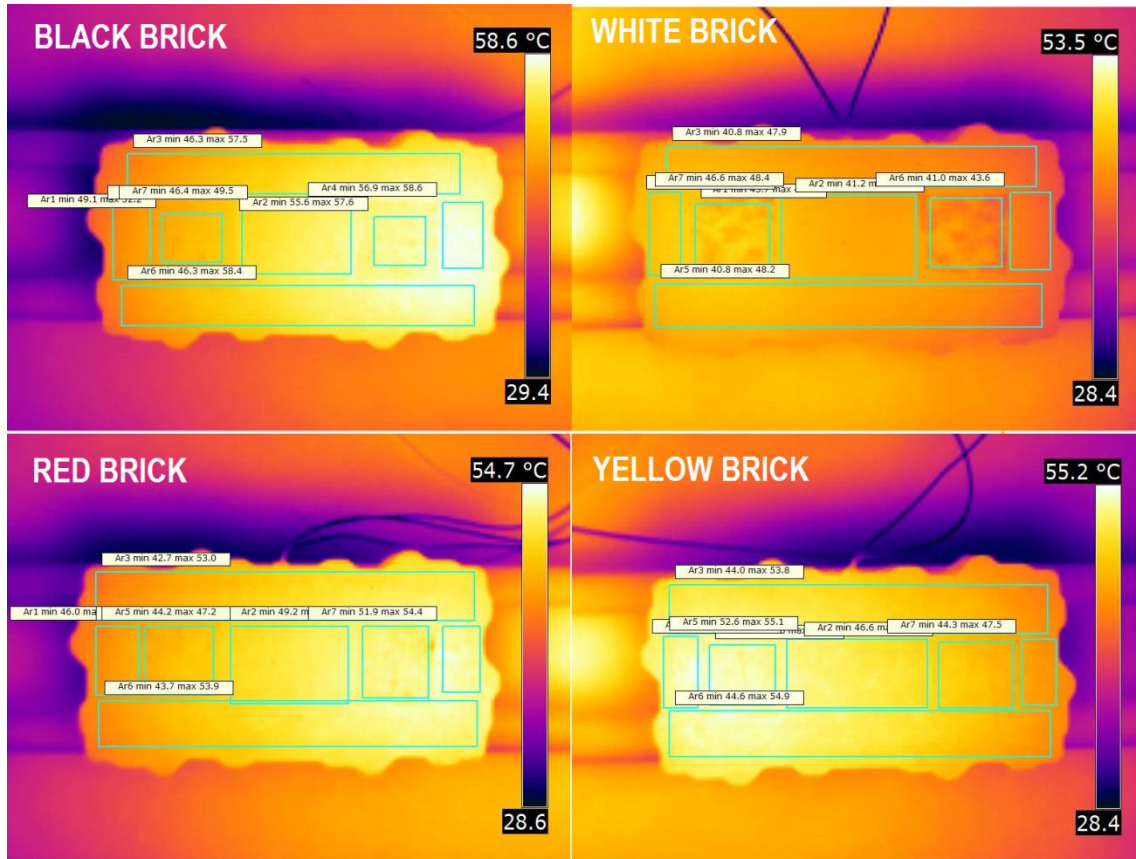


Figure 35: FLIR QUICK REPORTER screenshots

The worked out emissivities are shown in Table 4.

MANUAL METHOD	ϵ
Black	0.95
White	0.96
Yellow	0.96
Red	0.94

Table 4: manual method emissivities

- THERMOCOUPLES METHOD

As for the manual method, the reflector method was used to get the apparent temperature and set it in the thermal camera (§ 2.2.1). After the installation of the thermocouples sensors, the bricks were heated up with the infrared lamp on the same conditions of the previous case. Then the lamp was turned off and one photo for each sample was taken (fig.36). Using FLIR Quick Reporter software, the emissivity of the

sample was changed until getting the same temperature recorder by the data logger connected to the thermocouples.

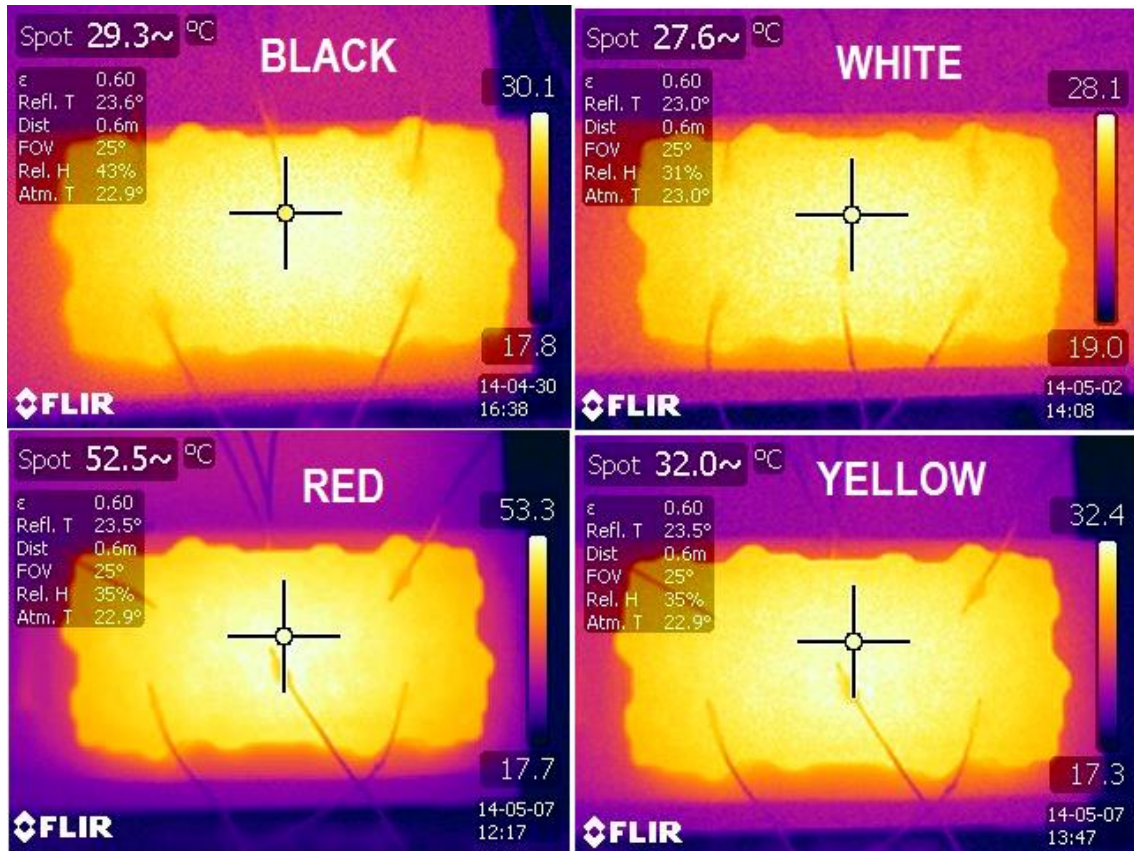


Figure 36: thermal photos

The worked out emissivities are shown in Table 5.

THERMOCOUPLES METHOD	ϵ
Black	0.94
White	0.92
Yellow	0.97
Red	0.93

Table 5: emissivities

- COMPARISON BETWEEN THE TWO METHODS

The resulting emissivities are similar, so it is possible to assume both methods as consistent (fig. 37). In particular, the only value presenting a noticeable variation is the white one. As the Figure 38 shows, that difference is small: 4 % (fig.38). That disparity

was supposed due to the shiny type of paint on the white sample surface, that make the thermic photo acquisition more dependent on the little differences of the enlightenment conditions in the room.

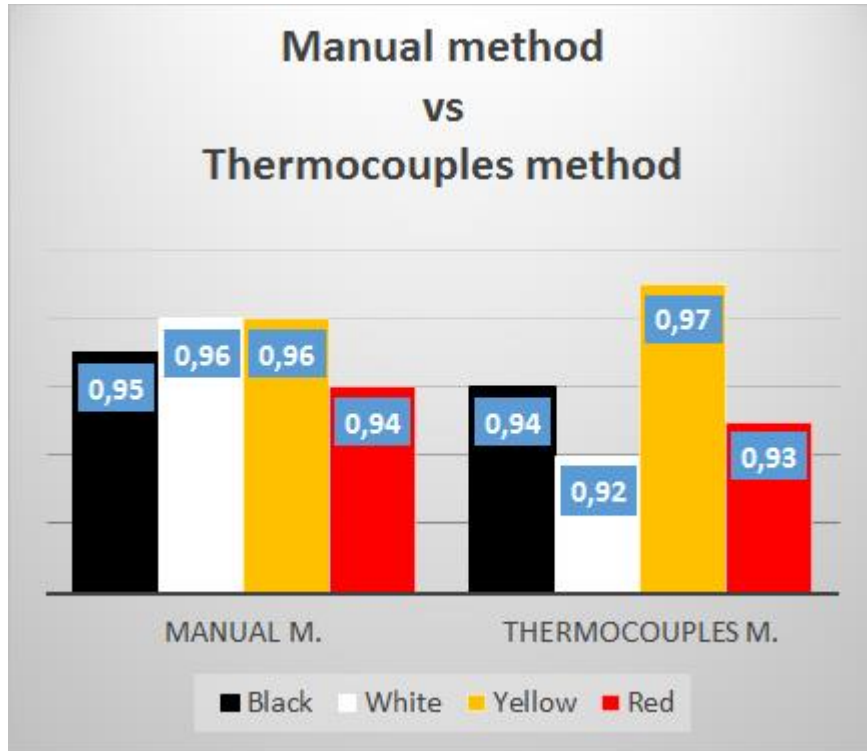


Figure 37: worked out emissivities comparison

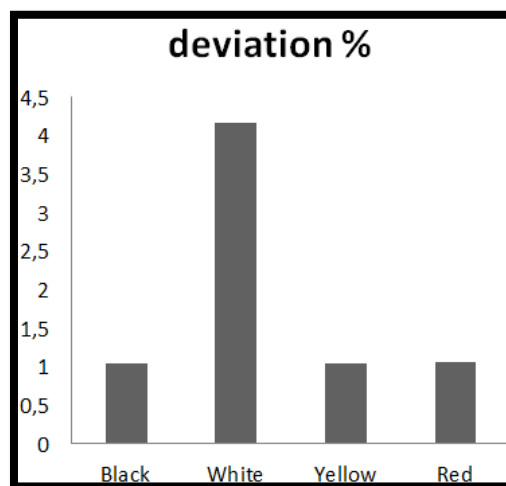


Figure 38: differences in emissivities values

It can be concluded that using the manual or the thermocouples method is a decision to take depending on the particular situation. For instance, in a controlled environment like a laboratory, the manual procedure could be a good solution as well as the

thermocouples one. On the other side, in an external situation it can be more practical to measure the temperature directly with a thermocouple, avoiding using the electrical tape, especially if the surface to investigate is not flat. In addition, a thermocouple can be installed permanently on the surface recording the temperature trend with a data logger, avoiding wastes of time waiting for reaching the same temperature between tape and surface. The important thing is to not forget to reach a 20°C difference in temperature between the sample and the environment, otherwise the thermal camera results could be inaccurate.

3.1.3 Heat release curves

In order to understand the influence of surface colour on the thermal performances of the bricks, and the general thermal behaviour of concrete interblocks, the samples were heated and the left cooling down. Thanks to the thermocouples installed it was possible to record the temperature variation on the surface and the inside of the samples (see § 2.4). Moreover thermal images were taken at regular time intervals.

As mentioned, five thermocouples were installed on the bricks surface and other three inside the bulk (fig. 39).

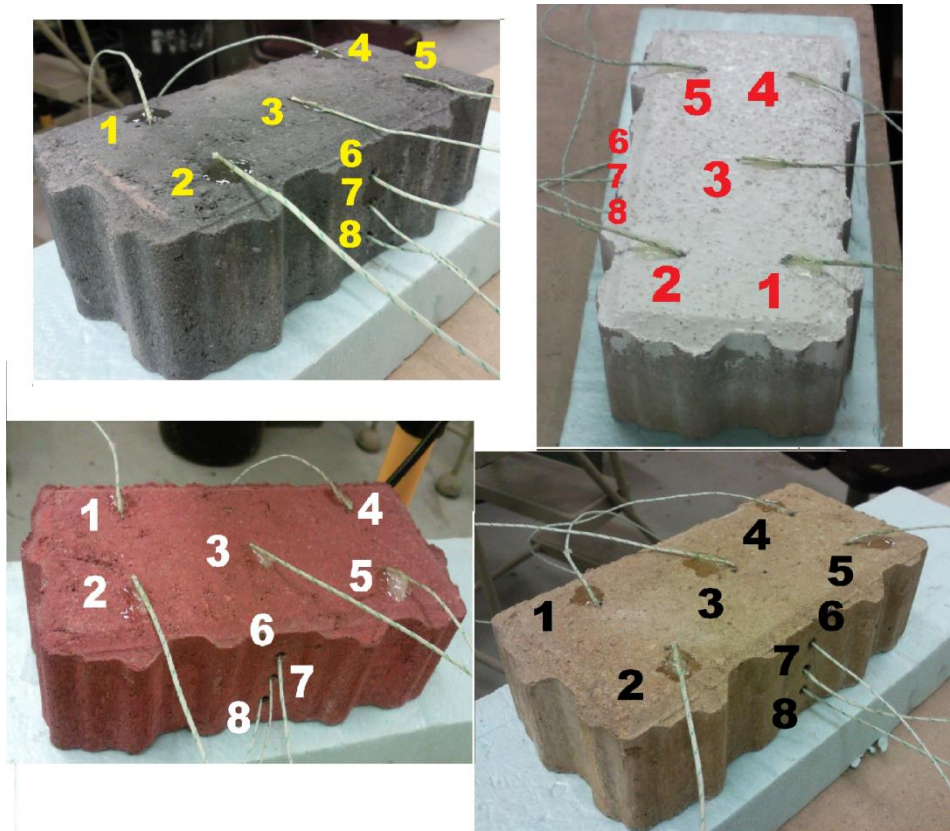


Figure 39: thermocouples positioning

The sensors were connected to a data logger able to record temperature at prearranged time intervals (10 minutes). The testing area was environmentally monitored throughout the experiment for air temperature, reflective temperature and humidity in order to not compromise results; the bricks were elevated off the table surface using blocks made of insulating material. The heat lamps were placed above the samples at a 30° angle. The lights were placed 600 mm above the top of the brick, allowing for localised heating onto the brick. The room temperature remained constant at 23°C.

The bricks were heated for two hours, with thermal photos being taken every half hour plus one shoot before turning on the lamp (fig.40). The data logger recorded the temperature every ten minutes. After two hours, the heat lamps were switched off and removed, and the cooling monitoring process began. Photos and temperatures were collected until two hours from the switch off, and four hours from the begin of testing.

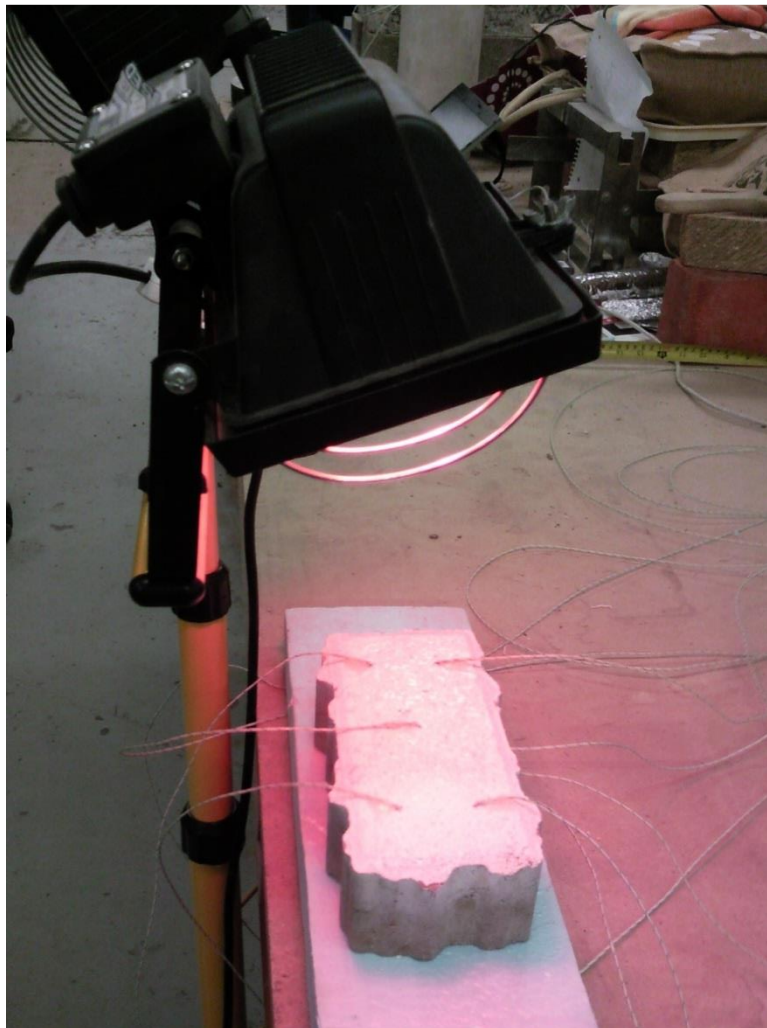


Figure 40: heating up the white sample

Once all experimentations were completed, all data from the thermocouples and the thermal imaging was gathered and placed into excel tables and graphs. Measurements collected are shown below for each brick (tabs.6-7-8-9). After that, different comparisons between the samples thermal performances are illustrated.

- THERMOCOUPLES RESULTS (ALL BRICKS)

BLACK	p1	p2	p3	p4	p5	p6	p7	p8	Av. Surf. T
0'	22.1	21.8	22.5	21.5	22.1	19.9	19.9	19.9	22.0
10'	37.5	35.8	39.1	37.9	37.5	28.5	24.7	22.1	37.6
20'	44.5	42.6	46.4	45.1	44.1	35.6	31.1	27.6	44.5
30'	49.6	47.5	51.5	50.3	48.2	41.5	36.9	33.3	49.4
40'	53.2	51.8	56.0	53.9	51.6	46.3	41.8	38.3	53.3
50'	56.7	54.2	59.9	57.4	55.8	50.5	46.2	42.8	56.8
1h	59.6	57.6	62.4	59.9	57.7	53.9	49.7	46.4	59.5
1h10'	61.8	59.6	63.6	61.4	60.3	56.8	52.7	49.4	61.4
1h20'	63.6	61.4	66.7	63.7	61.8	59.2	55.2	52.0	63.5
1h30'	64.4	63.0	67.7	64.5	63.4	61.1	57.3	54.2	64.6
1h40'	65.5	63.7	68.3	65.2	64.1	61.9	58.0	55.0	65.4
1h50'	66.2	64.7	69.3	66.4	64.7	62.8	59.0	55.9	66.3
2h	67.4	65.8	71.1	67.3	65.5	64.3	60.6	57.5	67.4
2h10'	63.6	62.9	66.3	63.7	62.7	65.5	61.8	58.8	63.9
2h20'	50.7	50.6	51.5	49.7	49.2	57.2	57.7	57.7	50.3
2h30'	46.2	46.2	47.1	45.7	45.3	51.8	52.7	53.3	46.1
2h40'	42.5	42.8	43.7	42.4	42.1	47.5	48.3	48.9	42.7
2h50'	39.4	39.9	40.8	39.4	39.3	43.9	44.5	45.1	39.8
3h	37.4	37.7	38.4	37.1	37.2	40.8	41.4	41.8	37.6
3h10'	35.3	35.6	36.1	35.0	35.1	38.2	38.7	39.1	35.4
3h20'	33.6	33.8	34.2	33.5	33.0	36.0	36.4	36.8	33.6
3h30'	32.0	32.1	32.5	31.8	31.6	34.1	34.4	34.7	32.0
3h40'	30.8	30.8	31.0	30.4	30.3	32.4	32.7	32.9	30.6
3h50'	29.6	29.6	29.8	29.2	29.1	31.0	31.2	31.4	29.5
4h	28.5	28.4	28.6	28.1	28.2	29.7	29.9	30.1	28.4

Table 6: black brick temperatures

WHITE	pt1	pt2	pt3	pt4	pt5	pt6	pt7	pt8	Av.Sup.T
0'	21.0	20.7	20.4	20.4	20.4	20.3	20.3	20.3	20.6
10'	33.4	30.7	34.2	32.2	33.4	23.4	21.1	20.4	32.8
20'	37.8	34.8	38.6	37.3	37.5	27.6	24.5	23.4	37.2
30'	41.3	38.0	42.2	40.6	40.6	31.3	28.0	26.9	40.5
40'	43.5	40.3	44.1	42.7	42.7	34.1	30.9	29.8	42.7
50'	45.8	42.5	46.3	45.1	44.8	36.9	33.8	32.7	44.9
1h	47.5	44.2	48.2	46.8	46.4	39.2	36.2	35.1	46.6
1h10'	48.4	45.8	48.9	48.3	48.3	41.1	38.3	37.3	47.9
1h20'	50.2	46.9	50.8	49.8	48.9	42.7	39.9	38.9	49.3
1h30'	51.2	48.0	52.1	51.0	49.9	44.1	41.3	40.3	50.5
1h40'	51.7	48.8	52.6	51.9	50.6	45.2	42.4	41.5	51.1
1h50'	52.3	49.4	53.8	52.0	51.1	46.0	43.3	42.3	51.7
2h	53.0	50.3	54.4	52.7	51.6	47.0	44.3	43.4	52.4
2h10'	39.5	39.6	40.1	40.2	38.3	43.4	43.8	43.7	39.5
2h20'	37.2	37.5	37.6	37.4	36.7	40.7	41.3	41.5	37.3
2h30'	35.2	35.6	35.5	35.3	34.2	38.0	38.6	38.8	35.1
2h40'	34.2	34.5	34.2	34.0	33.2	36.5	37.1	37.2	34.0
2h50'	32.5	32.8	32.7	32.2	31.7	34.6	35.1	35.2	32.4
3h	31.6	31.8	31.8	31.3	30.9	33.3	33.7	33.8	31.5
3h10'	30.4	30.7	30.5	30.2	29.7	32.0	32.4	32.5	30.3
3h20'	29.3	29.5	29.4	29.0	28.5	30.5	30.9	30.9	29.1
3h30'	28.3	28.5	28.4	28.0	27.6	28.8	29.0	29.8	28.2
3h40'	27.4	27.5	27.5	27.1	26.6	26.9	27.8	28.1	27.2
3h50'	26.5	26.6	26.5	26.1	25.7	26.0	26.7	27.2	26.3
4h	25.5	25.6	25.6	25.3	24.7	24.9	25.4	26.4	25.4

Table 7: white brick temperatures

RED	pt1	pt2	pt3	pt4	pt5	pt6	pt7	pt8	Av.Sur.T
0'	21.3	21.0	20.5	20.3	20.3	20.2	20.3	20.2	20.7
10'	24.5	24.2	23.8	22.6	22.3	21.0	20.6	20.2	23.5
20'	38.3	38.7	39.5	37.3	37.5	27.4	24.0	22.7	38.3
30'	43.8	44.5	45.6	43.4	43.5	33.0	28.9	27.1	44.1
40'	45.3	46.8	47.3	45.4	45.7	35.2	30.5	29.6	45.8
50'	47.5	48.3	49.2	47.0	47.4	37.9	33.7	32.0	47.9
1h	50.2	50.8	51.7	50.5	49.8	41.7	37.7	36.0	50.6
1h10'	52.6	53.2	54.0	53.4	51.3	45.0	41.1	39.5	52.9
1h20'	54.9	55.2	55.7	54.3	53.9	47.9	44.1	42.5	54.8
1h30'	56.7	56.0	57.7	57.4	54.4	50.2	46.5	45.0	56.4
1h40'	58.1	57.6	58.7	58.6	56.1	52.1	48.6	47.1	57.8
1h50'	59.6	58.7	60.3	59.8	57.0	53.8	50.3	48.9	59.1
2h	61.3	60.3	60.2	62.2	58.6	56.5	53.1	51.8	60.5
2h10'	55.8	54.7	54.9	56.0	52.1	57.5	54.2	52.8	54.7
2h20'	44.5	42.5	44.9	44.6	41.9	50.5	51.2	51.5	43.7
2h30'	40.9	39.7	41.0	40.7	38.9	46.1	47.1	47.5	40.2
2h40'	38.7	37.7	38.0	38.5	37.1	42.9	43.8	44.2	38.0
2h50'	36.7	35.8	36.6	36.4	35.1	40.4	41.2	41.5	36.1
3h	34.6	33.9	34.7	34.5	33.2	37.7	38.5	38.7	34.2
3h10'	33.3	32.8	33.5	33.0	32.1	35.9	36.5	36.7	33.0
3h20'	32.0	31.5	32.0	31.5	30.6	34.1	34.7	34.8	31.5
3h30'	30.7	30.2	30.4	30.3	29.8	32.5	33.0	33.1	30.3
3h40'	29.8	29.5	29.7	29.3	28.9	31.3	31.7	31.8	29.4
3h50'	29.0	28.5	28.7	28.3	27.9	30.1	30.5	30.5	28.5
4h	27.6	27.3	27.3	27.0	26.6	28.3	28.6	28.6	27.1

Table 8: red brick temperatures

YELLOW	pt1	pt2	pt3	pt4	pt5	pt6	pt7	pt8	Av.T.Surf
0'	21.5	21.3	21	21	21	20.9	20.9	20.9	21.1
10'	24	23.6	23.1	21.9	22.4	21.4	21	20.9	23
20'	37.5	38.7	37.8	35.3	37.4	27.3	24.4	22.9	37.4
30'	40.3	39.6	41.6	38.4	40.2	29.9	25.8	24.3	40
40'	43.5	42.6	44.7	41.3	42.4	32.9	29.4	27.4	42.9
50'	47.3	46.6	48.6	45.2	46.5	37.9	34.3	32.2	46.8
1h	50.8	49.1	51.8	48.7	49.1	41.9	38.4	36.4	49.9
1h10'	53.5	51.7	54.6	51.1	51.7	45.5	42.2	40.3	52.5
1h20'	55.9	53.2	57.5	53.8	53.7	48.5	45.2	43.4	54.8
1h30'	56.9	55.3	58.4	54.9	55.4	50.7	47.5	45.7	56.2
1h40'	59.1	55.7	61.1	57.2	56.5	52.7	49.6	47.8	57.9
1h50'	59.5	57.3	61.4	57.8	57.8	54.3	51.3	49.6	58.8
2h	60.8	59.6	63.3	59.7	59.5	56.6	53.6	52	60.6
2h10'	55.7	53.4	58.3	56.3	53.5	58	55	53.4	55.4
2h20'	45.1	43.3	46.1	45.5	43.9	50.8	51.2	51.3	44.8
2h30'	42.1	40.6	43.4	42.2	40.3	46.7	47.3	47.7	41.7
2h40'	40	38.5	40.2	39.7	38.3	43.6	44.1	44.5	39.3
2h50'	37.5	36	38	37.1	36.2	40.8	41.3	41.6	37
3h	35.7	34.4	36.3	35.6	34.6	38.6	39.1	39.3	35.3
3h10'	34.2	33.2	34.6	34	33.2	36.6	37	37.2	33.8
3h20'	32.8	32.1	32.9	32.5	32	34.8	35.2	35.4	32.5
3h30'	31.4	30.8	31.8	31.1	30.8	33.2	33.5	33.7	31.2
3h40'	30.3	29.5	30.4	29.9	29.4	31.7	31.9	32	29.9
3h50'	29.4	28.9	29.6	29.3	28.9	30.8	31	31.2	29.2
4h	27.8	27.3	27.8	27.4	27.3	28.6	28.8	28.9	27.5

Table 9: yellow brick temperatures

- BRICKS SURFACE POINTS COMPARISON

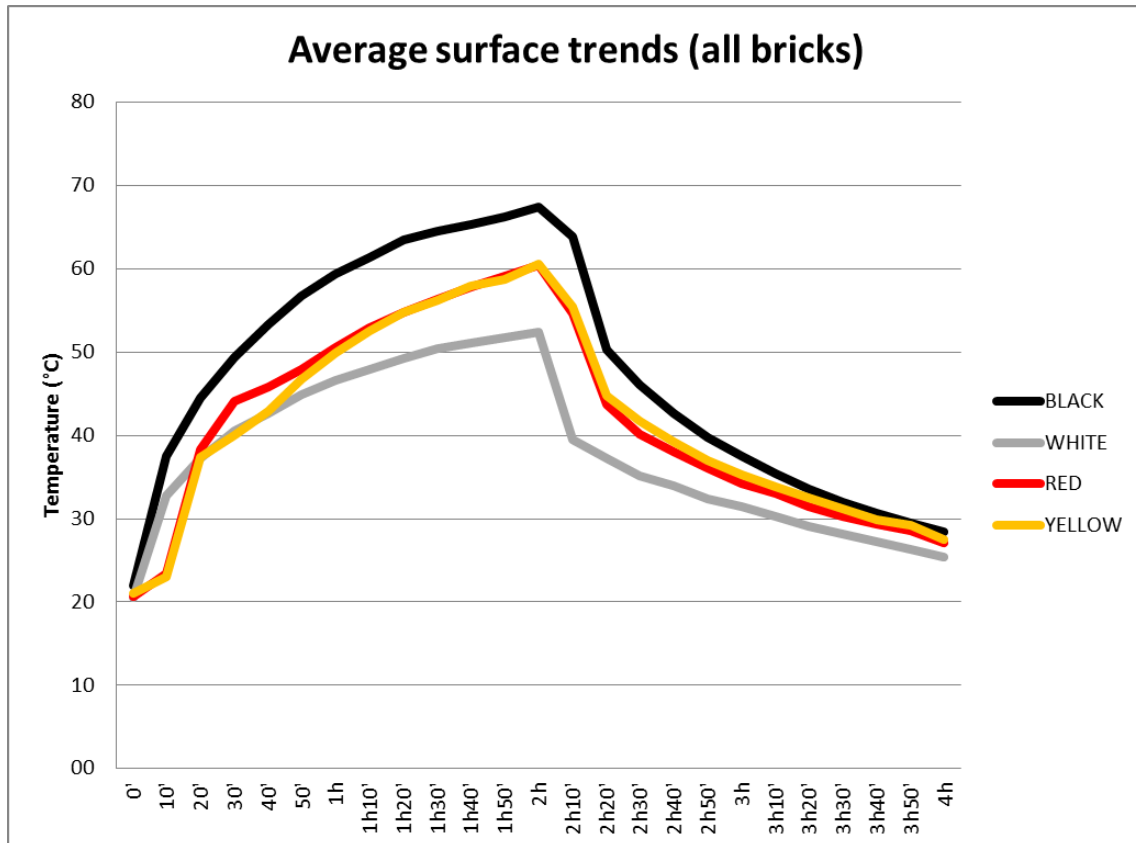


Figure 41: average surface temperature for all bricks

Analysing the surface thermocouples measurements (fig.41) it is clearly visible that the black sample absorbed the greatest amount of heat, with a peak value of 67.4°C. This fact confirms how the darkest colours affects the thermal behaviour, determining how much energy will be stored and how much will be reflected. It is also clear that the white shiny paint on the white brick has a good cooling effect, reflecting a significant amount of heat. In fact, it reaches a peak of 52.4°C, a difference of 15°C with the black (22.3%). The red sample peak is 60.5°C, with a difference of 6.9°C (10.2%), the yellow is 60.6°C, with a difference of 6.8°C (10.1%).

The cooling part of the curves presents two distinct phases. The first one (immediately after turning off the lamp) shows a quick heat loss, due to the first layer of material cooling down. In this step, the samples lose, in 20 minutes, 17.1°C (25.4%) for the black, 16.8°C (27.8%) for the red, 15.8°C (26.1%) for the yellow and 12.9°C (24.6%) for the white. After this, a slower heat release in all the bricks is recorded, due to the progressive cooling down of the internal layers. It can be noticed how the yellow specimen and the red one show a pretty identical behaviour. Practically the intermediate colours do not significantly affect the thermal behaviour.

- BRICKS INTERNAL POINTS COMPARISON

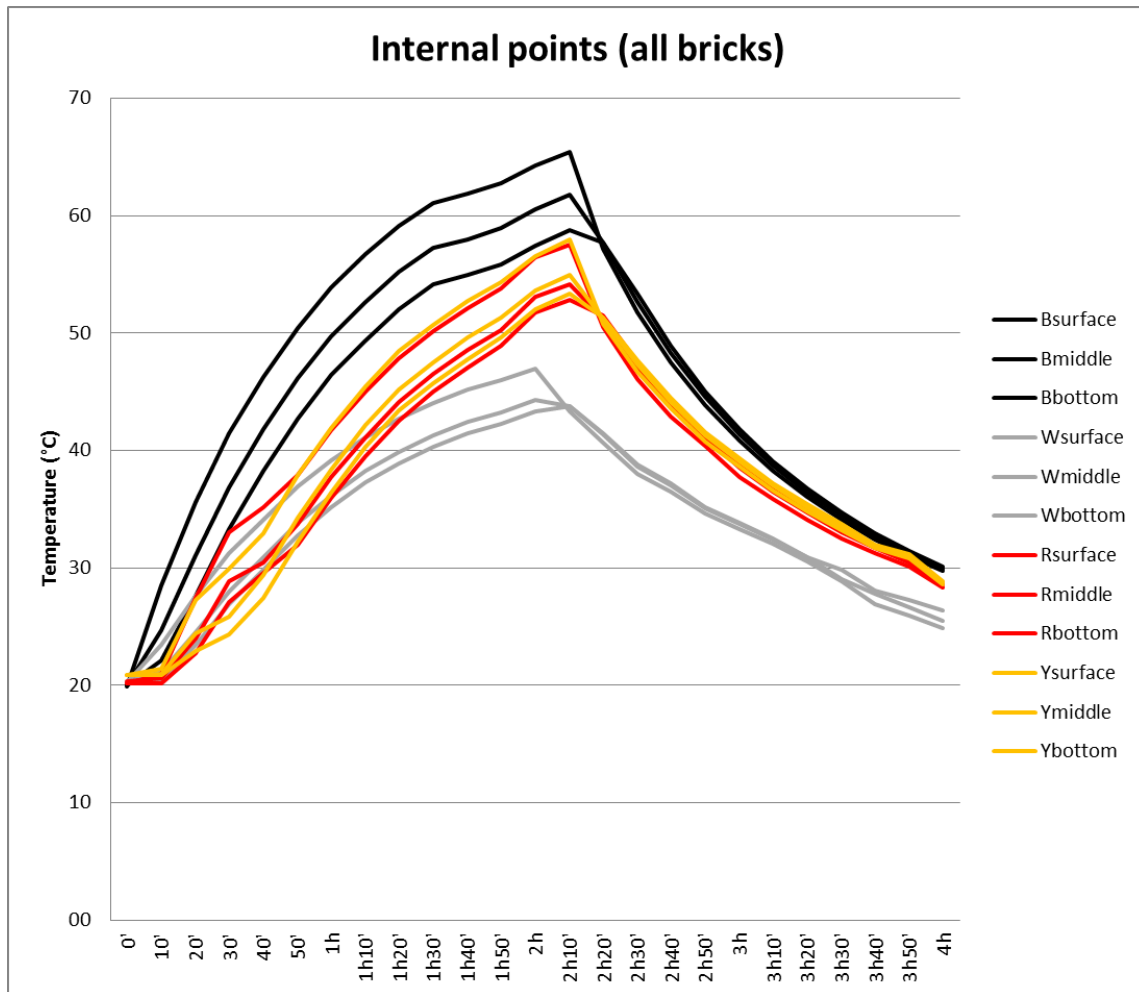


Figure 42: internal temperatures for all bricks

Looking at all the internal points temperature trends together (fig.42) it can be seen that the trends shape is similar for all the bricks, as the internal material is the same. The black one is the warmest, the white one the coolest. The red and yellow bricks have almost the same performance. It can be deduced that the black sample has the worst thermal behaviour, probably due to the high light absorbing capabilities of black colour. This means that the underlying layers would have a larger amount of heat received from the surface. Although choosing the yellow one or the red one could be the same, choosing the white one would give the best benefits.

• SURFACE THERMOCOUPLES POINTS vs THERMAL CAMERA DATA

BLACK	Tcouples	Tcamera	\Delta T	WHITE	Tcouples	Tcamera	\Delta T
0'	22.0	29.5	7.5	0'	20.6	29.1	8.5
30'	49.4	51.7	2.3	30'	40.5	39.0	1.5
1h	59.5	60.4	0.9	1h	46.6	45.6	1.0
1h30'	64.6	65.7	1.1	1h30'	50.5	49.7	0.8
2h	67.4	66.1	1.3	2h	52.4	52.3	0.1
2h30'	46.1	44.7	1.4	2h30'	35.1	37.2	2.1
3h	37.6	36.9	0.7	3h	31.5	32.3	0.8
3h30'	32.0	31.9	0.1	3h30'	28.2	28.9	0.7
4h	28.4	28.8	0.4	4h	25.4	26.9	1.6
RED	Tcouples	Tcamera	\Delta T	YELLOW	Tcouples	Tcamera	\Delta T
0'	20.7	28.5	7.8	0'	21.1	28.5	7.4
30'	44.1	45.1	1.0	30'	40.0	42.6	2.6
1h	50.6	52.4	1.8	1h	49.9	51.0	1.1
1h30'	56.4	58.8	2.4	1h30'	56.2	57.7	1.5
2h	60.5	58.9	1.6	2h	60.6	59.2	1.4
2h30'	40.2	40.8	0.6	2h30'	41.7	40.7	1.0
3h	34.2	34.7	0.5	3h	35.3	34.7	0.6
3h30'	30.3	30.9	0.6	3h30'	31.2	30.4	0.8
4h	27.1	28.2	1.1	4h	27.5	28.3	0.8

Table 10: thermocouples and thermal camera temperatures

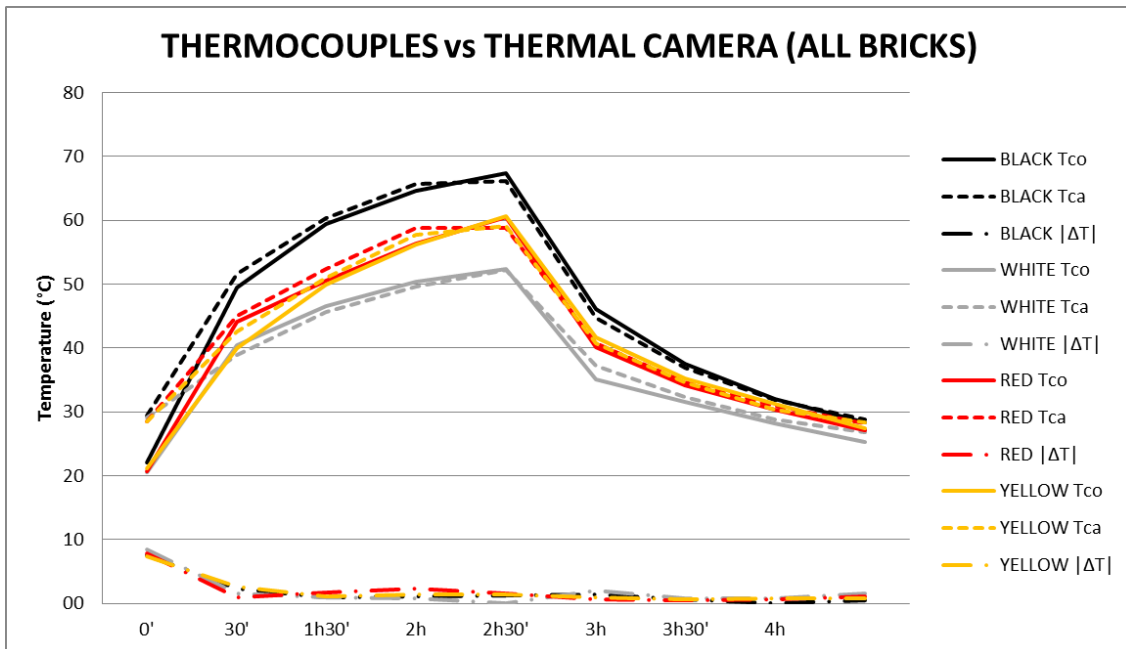


Figure 43: thermocouples and thermal camera readings comparison

The comparison between thermocouples and thermal camera data (fig.43) showed a discrepancy in the temperature trends. This fact is probably caused by the part of light

coming from the lamp and directly reflected away from the surface of the specimens. This disturbance cannot be compensated by the apparent temperature, which is calculated when the infrared lamp is turned off. The temperature difference ranges between 0.1 and 7.5°C for the black brick, 0.1 and 8.5 °C for the white one, 0.5 and 7.8°C for the red one, 0.6 and 7.4°C for the yellow one. It can be noticed how the difference is larger during the first 30 minutes, when the samples are relatively cold. In fact, the thermal camera's manual specifies that a 20°C difference in temperature between the environment and the specimen is necessary, value reached for each sample after half hour of heating. It can be seen how the ΔT decreases when this specification is respected. Excluding the first 30 minutes, the difference in all the samples ranges between 2.4°C and 0.1°C.

3.2 Outside investigation

The main purpose of this research is to investigate the thermal performances of different paved surfaces to assess how they behave in relation to the Urban Heat Island phenomenon. With this perspective four different paved urban surfaces were chosen, and their albedo and emissivity parameters were measured. Furthermore, a typical summer day was chosen, and the daily temperatures of surfaces and atmosphere were measured. The original idea was to set the data collected in a simulative software in order to create improving urban scenarios in terms of UHI mitigation. Unfortunately, it was not possible to modelling the scenario to reproduce the actual situation. This will be discussed in § 4.1.2.

The selected area is located in the Nottingham Trent University City Centre campus, near the Maudslay building (fig.44). The surface investigated were:

- MAUDSLAY LABORATORY'S CAR PARKING → AGED DENSE ASPHALT
- GOLDSMITH ROAD → GENERIC DENSE ASPHALT
- SIDEWALK → CONCRETE BRICKS
- SIDEWALK → GRANITE BLOCK ELEMENTS (fig.45)



Figure 44: investigated area [40]

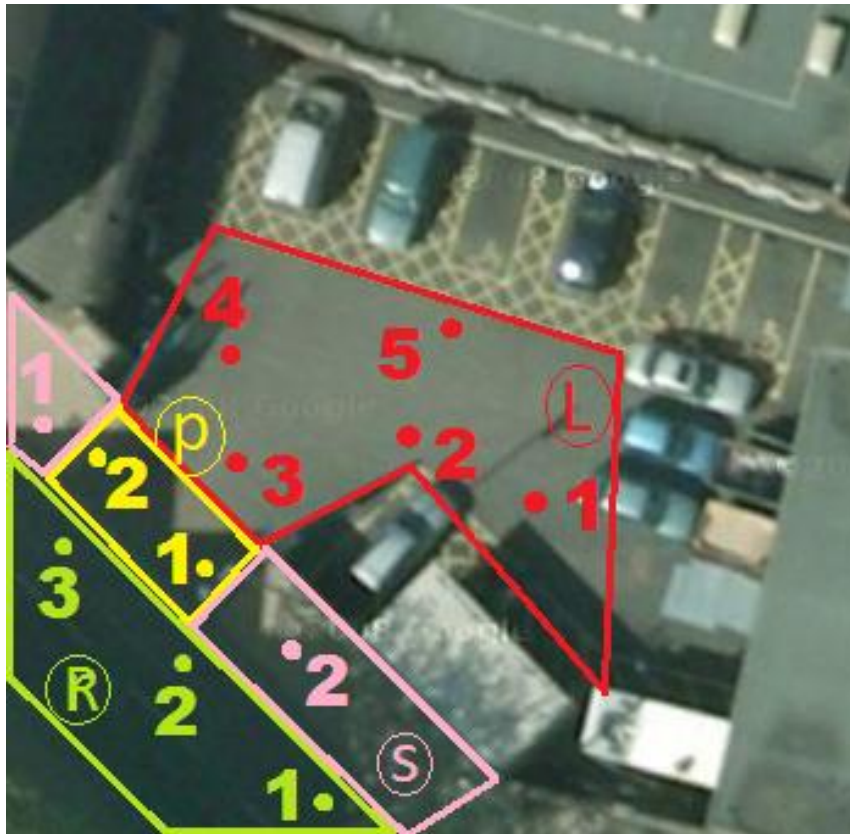


Figure 45: selected surfaces

Surfaces:

- RED AREA “L”: Maudslay Lab car parking → asphalt
- GREEN AREA “R”: Goldsmith Street → asphalt
- YELLOW AREA “p”: sidewalk → concrete bricks
- PINK AREA “s”: sidewalk → granite block elements (fig.46)

3.2.1 Emissivity evaluation

The equipment employed was composed by the FLIR B200 thermal camera, the Extech Hygro-Thermometer Humidity Alert, a portable thermocouple and a black electrical tape. Emissivity measurements were performed in 6 different points (fig.47):

- Points 1,2,3 for the asphalt Maudslay laboratory car parking
- Point 4 for the concrete bricks sidewalk
- Point 5 for the granite sidewalk
- Point 6 for the asphalt Goldsmith Street



Figure 46: investigated surfaces

The FLIR B200 manual's procedure was used for points 1,2,3. In order to check if the 20°C difference gap between surface and atmosphere was verified, surfaces temperature was measured with the thermocouple and the atmospheric temperature with the weather station. Thermocouples procedure was used for points 4,5,6 because it was not possible to leave the piece of black tape on the surfaces, due to the vehicles and the pedestrians transit. All the measurements were performed on the 16th of July 2014. The weather was sunny with a clear sky all day long.



Figure 47: emissivity measurement points

- MAUDSLAY BUILDING CAR PARKING

Following are the thermographic photos taken for the points 1,2 and 3 (figg.48,49,50), with the resulted emissivity values worked out by FLIR QUICK REPORTER software analysis.

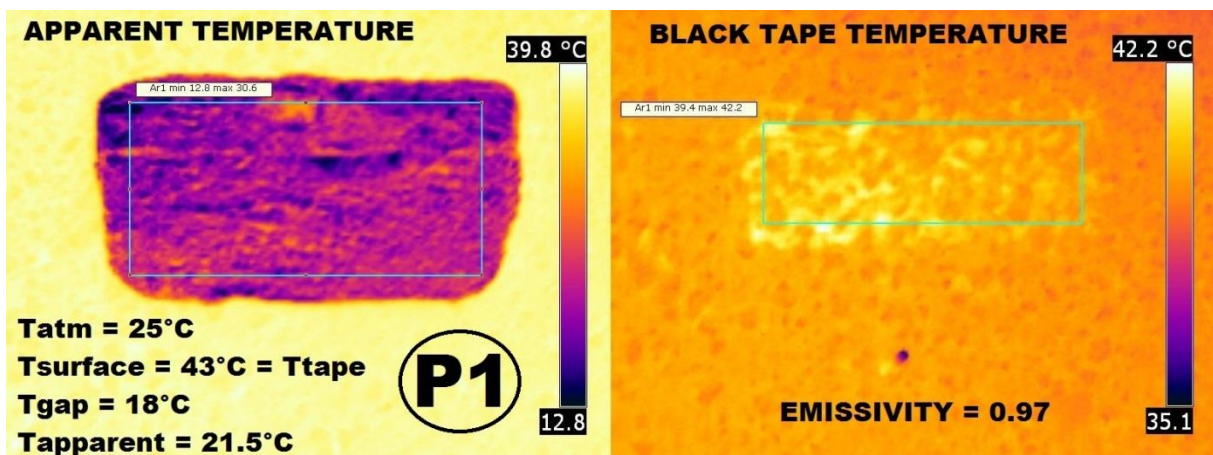


Figure 48: point 1

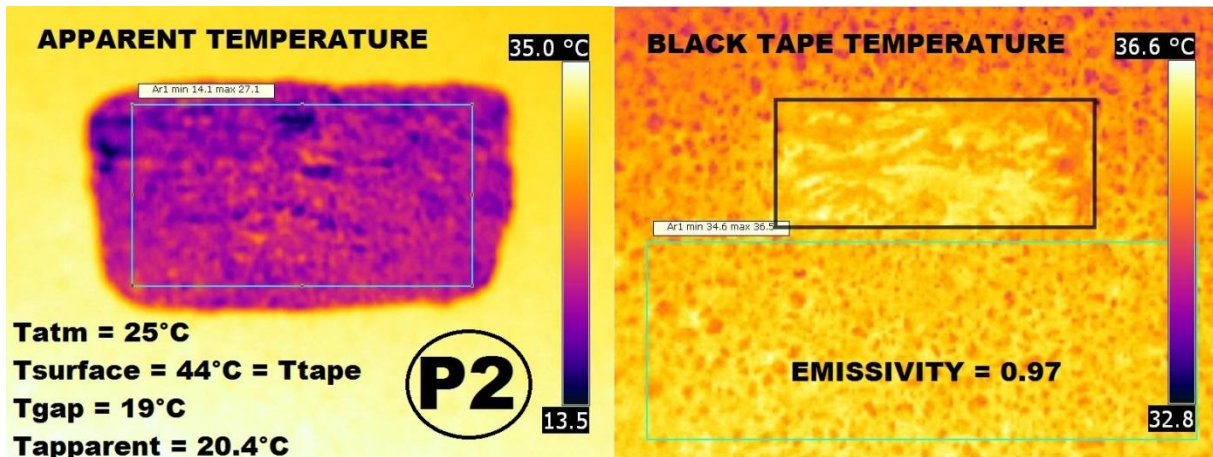


Figure 49: point 2

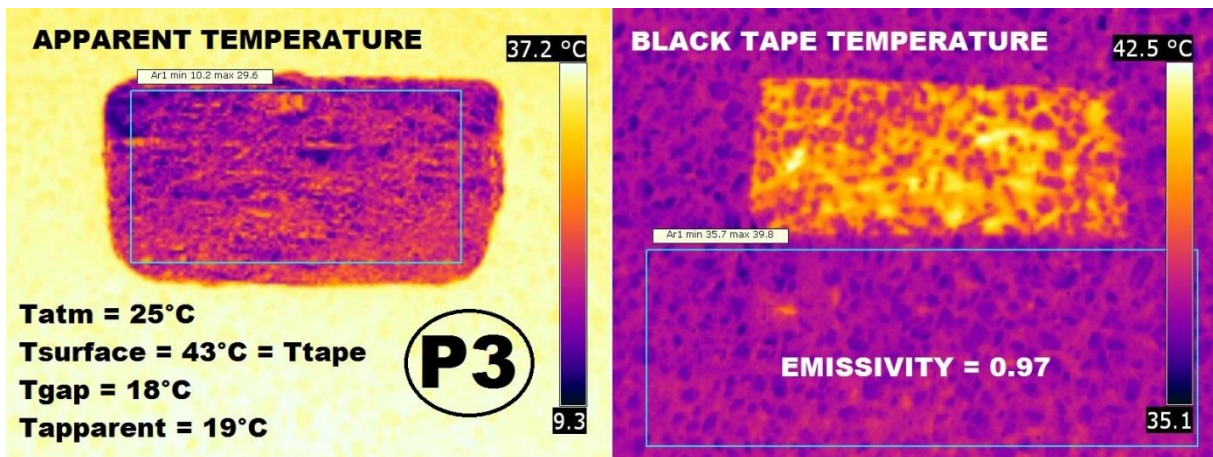


Figure 50: point 3

It can be seen how the worked out emissivities are the same for all measurements points, giving a validation of the accuracy of the value.

As expected, the emissivity of the asphalt is high, a typical value for an asphalt (see § 1.5).

- SIDEWALK (CONCRETE AND GRANITE)

Following are the thermographic photos taken for the points 4 and 5 (figg.51,52), with the resulted emissivity values worked out by FLIR QUICK REPORTER software analysis.

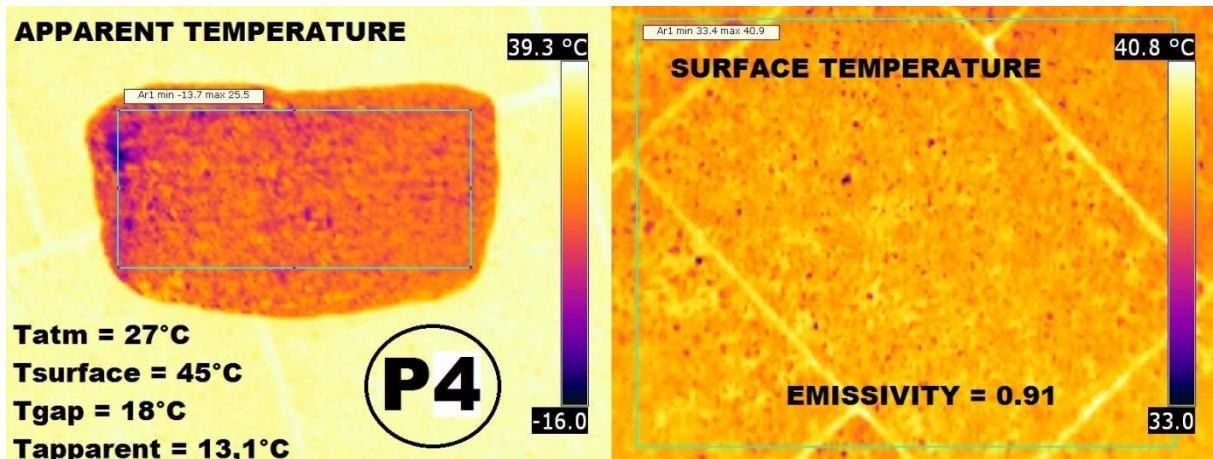


Figure 51: point 4

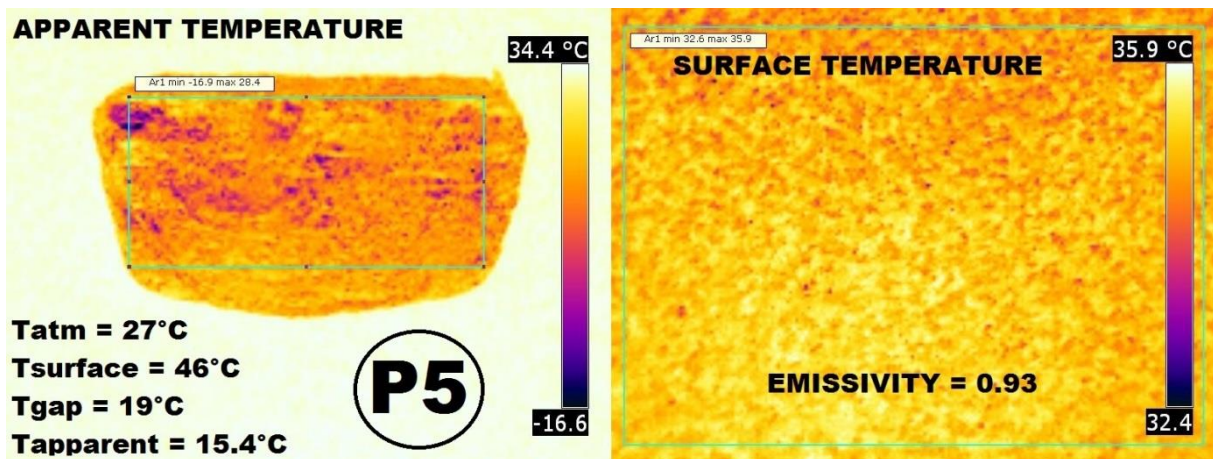


Figure 52: point 5

The emissivities are lower than those found at Maudslay car parking, due to the difference in component materials. In fact, asphalt is a greater heat emitter compared to concrete and granite. The values are consistent with materials features in literature (§ 1.5).

- GOLDSMITH ROAD

Following are the thermographic photos taken for the point 6 (fig.53), with the resulted emissivity values worked out by FLIR QUICK REPORTER software analysis.

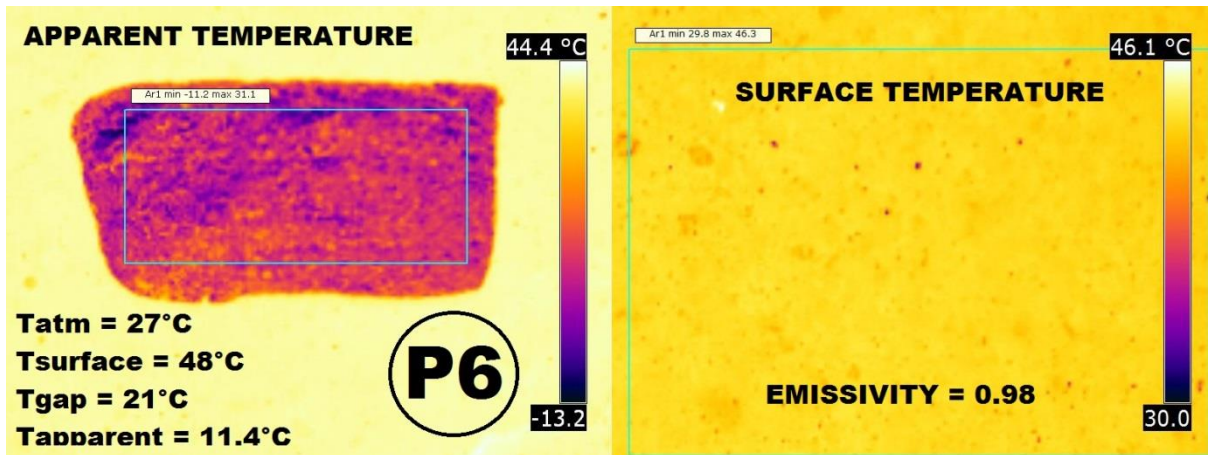


Figure 53: point 6

Also this emissivity is consistent with typical values for asphalts.

A summary of the measured emissivities for the different points is given in tab.11.

POINTS	T atm [°C]	T surface [°C]	T tape [°C]	T rifl app [°C]	Emissivity
Point1	25	43	43	21.5	0.97
Point2	25	44	44	20.4	0.97
Point3	25	43	43	19	0.97
Point4	27	45	-	13.1	0.91
Point5	27	46	-	15.4	0.93
Point6	27	48	-	11.4	0.98

Table 11: emissivities data

3.2.2 Albedo measurements

The SPN1 Sunshine Pyranometer was used to get the albedo parameter of the investigated surfaces. The standard ASTM E1918-06 was followed (see § 2.3). Regarding the measurements performed at the Maudslay laboratory's car parking, in addition to the simple albedo value of the pavement, different experimentations related to the impact of some external factors were carried out. In particular, the influence of parking painting lines and the effects of height sonde were assessed. This last factor was investigated in two weather conditions: clear sky and haze. Unfortunately, the albedo parameters of the sidewalk (both concrete and granite) and Goldsmith Road could not be measured, due to technical difficulties on placing the instrument in trafficked areas.

- MAUDSLAY BUILDING CAR PARKING

The albedo investigations were performed the 21st of May, the 6th of June and the 2nd of July 2014 (fig.54). The albedo value of the parking was determined on a flat portion of

asphalt pavement far away from painted lines, objects, shadows or whatever could affect the readings. The pyranometer height was set at 50 cm. Shown below the data collected and the average value (tab.12).



Figure 54: albedo measurement

Time	Incoming	Reflected	Albedo
09:58	711.0	151.0	0.212
10:01	708.0	140.5	0.198
10:04	693.0	140.6	0.203
10:10	723.5	148.0	0.205
10:13	732.3	153.7	0.210
10:15	730.0	154.3	0.211
10:31	794.0	166.0	0.209
10:34	776.0	157.0	0.202
10:37	797.0	162.4	0.204
10:40	788.0	162.0	0.206
10:46	781.4	163.0	0.209
10:52	775.2	161.0	0.208
11:00	796.8	168.2	0.211
11:02	790.0	162.0	0.205
11:05	793.0	165.0	0.208
11:09	798.0	164.7	0.206

11:15	829.0	180.5	0.218
11:19	825.0	176.0	0.213
11:22	829.0	173.7	0.210
11:26	830.0	172.4	0.208
11:30	835.8	178.0	0.213
11:33	830.0	174.0	0.210
11:36	837.0	174.0	0.208
11:40	829.0	167.0	0.201
11:43	825.0	168.0	0.204
11:46	858.0	171.0	0.199
11:49	849.0	173.0	0.204
11:52	845.0	177.0	0.209
11:56	876.0	175.7	0.201
11:59	859.0	167.0	0.194
12:02	869.0	170.0	0.196
average			0.206

Table 12: car parking albedo

The average value was 0.206, a typical albedo value for an aged asphalt.

The influence of parking painted lines on albedo was assessed changing the horizontal distance between the sonde and the lines, respectively 2 m, 1 m, 0.2 m and 0 m (directly above the lines) (figg.55,56).



Figure 55: distances from the parking lines [40]

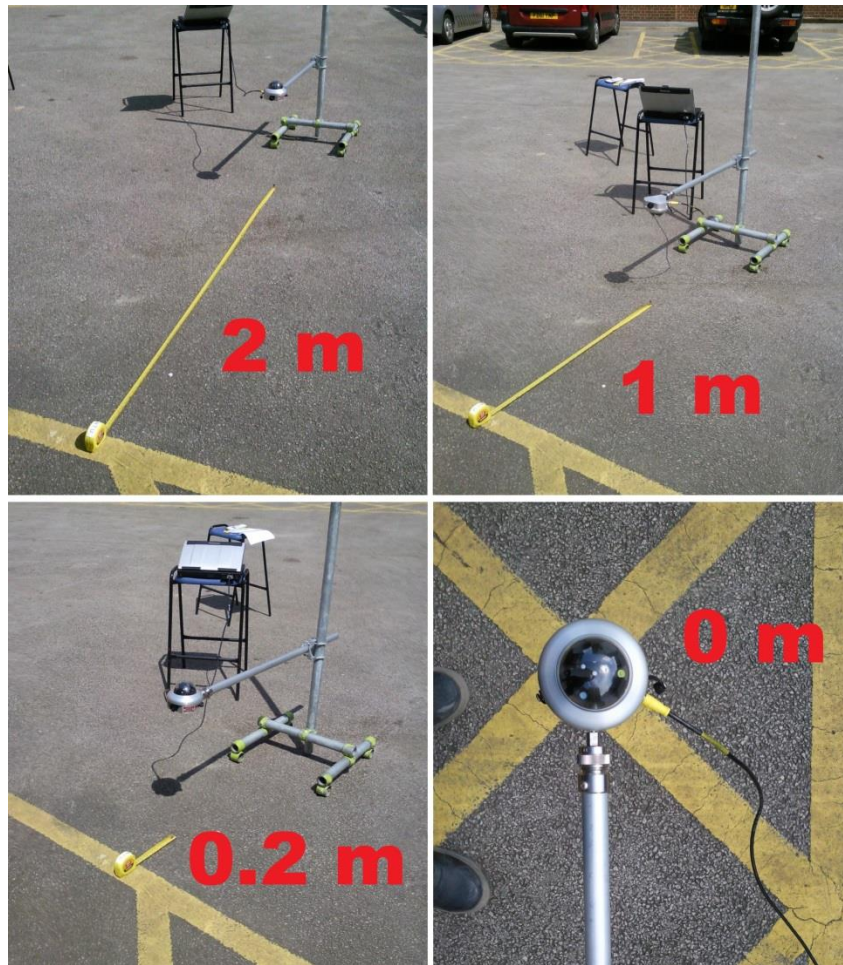


Figure 56: distances from park lines

The data collected and the average values are shown below (tabs.13-14-15-16).

It can be noticed how the yellow lines increase albedo significantly. The parameter range from 0.198 ($D = 2$ m) to 0.227 ($D = 0$ m), with a difference of 0.029 (12.8%). Paint acts like a shield against sunlight, enhancing the part of energy reflected. It is obvious that this solution cannot be employed on large urban surfaces (e.g. a whole car parking or a road), but covering small surfaces like sidewalks, pedestrian crosses, parking lots and similar places, can be enough to affect the overall albedo value of an urban area.

1: $D = 2$ m			
Time	Incoming	Reflected	Albedo
11.25	783	175	0.223
11.31	852	169	0.198
11.33	843	160	0.19
11.36	842	168	0.2

11.43	823	160	0.194
11.45	820	162	0.197
11.50	790	152	0.192
11.54	797	142	0.178
12.03	831.4	169.4	0.204
12.05	775	155	0.2
12.07	720	146	0.203
average			0.198

Table 13: D = 2 m

2: D = 1 m

Time	Incoming	Reflected	Albedo
12.21	788	155	0.197
12.23	856	168	0.196
12.35	800	158	0.197
average			0.197

Table 14: D = 1 m

3: D = 0,2 m

Time	Incoming	Reflected	Albedo
12.55	848	182	0.215
12.57	872	183.7	0.211
13.01	880	181	0.206
13.05	850	173	0.203
13.08	780	160	0.205
13.10	830	172	0.207
average			0.208

Table 15: D = 0.2 m

4: D = 0

Time	Incoming	Reflected	Albedo
13.19	950	220	0.231
13.24	945	212	0.224
13.26	920	211	0.229
13.29	938	209	0.223
average			0.227

Table 16: D = 0 m

The influence of the height of the pyranometer sonde was assessed changing the height in two different weather conditions: clear sky (tab.17) and haze (tab.18).

h=50cm			
Time	Incoming	Reflected	Albedo
10:30	734	143.5	0.195
10:33	744	146	0.196
10:35	747	147	0.197
average			0.196

h=40cm			
Time	Incoming	Reflected	Albedo
11:05	758	158	0.208
11:09	752	154	0.205
11:11	752	151	0.201
average			0.205

h=30cm			
Time	Incoming	Reflected	Albedo
11:15	743	150	0.202
11:18	750	151	0.203
11:21	753	155	0.206
average			0.204

h=20cm			
Time	Incoming	Reflected	Albedo
11:28	755	154	0.204
11:31	800	165	0.206
11:48	760	160	0.21
average			0.207

Table 17: height influence with clear sky on albedo

h=60cm			
time	upward	downward	albedo
14:06	550	86	0.156
14:08	500	79	0.158
14:12	511	80	0.156
average			0.157

h=45cm			
time	upward	downward	albedo
14:16	428	72	0.168
14:19	425	68	0.16
14:21	405	64	0.158
average			0.162

h=30cm			
time	upward	downward	albedo
14:25	392	69	0.176
14:32	382	71	0.186
14:34	402	72	0.179
average			0.180

h=15cm			
time	upward	downward	albedo
14:51	282	52	0.184
15:03	256	47	0.184
15:07	265	50	0.188
average			0.185

Table 18: height influence with haze on albedo

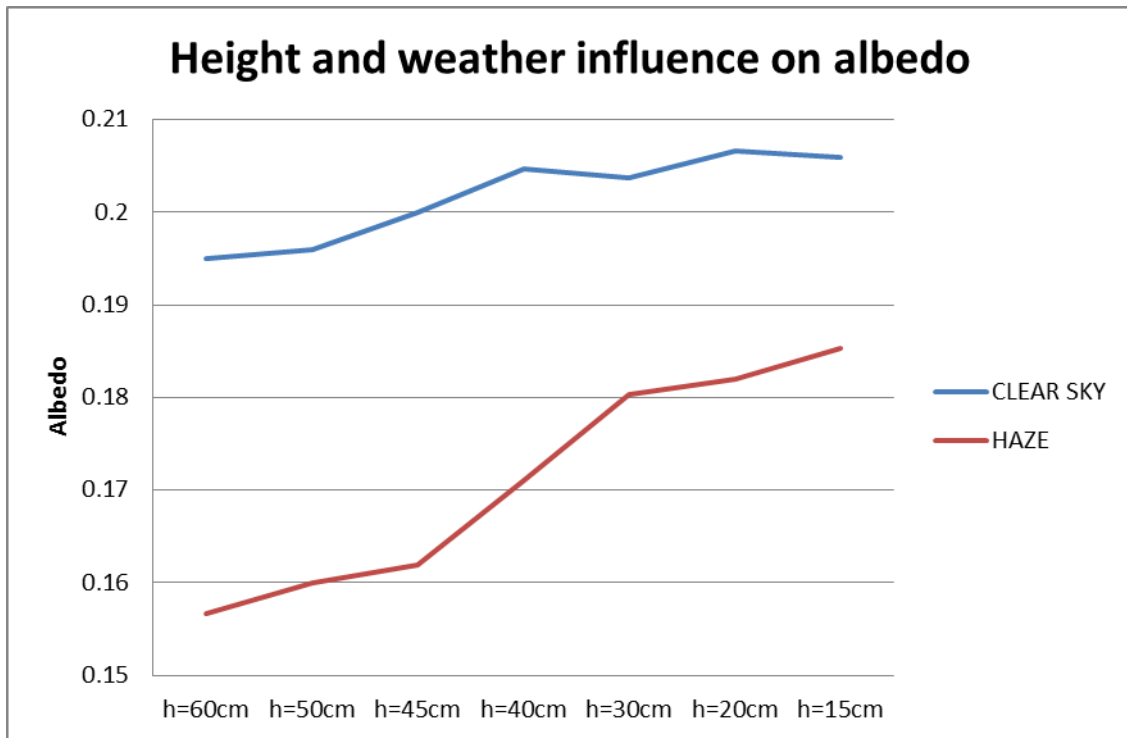


Figure 57: influence of height and haze

From the graph in fig.57 it can be deduced that weather conditions can influence albedo measurement, especially when the sonde is relatively far from the surface. However, the measurements performed with haze condition provided albedo values quite different from the average value previously found (≈ 0.21). This fact is probably due to the haze placed between the pyranometer and the pavement which caused a disturbance in readings. With clear sky, the readings provided results relatively reliable, considering the fact that just 3 readings were performed for each height, whilst the average albedo is calculated on 31 readings (for this reason average albedo value of 0.21 is considered correct).

3.2.3 Temperature readings

Temperature readings were collected in order to calibrate the simulative model in the software. For this reason, on the 21st of July 2014, an all-day measurements campaign was performed. The thermal camera was used on the 4 areas previously selected (fig.58):

- RED AREA “L”: Maudslay lab car parking → asphalt
- GREEN AREA “R”: Goldsmith Road → asphalt
- YELLOW AREA “p”: sidewalk → concrete bricks
- PINK AREA “s”: sidewalk → granite block elements

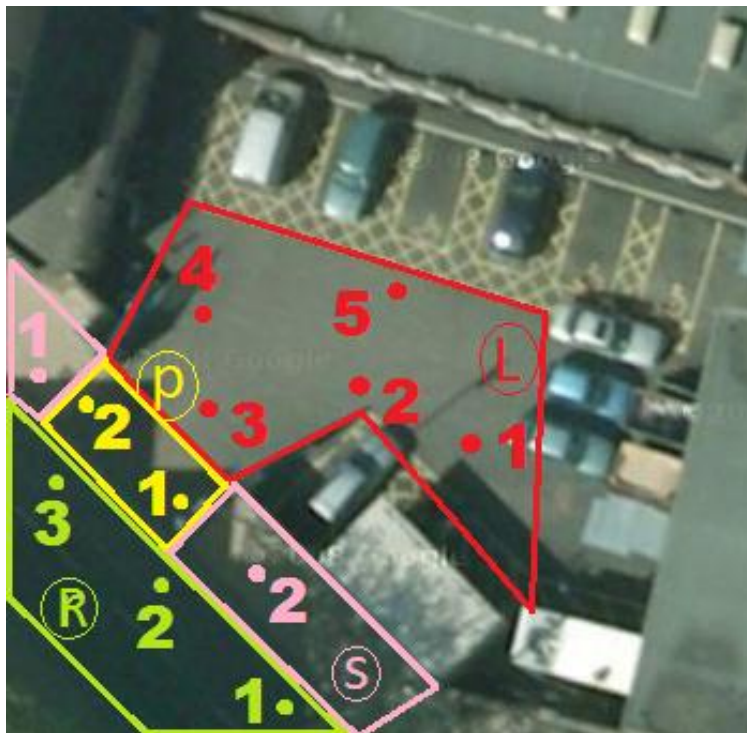


Figure 58 [40]

The measures collected with the thermal camera are shown below (tab.19).

h 9.00	L [°C]	p [°C]	s [°C]	R [°C]
pt1	22.8	23.4	24.1	24.1
pt2	24.9	25.1	22.5	24.8
pt3	24.9	-	-	26
pt4	24.9	-	-	-
pt5	24.8	-	-	-
average	24.5	24.3	23.3	25.0
h 11.00	L [°C]	p [°C]	s [°C]	R [°C]
pt1	27	26.8	25.2	27.4
pt2	27.7	28.2	26.7	28.5
pt3	27.5	-	-	29.3

pt4	28	-	-	-
pt5	27.9	-	-	-
average	27.6	27.5	26.0	28.4
h 13.00	L [°C]	p [°C]	s [°C]	R [°C]
pt1	39	35.7	32.8	35.4
pt2	39.3	36.5	34.8	35.6
pt3	38.9	-	-	39.2
pt4	38.3	-	-	-
pt5	39.9	-	-	-
average	39.1	36.1	33.8	36.7
h 15.00	L [°C]	p [°C]	s [°C]	R [°C]
pt1	46.3	39.9	43.6	46.7
pt2	46.5	44.7	42	37.2
pt3	46.3	-	-	46.6
pt4	46.1	-	-	-
pt5	47.3	-	-	-
average	46.5	42.3	42.8	43.5

Table 19: surfaces temperatures

Atmosphere temperature and humidity were measured with the portable weather station, placed at 1 m from the ground (tab.20).

Time	Air T [°C]	Hum. %
09:00	22.1	63
11:00	25.7	47
13:00	30.1	32
15:00	28.6	34

Table 20: atmosphere temperatures and humidity

CHAPTER 4:

CASE STUDY MODELLING

The last step of this research is the simulative phase. The aim is to assess the thermal behaviour of the investigated materials figuring out how they could be employed to mitigate the UHI. In order to do that, a freeware software called “*ENVI-met*” has been used. The software is able to reproduce the microclimatic dynamics of urban areas.

4.1 ENVI-met software (version 3.1)

ENVI-met is a three-dimensional microclimate model designed to simulate the surface-plant-air interactions in urban environment. Typical areas of application are Architecture, Landscape Architecture, Building Design or Environmental Planning. The software includes the simulation of:

- Flow around and between buildings
- Exchange processes at the ground surface and at building walls
- Building physics
- Impact of vegetation of the local microclimate
- Bioclimatology
- Pollutant dispersion [41]

The software can to simulate urban micro-areas with a spatial resolution ranging between 0.5 and 10 meters, with a time period varying between 24 and 48 hours and a maximum time-step of 10 seconds. ENVI-met implements Computational Fluid Dynamics Models (CFD).

The effectiveness of this software have been confirmed by different papers and research conducted in this field of studies [42-43-44-45-46-47].

4.1.1 Software architecture

The software structure is organized in 4 different interfaces (fig.59):

- INPUT
- SIMULATION
- OUTPUT
- DATA MANAGEMENT (fig.54)

The INPUT interface is formed of 3 main files: the AREA file, the CONFIGURATION file and the DATABASE file.

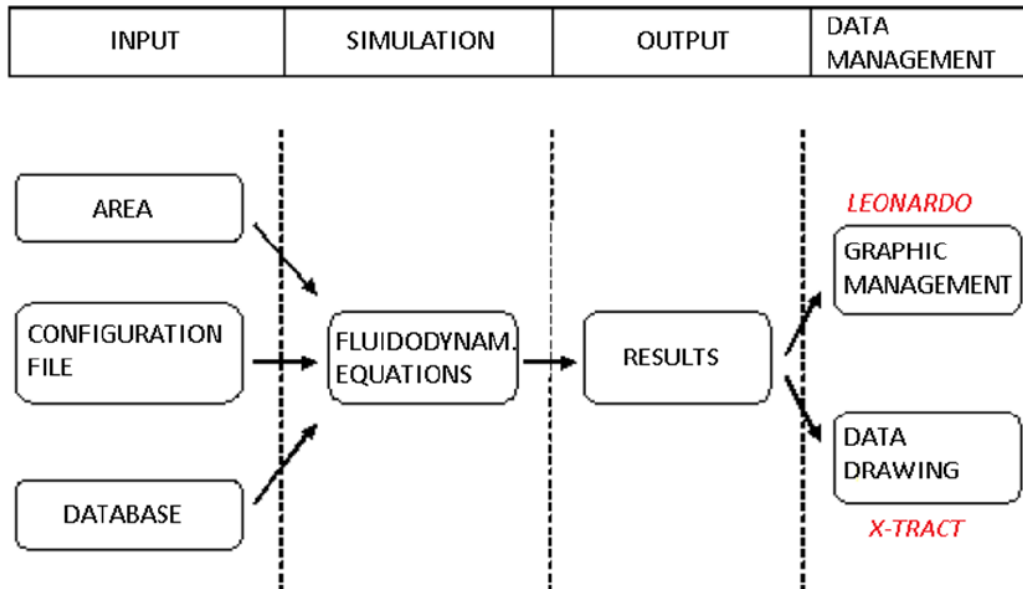


Figure 59: software structure

The AREA file (*_.in*) is a 2D graphic file necessary to build up the geometry of the area. It contains the geometric data of the simulation model:

- Area dimensions
- Surfaces and materials
- Buildings
- Vegetation
- Roads
- Water bodies

The model domain is organised as a rectangular area which extends in x-, y- and z-direction. The z-direction is not visualized as the domain is represented from above, in a 2D configuration. Nevertheless, is possible to set buildings heights although working in the horizontal view (fig.60). By changing the visualization mode it is possible to assign the materials of the surfaces.

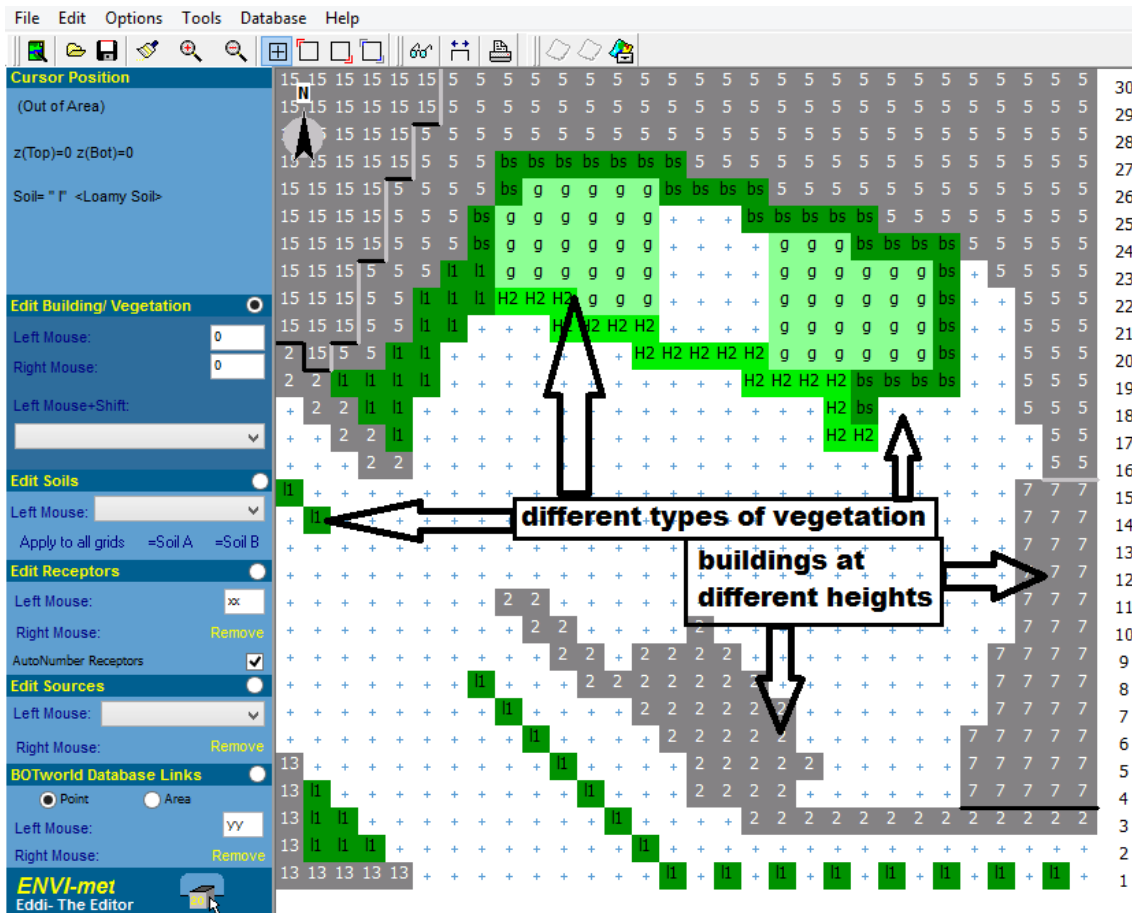


Figure 60: building and vegetation settings

Materials are visualised as acronyms in the map, called “IDs” (fig.61).

ENVI-met has a library where some default materials are contained. It is possible to set a layer composed by default materials or to create new layers with other default materials or new materials. Materials, vegetation and layers are included in 3 DATABASE files, respectively SOILS.DAT, PLANTS.DAT and PROFILS.DAT.

The most important DATABASE file for the scopes of this research is PROFILS.DAT. The file encloses a list of the available layers of materials, and can be freely modified, even though respecting some compilation rules. The file is structured in columns and rows. Each layer is represented by a row and each column contains values referring to the layer composition and to the material’s parameters. The columns labelled “-.015” to “-.1.75” are the vertical grid boxes of the soil model. The last three columns contain the material parameters: **z0** is the roughness length of the surface in [m], **a** is the short-wave albedo of the surface and **em** is the long-wave emissivity of the surface (fig.62).

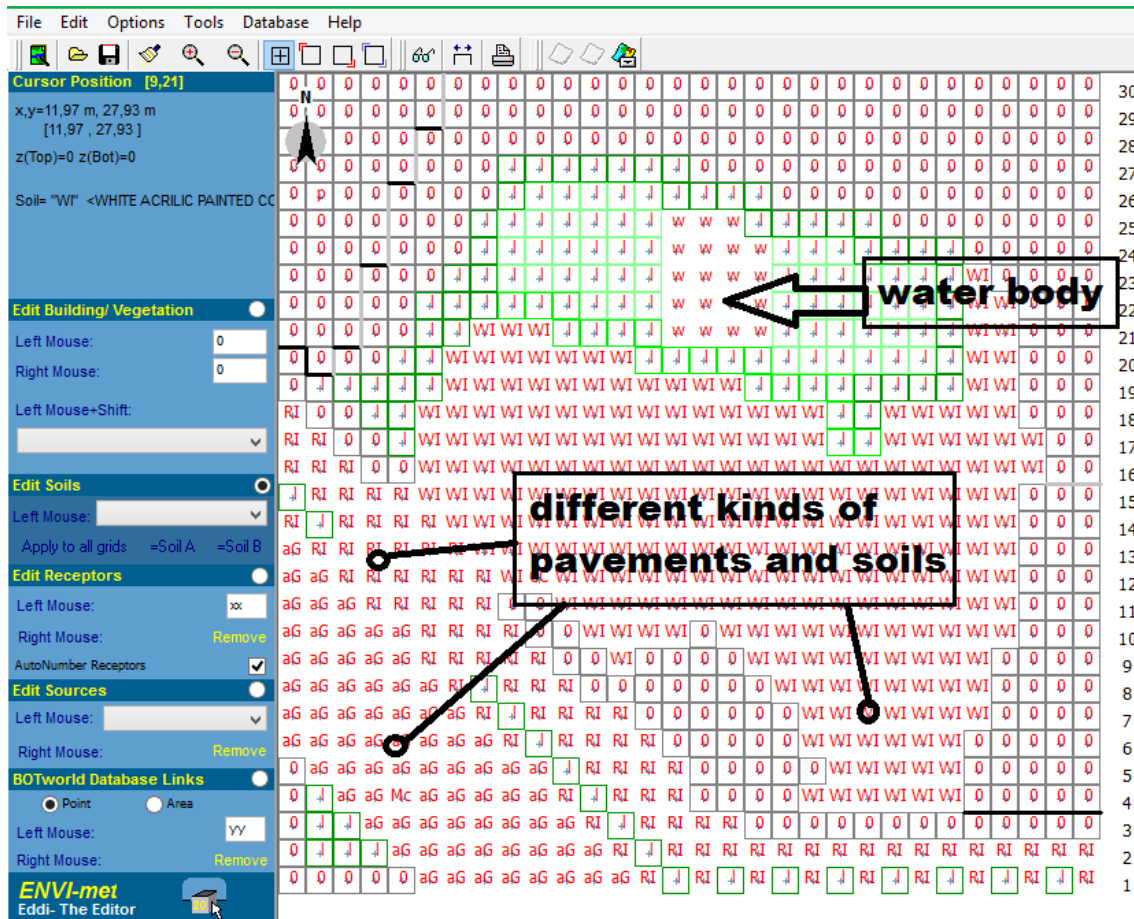


Figure 61: materials settings

The software allows the user to change the geographic location by choosing the city from a default list or by setting latitude and longitude. In fact, the simulation needs for different parameters related to the sun and to the month. These values differ depending on the geographic position on earth.

In the same window it is possible to define all the geometric parameters of the simulation:

- Number of cells in the grid
- Nesting grids
- Soils for the nesting grids
- Cells size
- Generation of vertical grid (fig.63)

ENVI-met splits the simulation volume into finite elements, that are 3D cells. The dimensions of these elements can be set in the command window (cells size), ranging

between 0.5 and 10 m for each spatial direction. Nevertheless, the resulting model height is not enough and some calculation data are necessary up the altitude of 2500 m.

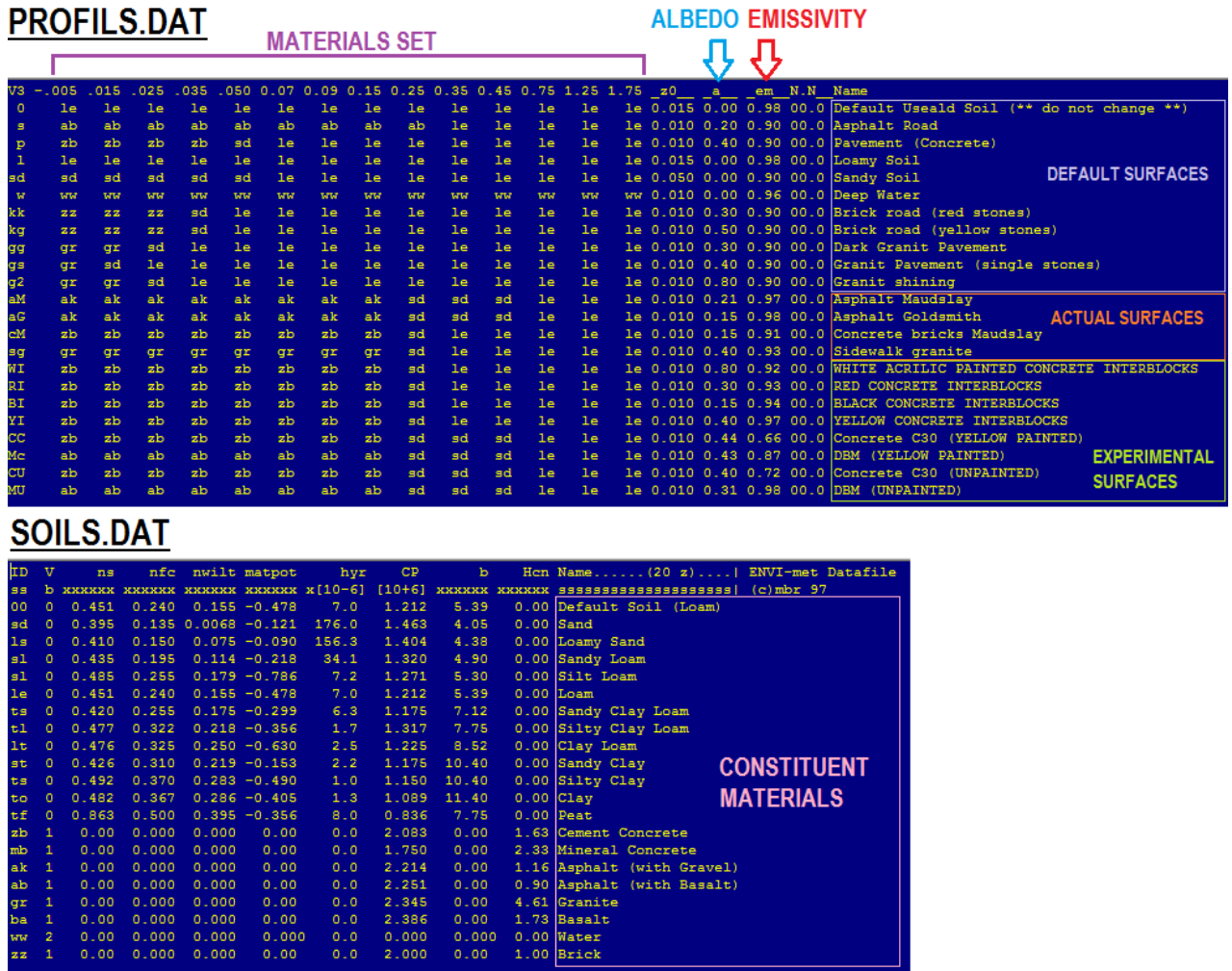


Figure 62: PROFILS.DAT and SOILS.DAT

Since would be senseless to use a 3D model up to 2500 m due to the large amount of calculations needed, typically the 3D model ends at a height twice as much the highest building in the scenario. After this height a 1D model begins, up to 2500 m.

The software allows the user to choose the most adequate boundary conditions, in order to have reliable results at the limits of the geometry. Regarding this fact, ENVI-met puts a number of *nesting grids* outside the shaped area (the number and the material components the soil can be changed in the AREA file). These additional cells are useful to mitigate the errors occurring at the boundaries. Besides, they help in avoiding divergences in calculation.

Figure 63: domain parameters

The CONFIGURATION file (`_CF`) defines the settings for the simulation to run. It contains:

- Name of the simulation
- Directory for the area file
- Name of the file-base output
- Directory for the output files
- Day of simulation
- Duration of simulation
- Wind direction and speed
- Initial roughness
- Initial atmosphere temperature
- Specific humidity at 2500 m
- Relative humidity at 2 m (fig.64)

Additionally it is possible to add other sections relative to many simulation parameters. If these parameters are not changed, they keep their default value.

```

File Edit Add Section Help Window
% ---- Basic Configuration File for ENVI-met Version 3 ----
% ---- MAIN-DATA Block ----
Name for Simulation (Text):           = Prova2giugno
Input File Model Area                 =\\nasstudusers\2\N0556329\master thesis\work\ENVI-MET\files\NewArea2giugno.in
Filebase name for Output (Text):      =PROVA2GIUGNO
Output Directory:                    =\\nasstudusers\2\N0556329\master thesis\work\ENVI-MET\files\OUTPUT2GIUGNO
Start Simulation at Day (DD.MM.YYYY): =2.06.2014
Start Simulation at Time (HH:MM:SS):  =06:00:00
Total Simulation Time in Hours:       =24.00
Save Model State each ? min          =60
Wind Speed in 10 m ab. Ground [m/s]  =3
Wind Direction (0:N..90:E..180:S..270:W..) =90
Roughness Length z0 at Reference Point =0.1
Initial Temperature Atmosphere [K]    =283
Specific Humidity in 2500 m [g Water/kg air] =7
Relative Humidity in 2m [%]           =50
Database Plants                       =[input]\Plants.dat

( -- End of Basic Data --)
( -- Following: Optional data. The order of sections is free. --)
( -- Missing Sections will keep default data. --)
( Use "Add Section" in ConfigEditor to add more sections )
( Only use "=" in front of the final value, not in the description)
( This file is created for ENVI-met V3.0 or better )

```

Figure 64: configuration file

All these parameters are used in the CFD equations solved by the software at each time-step.

The SIMULATION interface is the central part of the software and is represented by a control panel (fig.65). In this window is possible to test the model configuration (if any error occurs, the software displays an alert message), launch the simulation, monitor the calculation progress, the simulation time, the possible simulation errors.

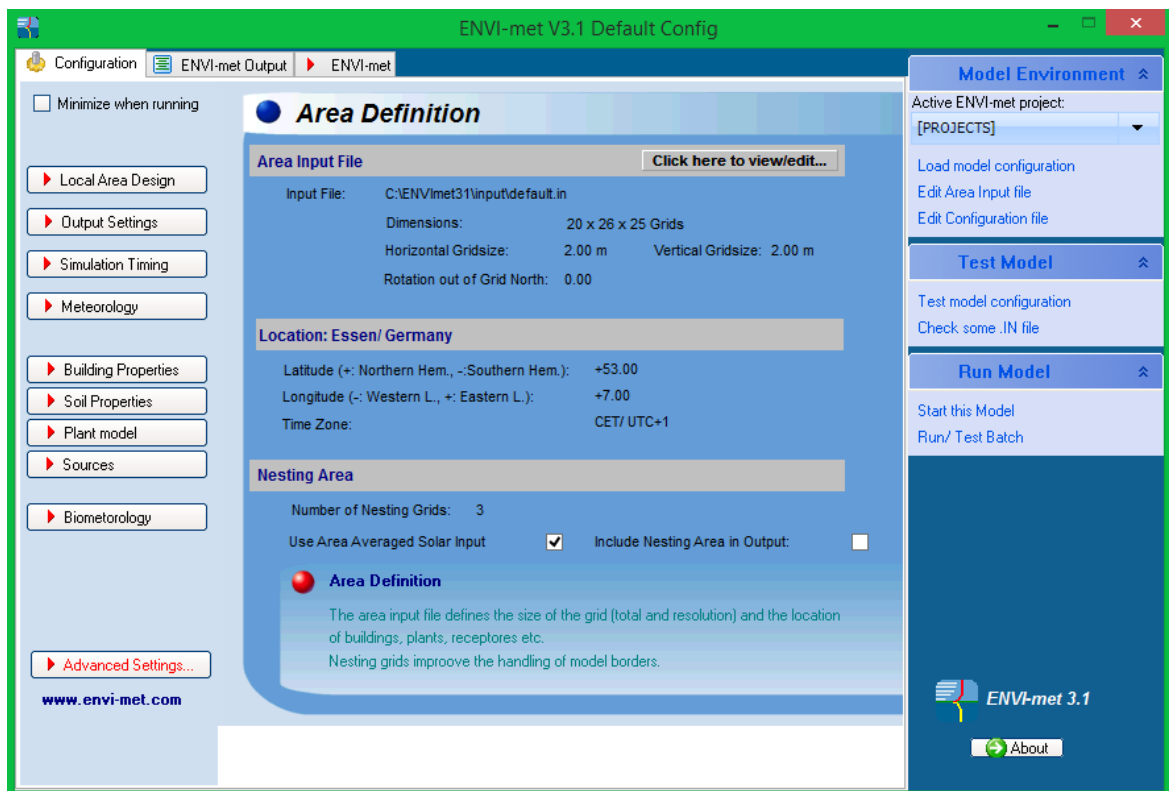


Figure 65: simulation interface

The OUTPUT FILES worked out are placed in a dedicated folder (the directory has been already set in the configuration file). ENVI-met produces a lot of results and divides them into sub-folders related to the associated datafield. The sub-folders produced are:

- Atmosphere
- BOTworld
- Inflow
- Log
- Receptors
- Soil
- Surface

Atmosphere folder contains hourly files relative to the air. In particular, there is the air temperature for all the simulation hours, cells and heights. It is important to highlight the fact that only one value is worked out for each element, to take in consideration in when choosing the number of grids volumes.

BOTworld files are referred to the calculation of the thermo-hygroscopic comfort of a virtual user.

Inflow contains data relative to the 1D model built over the 3D model.

Log files are useful to the program to connect the Area model and the Configuration model.

Receptors folder contains all the data relative to the receptors previously placed in the model. Receptors are special points in the map, typically representing the position of interesting elements of the scenario.

Soils files give information about the soil temperature and the contained water.

Surface folder presents all the resulting parameters of the pavements and soils. In particular, there is the surfaces temperature for all the simulation hours and cells, at the height $z = 0$.

ENVI-met provides two tools for the DATA MANAGEMENT: *Leonardo* and *Xtract*.

Leonardo is a graphic interface useful to visualize and analyse 3D data on a quality level. When a file is imported, it is possible to show graphic data in different ways, depending on the specific parameter needed (fig.66). There are 4 graphic methods:

- Data: data are visualized in chromatic scale, with a legend reporting the colour significance.
- Vector: data are visualized using arrows, with direction and modulus proportional to the value of the parameter.
- Special: it allows to show specific data with a single value.
- Isoline: data are shown using curves characterized by a constant value of a parameter.

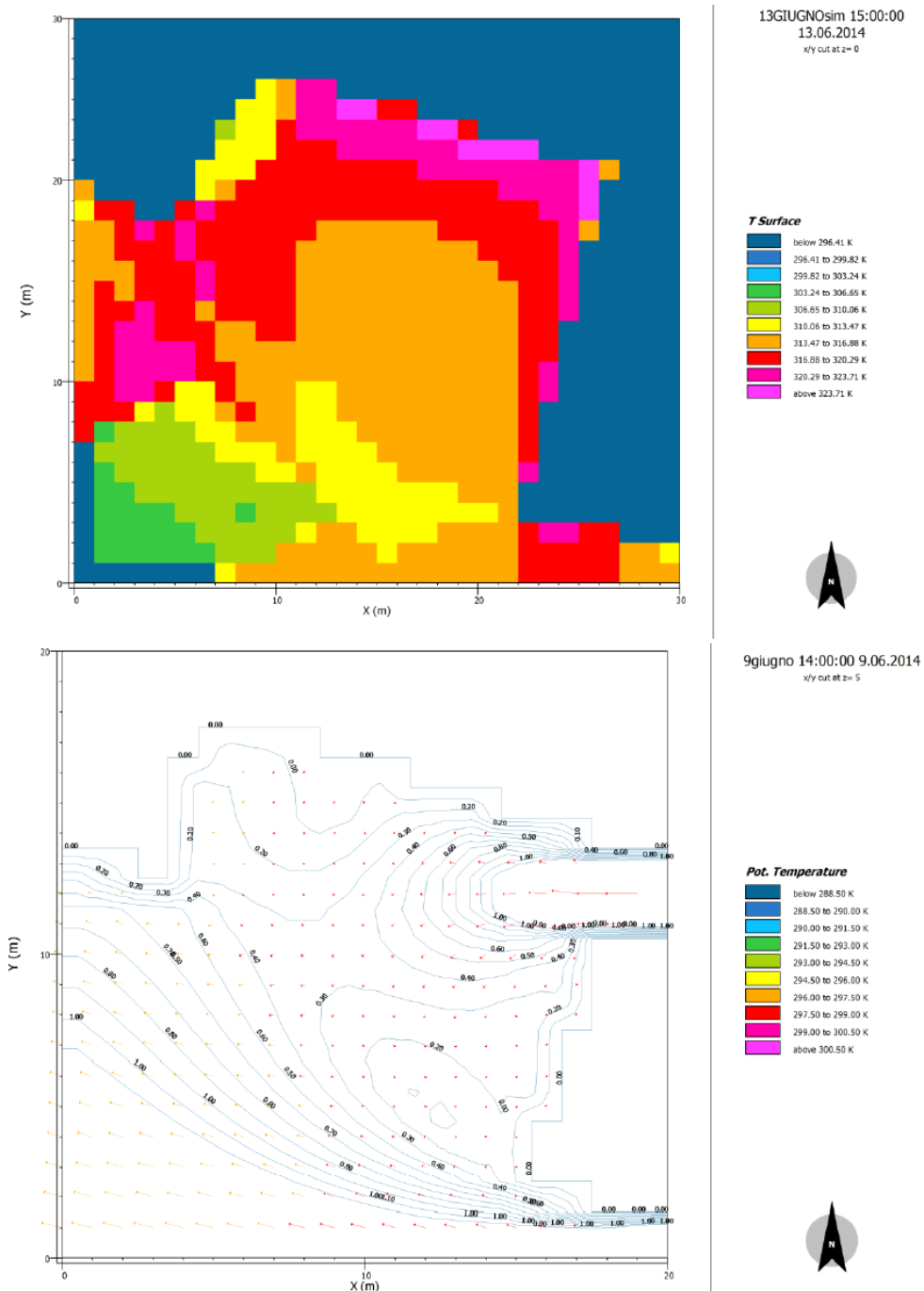


Figure 66: Leonardo graphic modes: data and isoline

Xtract is a tool able to extract data on a quantitative level. The values extracted can be read as a text file. Data are selected with a vertical or horizontal cut, but just a single parameter at a time (fig.67).

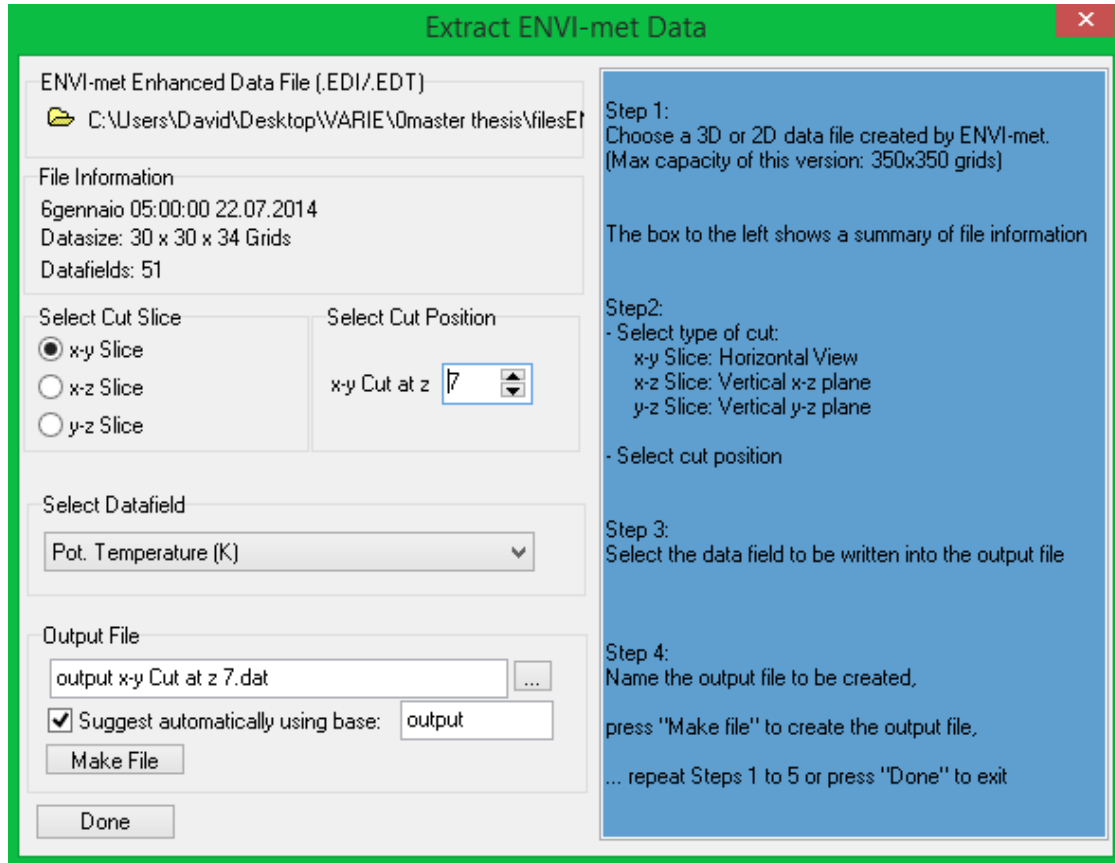


Figure 67: Xtract tool

4.1.2 Simulation models

The original idea was to build up the real scenario, formed of the area where the outside measurements and experimentations were carried out, with the aim of assessing the thermal behaviour of the existing surfaces (fig.68). The following phase would be to substitute those surfaces with the investigated materials, trying to figure out how they could be employed to mitigate the UHI problem. In order to do this, the simulative model shall reproduce the real situation, working out results close to the reality. This is called “*calibration phase*” and it is essential to prove that the built model works properly. Once the calibration phase is done, the model can be used to simulate hypothetical scenarios reliably. That was the scope of the all-day measurements campaign conducted on the 21st of July 2014 (see § 3.2.3): to collect data on surfaces and air temperature and to use these measurements to check out if the simulation model

could reproduce them. Unfortunately it has not been possible to accomplish that result. Different reasons have led to this. First of all, it was not possible to measure some parameters such as the building's walls transmittance, albedo and emittance. In addition, due to technical problems, it was not possible to use the meteorological station placed on Maudslay building's roof, more accurate and reliable than the portable weather station. Another important reason is that ENVI-met asks to specify which materials compose the surface layers, from the sub-base to the surface, and there was a lack of information on this. All these reasons have prevented the calibration of the model.

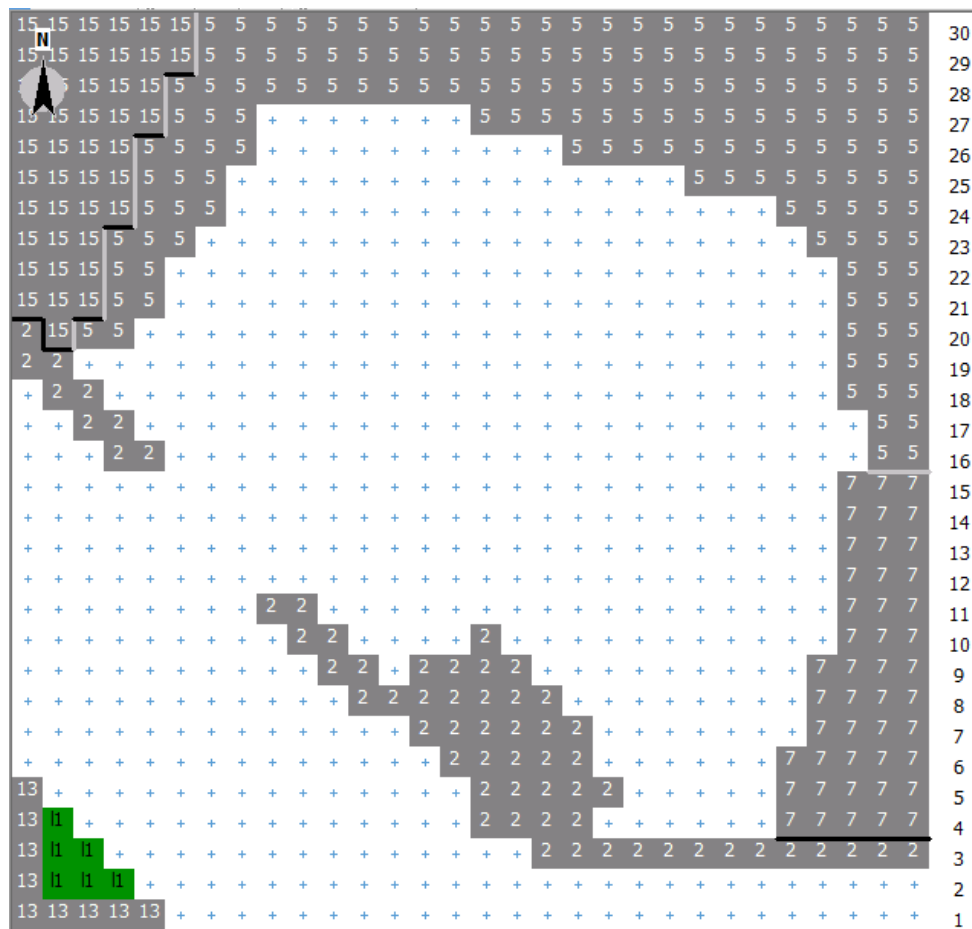


Figure 68: simulation model

Nevertheless, measurements collected have been used to test the materials in two typical urban situations: the *urban canyon* and the *urban heat basin*.

An urban canyon is a place where a relatively narrow street is flanked by tall buildings, creating a canyon-like environment (fig.69). This situation has an impact on different local conditions, such as temperature, wind, air quality, GPS and radio signals.

Urban canyons worsen the UHI effect, elevating temperatures inside. The main factors affecting the temperature inside a urban canyon are irradiance, angle of incidence, albedo, emissivity, temperature and Sky View Factor (SVF). In particular, with high SVF the temperature decreases quickly, because more sky is available to absorb the energy irradiated by the buildings. Low SVF can lead to a high heat release during the night-time, when buildings and surface dissipate the energy stored during the day. It has been seen that the amount of surface energy at various times within the canyon depends on canyon geometry and orientation. Canyons with north-south orientation have been found to be the most active energy site. In fact, 30% of midday solar radiation is trapped and stored in the buildings. As a result, during the night the air does not cool down, due to the heat release of the materials in the atmosphere. The phenomenon contributes significantly to the UHI effect [48].

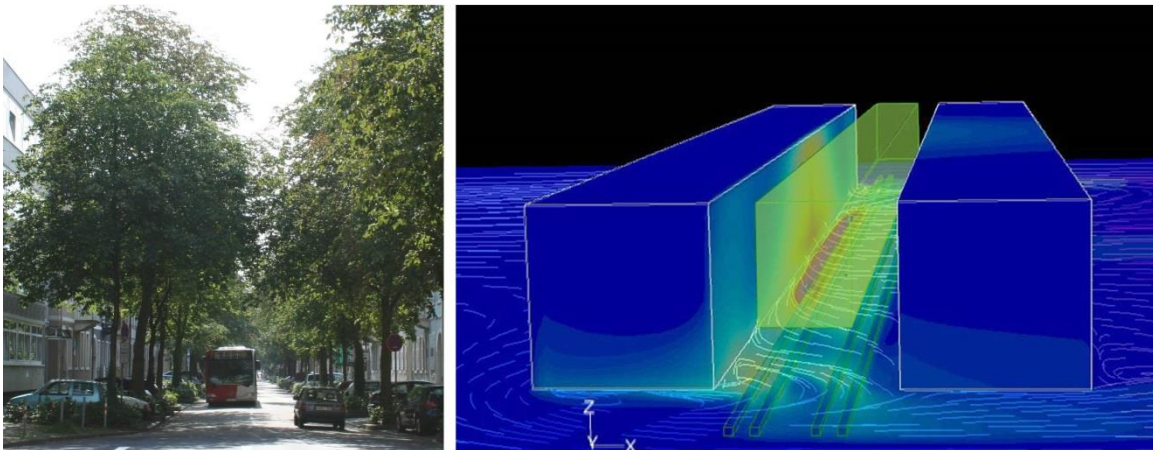


Figure 64: Urban street canyon with avenue-trees (left), CFD simulation of flow and pollutant dispersion in street canyon model with densely spaced avenue-trees [49]

A urban heat basin is another typical urban configuration, represented by an empty space enclosed by a number of buildings (fig.70). This situation has not been treated in previous researches so far, but it can be considered as a potential factor affecting the thermal performances of a zone. In fact, the disturbance that buildings create in the wind circulation, can influence the thermal dynamics, preventing the natural cooling effect given by the wind. In this optic, also this situation can represent a source of a bad thermal behaviour of a city. This is just a hypothesis that needs to be proved and confirmed with future studies.



Figure 70: a potential urban basin [50]

The two urban configurations presented have been chosen in order to represent two actual situations of the real scenario.

The investigated area can be divided into two portions:

- the Maudslay building car parking, presenting a flat empty surface surrounded by three buildings with different heights → URBAN HEAT BASIN
- the Goldsmith Road, representing a geometry similar to an urban canyon, with a side covered in vegetation → URBAN CANYON (fig.71)

Simulations were performed for both the scenarios individually.



Figure 71: the two configurations

Five simulations there were carried out for the Goldsmith Street urban canyon and 10 simulations for the Maudslay building car parking.

All the simulations were set with the same geometrical, geographic and meteorological parameters. In the model domain were set (fig.72):

- Number of elements: $30 \times 30 \times 30 = 27,000$ cells
- Cell size: $1 \times 1 \times 1 \text{ m} = 1 \text{ m}^3$
- Area size: $30 \times 30 \text{ m} = 900 \text{ m}^2$
- Location: Nottingham

Weather data set in the configuration file (fig.73) were taken from *Weatherunderground.com* website, and are referred to 6 a.m. of the 21st of July 2014 (all-day measurement campaign performed):

- Wind speed: 3.3 m/s
- Wind direction: North-West
- Temperature: 288 K (15°C)
- Relative humidity in 2 m: 94%
- Specific humidity in 2500 m: 3.767 g water / kg air *

*The specific humidity in 2500 m of height were taken from a table directly provided by ENVI-met developer (fig.74).

Figure 72: model domain configuration

Other data set in the configuration file were:

- Start simulation at day: 21st July 2014
- Start simulation at time: 6 a.m.
- Simulation time: 24 h

```

$ --- Basic Configuration File for ENVI-met Version 3 -----
$ --- MAIN-DATA Block -----
Name for Simulation (Text):                =actual
Input file Model Area                      =C:\Users\David\Desktop\VARIE\
\actualAREA.in
Filebase name for Output (Text):           =actual
Output Directory:                          =C:\Users\David\Desktop\VARIE\
Start Simulation at Day (DD.MM.YYYY):      =21.07.2014
Start Simulation at Time (HH:MM:SS):       =06:00:00
Total Simulation Time in Hours:            =24.00
Save Model State each ? min                =60
Wind Speed in 10 m ab. Ground [m/s]       =3.3
Wind Direction (0:N..90:E..180:S..270:W..) =315
Roughness Length z0 at Reference Point     =0.01
Initial Temperature Atmosphere [K]        =288
Specific Humidity in 2500 m [g Water/kg air] =3.767
Relative Humidity in 2m [%]               =94
Database Plants                            =(input)\Plants.dat

( -- End of Basic Data --)
( -- Following: Optional data. The order of sections is free. --)
( -- Missing Sections will keep default data. --)
( Use "Add Section" in ConfigEditor to add more sections )
( Only use "=" in front of the final value, not in the description)
( This file is created for ENVI-met V3.0 or better )

```

Figure 73: configuration file

Temperature ($^{\circ}\text{C}$)	Saturation Pressure of Water Vapor (Pa)	Maximum Humidity Ratio (kg_w/kg_a)
0	609.9	0.003767
5	870	0.005387
10	1225	0.007612
15	1701	0.01062
20	2333	0.014659
25	3130	0.019826
30	4234	0.027125

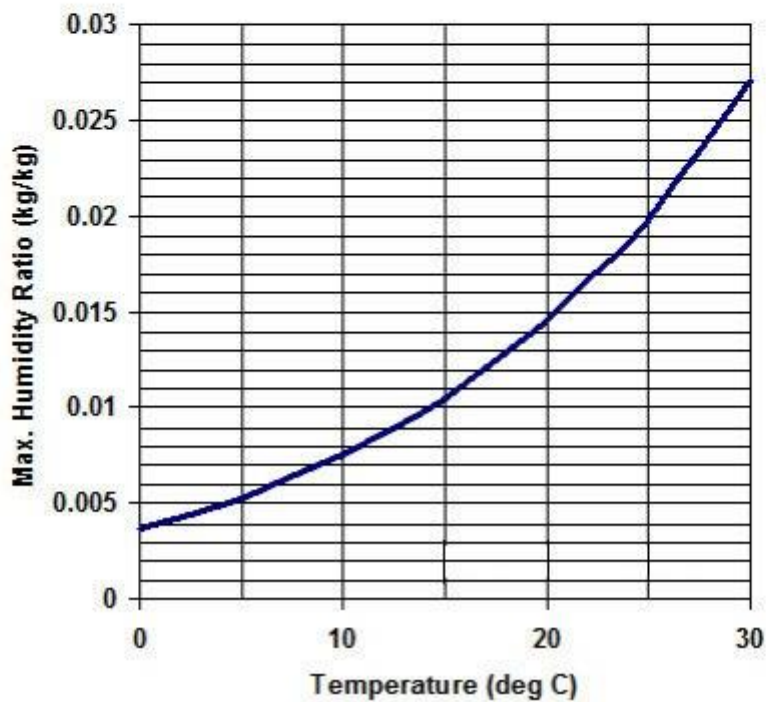


Figure 74: specific humidity in 2500 m determination

Materials used to build the two scenarios were directly defined in the *profils.dat* file (fig.75) without modifying the *soils.dat* file (where the materials forming the layers are contained). For each simulation only the pavements were changed, in order to maintain the same boundary conditions. In § 4.1.3 will be provided a description of each material used.

Albedo and emissivity are the two fundamental parameters defining the surfacing material. They only refer to the top of the layer. The underlying materials features are defined in the *soils.dat* file.

PROFILS.DAT

MATERIALS SET

ALBEDO EMISSIVITY

↓ ↓

V3	-.005	.015	.025	.035	.050	0.07	0.09	0.15	0.25	0.35	0.45	0.75	1.25	1.75	_z0	_a	_em	N.N	Name	
0	le	le	le	le	le	le	le	le	le	le	le	le	le	le	le	0.015	0.00	0.98	00.0	Default Useald Soil (** do not change **)
s	ab	ab	ab	ab	ab	ab	ab	ab	ab	le	le	le	le	le	le	0.010	0.20	0.90	00.0	Asphalt Road
p	zb	zb	zb	zb	sd	le	le	le	le	le	le	le	le	le	le	0.010	0.40	0.90	00.0	Pavement (Concrete)
l	le	le	le	le	le	le	le	le	le	le	le	le	le	le	le	0.015	0.00	0.98	00.0	Loamy Soil
sd	sd	sd	sd	sd	sd	le	le	le	le	le	le	le	le	le	le	0.050	0.00	0.90	00.0	Sandy Soil
w	ww	ww	ww	ww	ww	ww	ww	ww	ww	ww	ww	ww	ww	ww	ww	0.010	0.00	0.96	00.0	Deep Water
kk	zz	zz	zz	sd	le	le	le	le	le	le	le	le	le	le	le	0.010	0.30	0.90	00.0	Brick road (red stones)
kg	zz	zz	zz	sd	le	le	le	le	le	le	le	le	le	le	le	0.010	0.50	0.90	00.0	Brick road (yellow stones)
gg	gr	gr	sd	le	le	le	le	le	le	le	le	le	le	le	le	0.010	0.30	0.90	00.0	Dark Granit Pavement
gs	gr	sd	le	le	le	le	le	le	le	le	le	le	le	le	le	0.010	0.40	0.90	00.0	Granit Pavement (single stones)
gZ	gr	gr	sd	le	le	le	le	le	le	le	le	le	le	le	le	0.010	0.80	0.90	00.0	Granit shining
aM	ak	ak	ak	ak	ak	ak	ak	sd	sd	sd	sd	le	le	le	le	0.010	0.21	0.97	00.0	Asphalt Maudslay
aG	ak	ak	ak	ak	ak	ak	ak	sd	sd	sd	sd	le	le	le	le	0.010	0.15	0.98	00.0	Asphalt Goldsmith
cM	zb	zb	zb	zb	zb	zb	zb	sd	sd	sd	sd	le	le	le	le	0.010	0.15	0.91	00.0	Concrete bricks Maudslay
sg	gr	gr	gr	gr	gr	gr	gr	sd	sd	sd	sd	le	le	le	le	0.010	0.40	0.93	00.0	Sidewalk granite
WI	zb	zb	zb	zb	zb	zb	zb	sd	sd	sd	sd	le	le	le	le	0.010	0.80	0.92	00.0	WHITE ACRYLIC PAINTED CONCRETE INTERBLOCKS
RI	zb	zb	zb	zb	zb	zb	zb	sd	sd	sd	sd	le	le	le	le	0.010	0.30	0.93	00.0	RED CONCRETE INTERBLOCKS
BI	zb	zb	zb	zb	zb	zb	zb	sd	sd	sd	sd	le	le	le	le	0.010	0.15	0.94	00.0	BLACK CONCRETE INTERBLOCKS
YI	zb	zb	zb	zb	zb	zb	zb	sd	sd	sd	sd	le	le	le	le	0.010	0.40	0.97	00.0	YELLOW CONCRETE INTERBLOCKS
CC	zb	zb	zb	zb	zb	zb	zb	sd	sd	sd	sd	le	le	le	le	0.010	0.44	0.66	00.0	Concrete C30 (YELLOW PAINTED)
Mc	ab	ab	ab	ab	ab	ab	ab	sd	sd	sd	sd	le	le	le	le	0.010	0.43	0.87	00.0	DBM (YELLOW PAINTED)
CU	zb	zb	zb	zb	zb	zb	zb	sd	sd	sd	sd	le	le	le	le	0.010	0.40	0.72	00.0	Concrete C30 (UNPAINTED)
MU	ab	ab	ab	ab	ab	ab	ab	sd	sd	sd	sd	le	le	le	le	0.010	0.31	0.98	00.0	DBM (UNPAINTED)

Figure 75: materials used

4.1.3 Surfacing materials used

Simulated surfacing materials were (fig.76):

- ASPHALT MAUDSLAY [ID: “aM”]

Real pavement of the Maudslay car parking. Measured parameters:

Albedo:0.21

Emissivity:0.97

Hypothetic layer:

0 m → 0.005 m (0,5 cm) = asphalt (with gravel) [ID: “ak”]

0.005 m → 0.015 m (1 cm) = asphalt (with gravel)

0.015 m → 0.025 m (1 cm) = asphalt (with gravel)

0.025 m → 0.035 m (1 cm) = asphalt (with gravel)

0.035 m → 0.050 m (1.5 cm) = asphalt (with gravel)

0.050 m → 0.070 m (2 cm) = asphalt (with gravel)

0.070 m → 0.090 m (2 cm) = asphalt (with gravel)

0.090 m → 0.150 m (6 cm) = asphalt (with gravel)

0.150 m → 0.250 m (10 cm) = sand [ID: “sd”]

0.250 m → 0.350 m (10 cm) = sand

0.350 m → 0.450 m (10 cm) =sand

0.450 m → 0.750 m (30 cm) = loam [ID: “le”]

0.750 m → 1.250 m (50 cm) = loam

1.250 m → 1.750 m (50 cm) = loam

➤ ASPHALT GOLDSMITH [ID: “aG”]

Real pavement of the Goldsmith Road. Measured parameters:

Albedo:0.15

Emissivity:0.98

Hypothetic layer:

0 m → 0.005 m (0,5 cm) = asphalt (with gravel) [ID: “ak”]

0.005 m → 0.015 m (1 cm) = asphalt (with gravel)

0.015 m → 0.025 m (1 cm) = asphalt (with gravel)

0.025 m → 0.035 m (1 cm) = asphalt (with gravel)

0.035 m → 0.050 m (1.5 cm) = asphalt (with gravel)

0.050 m → 0.070 m (2 cm) = asphalt (with gravel)

0.070 m → 0.090 m (2 cm) = asphalt (with gravel)

0.090 m → 0.150 m (6 cm) = asphalt (with gravel)

0.150 m → 0.250 m (10 cm) = sand [ID: “sd”]

0.250 m → 0.350 m (10 cm) = sand

0.350 m → 0.450 m (10 cm) = sand

0.450 m → 0.750 m (30 cm) = loam [ID: “le”]

0.750 m → 1.250 m (50 cm) = loam

1.250 m → 1.750 m (50 cm) = loam

➤ CONCRETE BRICKS MAUDSLAY [ID: “cM”]

Real pavement of the sidewalk in front of Maudslay car parking. Measured parameters:

Albedo:0.15

Emissivity:0.91

Hypothetic layer:

0 m → 0.005 m (0,5 cm) = cement concrete [ID: “zb”]

0.005 m → 0.015 m (1 cm) = cement concrete

0.015 m → 0.025 m (1 cm) = cement concrete

0.025 m → 0.035 m (1 cm) = cement concrete

0.035 m → 0.050 m (1.5 cm) = cement concrete

0.050 m → 0.070 m (2 cm) = cement concrete

0.070 m → 0.090 m (2 cm) = cement concrete

0.090 m → 0.150 m (6 cm) = cement concrete

$0.150\text{ m} \rightarrow 0.250\text{ m}$ (10 cm) = sand [ID: "sd"]

$0.250\text{ m} \rightarrow 0.350\text{ m}$ (10 cm) = loam [ID: "le"]

$0.350\text{ m} \rightarrow 0.450\text{ m}$ (10 cm) = loam

$0.450\text{ m} \rightarrow 0.750\text{ m}$ (30 cm) = loam

$0.750\text{ m} \rightarrow 1.250\text{ m}$ (50 cm) = loam

$1.250\text{ m} \rightarrow 1.750\text{ m}$ (50 cm) = loam

➤ SIDEWALK GRANITE [ID: "sg"]

Real pavement of the sidewalk near the Goldsmith Road. Measured parameters:

Albedo:0.40

Emissivity:0.93

Hypothetic layer:

$0\text{ m} \rightarrow 0.005\text{ m}$ (0,5 cm) = granite [ID: "gr"]

$0.005\text{ m} \rightarrow 0.015\text{ m}$ (1 cm) = granite

$0.015\text{ m} \rightarrow 0.025\text{ m}$ (1 cm) = granite

$0.025\text{ m} \rightarrow 0.035\text{ m}$ (1 cm) = granite

$0.035\text{ m} \rightarrow 0.050\text{ m}$ (1.5 cm) = granite

$0.050\text{ m} \rightarrow 0.070\text{ m}$ (2 cm) = granite

$0.070\text{ m} \rightarrow 0.090\text{ m}$ (2 cm) = granite

$0.090\text{ m} \rightarrow 0.150\text{ m}$ (6 cm) = granite

$0.150\text{ m} \rightarrow 0.250\text{ m}$ (10 cm) = sand [ID: "sd"]

$0.250\text{ m} \rightarrow 0.350\text{ m}$ (10 cm) = loam [ID: "le"]

$0.350\text{ m} \rightarrow 0.450\text{ m}$ (10 cm) = loam

$0.450\text{ m} \rightarrow 0.750\text{ m}$ (30 cm) = loam

$0.750\text{ m} \rightarrow 1.250\text{ m}$ (50 cm) = loam

$1.250\text{ m} \rightarrow 1.750\text{ m}$ (50 cm) = loam

➤ WHITE ACRILIC PAINTED CONCRETE INTERBLOCKS [ID: "WI"]

Tested bricks. Measured parameters:

Albedo:0.80

Emissivity:0.92

Hypothetic layer:

$0\text{ m} \rightarrow 0.005\text{ m}$ (0,5 cm) = cement concrete [ID: "zb"]

$0.005\text{ m} \rightarrow 0.015\text{ m}$ (1 cm) = cement concrete

$0.015\text{ m} \rightarrow 0.025\text{ m}$ (1 cm) = cement concrete
 $0.025\text{ m} \rightarrow 0.035\text{ m}$ (1 cm) = cement concrete
 $0.035\text{ m} \rightarrow 0.050\text{ m}$ (1.5 cm) = cement concrete
 $0.050\text{ m} \rightarrow 0.070\text{ m}$ (2 cm) = cement concrete
 $0.070\text{ m} \rightarrow 0.090\text{ m}$ (2 cm) = cement concrete
 $0.090\text{ m} \rightarrow 0.150\text{ m}$ (6 cm) = cement concrete
 $0.150\text{ m} \rightarrow 0.250\text{ m}$ (10 cm) = sand [ID: "sd"]
 $0.250\text{ m} \rightarrow 0.350\text{ m}$ (10 cm) = loam [ID: "le"]
 $0.350\text{ m} \rightarrow 0.450\text{ m}$ (10 cm) = loam
 $0.450\text{ m} \rightarrow 0.750\text{ m}$ (30 cm) = loam
 $0.750\text{ m} \rightarrow 1.250\text{ m}$ (50 cm) = loam
 $1.250\text{ m} \rightarrow 1.750\text{ m}$ (50 cm) = loam

➤ RED CONCRETE INTERBLOCKS [ID: "RI"]

Tested bricks. Measured parameters:

Albedo:0.30

Emissivity:0.93

Hypothetic layer:

$0\text{ m} \rightarrow 0.005\text{ m}$ (0,5 cm) = cement concrete [ID: "zb"]
 $0.005\text{ m} \rightarrow 0.015\text{ m}$ (1 cm) = cement concrete
 $0.015\text{ m} \rightarrow 0.025\text{ m}$ (1 cm) = cement concrete
 $0.025\text{ m} \rightarrow 0.035\text{ m}$ (1 cm) = cement concrete
 $0.035\text{ m} \rightarrow 0.050\text{ m}$ (1.5 cm) = cement concrete
 $0.050\text{ m} \rightarrow 0.070\text{ m}$ (2 cm) = cement concrete
 $0.070\text{ m} \rightarrow 0.090\text{ m}$ (2 cm) = cement concrete
 $0.090\text{ m} \rightarrow 0.150\text{ m}$ (6 cm) = cement concrete
 $0.150\text{ m} \rightarrow 0.250\text{ m}$ (10 cm) = sand [ID: "sd"]
 $0.250\text{ m} \rightarrow 0.350\text{ m}$ (10 cm) = loam [ID: "le"]
 $0.350\text{ m} \rightarrow 0.450\text{ m}$ (10 cm) = loam
 $0.450\text{ m} \rightarrow 0.750\text{ m}$ (30 cm) = loam
 $0.750\text{ m} \rightarrow 1.250\text{ m}$ (50 cm) = loam
 $1.250\text{ m} \rightarrow 1.750\text{ m}$ (50 cm) = loam

➤ BLACK CONCRETE INTERBLOCKS [ID: “BI”]

Tested bricks. Measured parameters:

Albedo:0.15

Emissivity:0.94

Hypothetic layer:

0 m → 0.005 m (0,5 cm) = cement concrete [ID: “zb”]

0.005 m → 0.015 m (1 cm) = cement concrete

0.015 m → 0.025 m (1 cm) = cement concrete

0.025 m → 0.035 m (1 cm) = cement concrete

0.035 m → 0.050 m (1.5 cm) = cement concrete

0.050 m → 0.070 m (2 cm) = cement concrete

0.070 m → 0.090 m (2 cm) = cement concrete

0.090 m → 0.150 m (6 cm) = cement concrete

0.150 m → 0.250 m (10 cm) = sand [ID: “sd”]

0.250 m → 0.350 m (10 cm) = loam [ID: “le”]

0.350 m → 0.450 m (10 cm) = loam

0.450 m → 0.750 m (30 cm) = loam

0.750 m → 1.250 m (50 cm) = loam

1.250 m → 1.750 m (50 cm) = loam

➤ YELLOW CONCRETE INTERBLOCKS [ID: “YI”]

Tested bricks. Measured parameters:

Albedo:0.40

Emissivity:0.97

Hypothetic layer:

0 m → 0.005 m (0,5 cm) = cement concrete [ID: “zb”]

0.005 m → 0.015 m (1 cm) = cement concrete

0.015 m → 0.025 m (1 cm) = cement concrete

0.025 m → 0.035 m (1 cm) = cement concrete

0.035 m → 0.050 m (1.5 cm) = cement concrete

0.050 m → 0.070 m (2 cm) = cement concrete

0.070 m → 0.090 m (2 cm) = cement concrete

0.090 m → 0.150 m (6 cm) = cement concrete

$0.150\text{ m} \rightarrow 0.250\text{ m}$ (10 cm) = sand [ID: "sd"]

$0.250\text{ m} \rightarrow 0.350\text{ m}$ (10 cm) = loam [ID: "le"]

$0.350\text{ m} \rightarrow 0.450\text{ m}$ (10 cm) = loam

$0.450\text{ m} \rightarrow 0.750\text{ m}$ (30 cm) = loam

$0.750\text{ m} \rightarrow 1.250\text{ m}$ (50 cm) = loam

$1.250\text{ m} \rightarrow 1.750\text{ m}$ (50 cm) = loam

Except for the Maudslay car parking, albedo was not investigated (see § 3.2.2). Values used in simulations were found in technical specifications about surfacing materials [51,52].

The following 4 materials were taken from Di Maria's Master Thesis work [34].

➤ CONCRETE C30 (YELLOW PAINTED) [ID: "CC"]

Concrete C30 with a characteristic strength of 30 N/mm^2 , painted by a primer white paint and a second thin layer of yellow paint. Measured parameters:

Albedo:0.44

Emissivity:0.66

Hypothetic layer:

$0\text{ m} \rightarrow 0.005\text{ m}$ (0,5 cm) = cement concrete [ID: "zb"]

$0.005\text{ m} \rightarrow 0.015\text{ m}$ (1 cm) = cement concrete

$0.015\text{ m} \rightarrow 0.025\text{ m}$ (1 cm) = cement concrete

$0.025\text{ m} \rightarrow 0.035\text{ m}$ (1 cm) = cement concrete

$0.035\text{ m} \rightarrow 0.050\text{ m}$ (1.5 cm) = cement concrete

$0.050\text{ m} \rightarrow 0.070\text{ m}$ (2 cm) = cement concrete

$0.070\text{ m} \rightarrow 0.090\text{ m}$ (2 cm) = cement concrete

$0.090\text{ m} \rightarrow 0.150\text{ m}$ (6 cm) = cement concrete

$0.150\text{ m} \rightarrow 0.250\text{ m}$ (10 cm) = sand [ID: "sd"]

$0.250\text{ m} \rightarrow 0.350\text{ m}$ (10 cm) = sand

$0.350\text{ m} \rightarrow 0.450\text{ m}$ (10 cm) = sand

$0.450\text{ m} \rightarrow 0.750\text{ m}$ (30 cm) = loam [ID: "le"]

$0.750\text{ m} \rightarrow 1.250\text{ m}$ (50 cm) = loam

$1.250\text{ m} \rightarrow 1.750\text{ m}$ (50 cm) = loam

➤ DBM C30 (YELLOW PAINTED) [ID: “Mc”]

Dense Bitumen Macadam, painted by a primer white paint and a second thin layer of yellow paint. Measured parameters:

Albedo:0.43

Emissivity:0.87

Hypothetic layer:

0 m → 0.005 m (0,5 cm) = asphalt (with basalt) [ID “ab”]

0.005 m → 0.015 m (1 cm) = asphalt (with basalt)

0.015 m → 0.025 m (1 cm) = asphalt (with basalt)

0.025 m → 0.035 m (1 cm) = asphalt (with basalt)

0.035 m → 0.050 m (1.5 cm) = asphalt (with basalt)

0.050 m → 0.070 m (2 cm) = asphalt (with basalt)

0.070 m → 0.090 m (2 cm) = asphalt (with basalt)

0.090 m → 0.150 m (6 cm) = asphalt (with basalt)

0.150 m → 0.250 m (10 cm) = sand [ID: “sd”]

0.250 m → 0.350 m (10 cm) = sand

0.350 m → 0.450 m (10 cm) = sand

0.450 m → 0.750 m (30 cm) = loam [ID: “le”]

0.750 m → 1.250 m (50 cm) = loam

1.250 m → 1.750 m (50 cm) = loam

➤ CONCRETE C30 (UNPAINTED) [ID: “CU”]

Concrete C30 with a characteristic strength of 30 N/mm². Measured parameters:

Albedo:0.40

Emissivity:0.72

Hypothetic layer:

0 m → 0.005 m (0,5 cm) = cement concrete [ID: “zb”]

0.005 m → 0.015 m (1 cm) = cement concrete

0.015 m → 0.025 m (1 cm) = cement concrete

0.025 m → 0.035 m (1 cm) = cement concrete

0.035 m → 0.050 m (1.5 cm) = cement concrete

0.050 m → 0.070 m (2 cm) = cement concrete

0.070 m → 0.090 m (2 cm) = cement concrete

0.090 m → 0.150 m (6 cm) = cement concrete

0.150 m → 0.250 m (10 cm) = sand [ID: "sd"]

0.250 m → 0.350 m (10 cm) = sand

0.350 m → 0.450 m (10 cm) = sand

0.450 m → 0.750 m (30 cm) = loam [ID: "le"]

0.750 m → 1.250 m (50 cm) = loam

1.250 m → 1.750 m (50 cm) = loam

➤ **DBM C30 (UNPAINTED) [ID: "MU"]**

Dense Bitumen Macadam. Measured parameters:

Albedo:0.31

Emissivity:0.98

Hypothetic layer:

0 m → 0.005 m (0,5 cm) = asphalt (with basalt) [ID "ab"]

0.005 m → 0.015 m (1 cm) = asphalt (with basalt)

0.015 m → 0.025 m (1 cm) = asphalt (with basalt)

0.025 m → 0.035 m (1 cm) = asphalt (with basalt)

0.035 m → 0.050 m (1.5 cm) = asphalt (with basalt)

0.050 m → 0.070 m (2 cm) = asphalt (with basalt)

0.070 m → 0.090 m (2 cm) = asphalt (with basalt)

0.090 m → 0.150 m (6 cm) = asphalt (with basalt)

0.150 m → 0.250 m (10 cm) = sand [ID: "sd"]

0.250 m → 0.350 m (10 cm) = sand

0.350 m → 0.450 m (10 cm) = sand

0.450 m → 0.750 m (30 cm) = loam [ID: "le"]

0.750 m → 1.250 m (50 cm) = loam

1.250 m → 1.750 m (50 cm) = loam

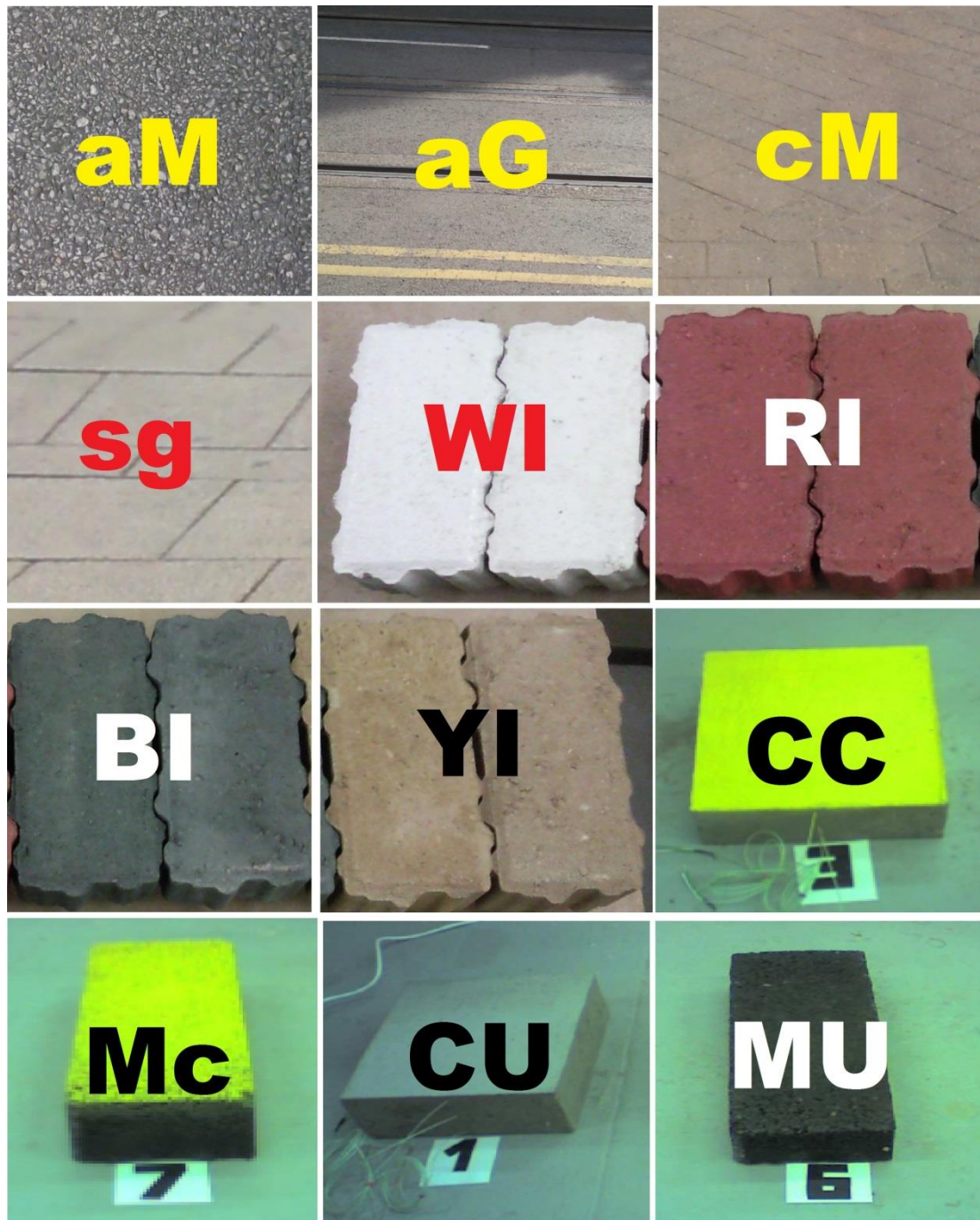


Figure 76: simulated surfacing materials

4.1.4 Urban canyon simulations

Urban canyon scenario was recreated in the most simple way, in order to make easy to figure out the effects of the pavements changes. The geometry was conceived to be similar to the real situation of the Maudslay car parking and Goldsmith Road (fig.77,78). On the right side of the road, a series of building was placed. Heights were 5 m, 10 m and 14 m. On the left side, 15 m tall trees were placed, to recreate the typical

urban vegetation of a urban road. Only the road pavement was varied, leaving all the other parameters unvaried. Weather conditions are those of 21st of July 2014.

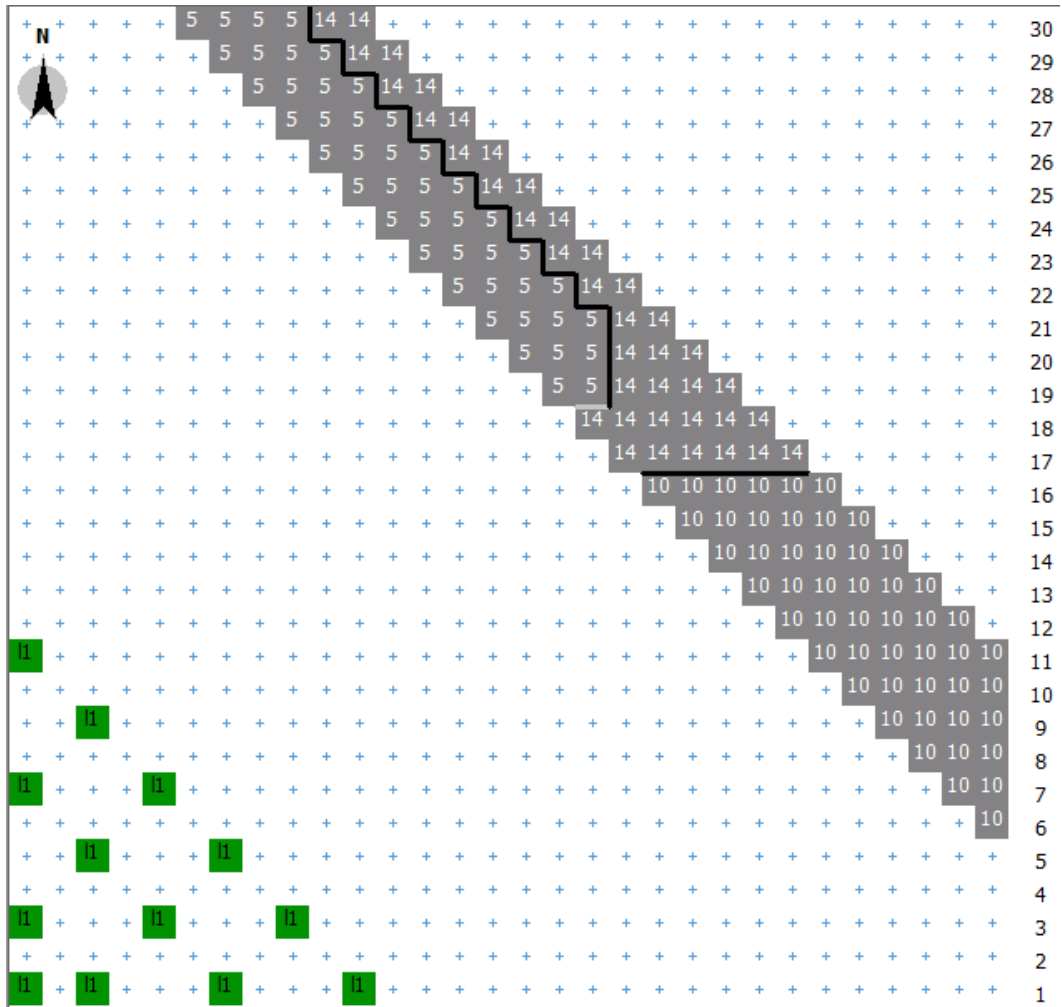


Figure 77: canyon geometry

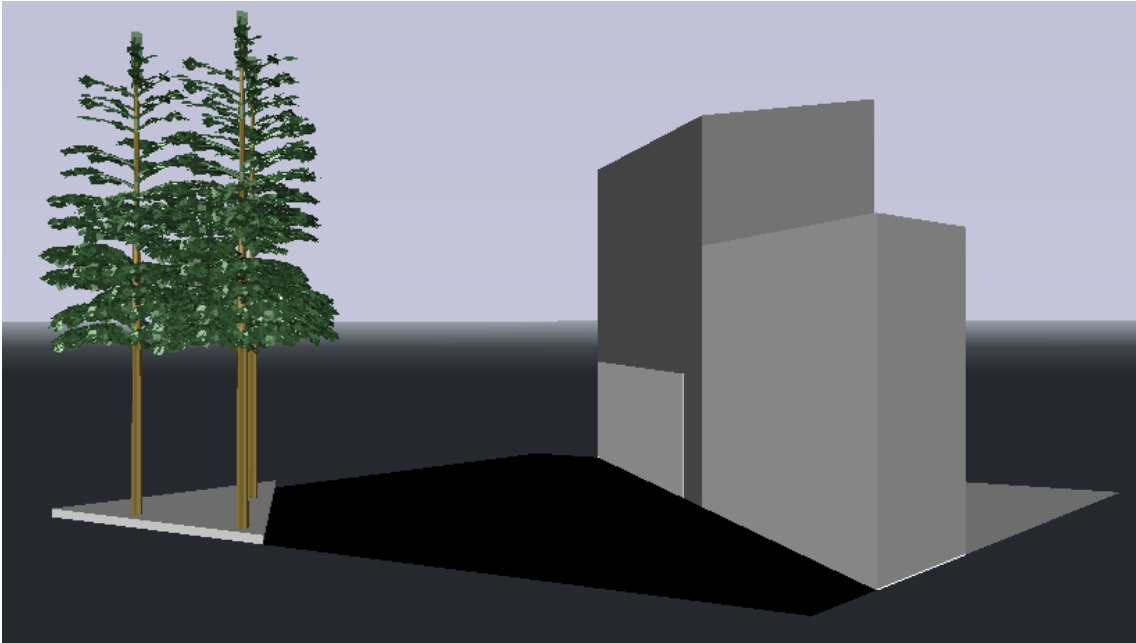


Figure 78: canyon 3D geometry

Five simulations were carried out by changing pavement materials:

- ACTUAL → measured asphalt Goldsmith
- C30 U → concrete C30 unpainted
- C30 P → concrete C30 yellow painted
- DBM U → Dense Bitumen Macadam unpainted
- DBM P → Dense Bitumen Macadam yellow painted

Atmospheric temperatures were extracted at 1 m from the ground. This height was considered to be representative of the air level affecting the thermal comfort. Following are the simulations results (see Tables 21-25).

ACTUAL	T surf [°C]	T atm [°C]
h 7.00	18.7	17.9
h 8.00	19.9	18.5
h 9.00	24.9	19.8
h 10.00	29.9	23
h 11.00	33.9	26
h 12.00	35.9	27.4
h 13.00	36.8	28.1
h 14.00	37	28.5
h 15.00	36.2	28.3

h 16.00	34.4	27.6
h 17.00	32.4	26.8
h 18.00	29.8	25.8
h 19.00	26.8	24.6
h 20.00	24.2	23.7
h 21.00	23	22.8
h 22.00	22	22
h 23.00	21.2	21.4
h 0.00	20.6	20.7
h 1.00	20.1	20.3
h 2.00	19.6	19.7
h 3.00	19.2	19.4
h 4.00	18.8	19
h 5.00	18.6	18.6
h 6.00	19	18.7

Table 21: actual material temperatures

C30 U	T surf [°C]	T atm [°C]
h 7.00	18.8	17.8
h 8.00	20.2	18.4
h 9.00	23.3	19.5
h 10.00	26.6	22.1
h 11.00	29.7	24.5
h 12.00	32	25.6
h 13.00	32.7	26.1
h 14.00	32.6	26.2
h 15.00	32	26
h 16.00	31.2	25.7
h 17.00	29.9	25.3
h 18.00	28.1	24.6
h 19.00	26	23.8
h 20.00	24	22.8
h 21.00	22.6	22
h 22.00	21.7	21.3
h 23.00	21	20.7
h 0.00	20.7	20.2
h 1.00	20.3	19.8
h 2.00	19.9	19.4
h 3.00	19.5	19.1

h 4.00	19.2	18.8
h 5.00	19.1	18.5
h 6.00	19.5	18.5

Table 22: unpainted concrete temperatures

C30 P	T surf [°C]	T atm [°C]
h 7.00	18.3	17.6
h 8.00	19.7	18
h 9.00	21.7	18.7
h 10.00	24.5	21.1
h 11.00	27	23.8
h 12.00	28.6	24.8
h 13.00	29.4	25.3
h 14.00	30	25.2
h 15.00	29.6	25
h 16.00	28.9	24.7
h 17.00	27.8	24.3
h 18.00	26.4	23.6
h 19.00	24.2	22.8
h 20.00	22.7	21.8
h 21.00	21.5	21
h 22.00	21	20.3
h 23.00	20.4	19.7
h 0.00	19.8	19.2
h 1.00	19.2	18.8
h 2.00	18.9	18.6
h 3.00	18.3	18.5
h 4.00	18	18.2
h 5.00	18.5	18
h 6.00	18.8	18

Table 23: painted concrete temperatures

DBM U	T surf [°C]	T atm [°C]
h 7.00	19	18.1
h 8.00	20.4	18.8
h 9.00	24	19.9
h 10.00	27.8	22.5
h 11.00	31.3	24.9
h 12.00	33	26
h 13.00	34	26.6
h 14.00	33.8	26.6
h 15.00	33.2	26.4
h 16.00	32.2	26.1
h 17.00	30.8	25.6

h 18.00	28.8	25
h 19.00	26.8	24.1
h 20.00	24	23.1
h 21.00	22.8	22.3
h 22.00	22	21.6
h 23.00	21.5	21
h 0.00	21	20.6
h 1.00	20.6	20.1
h 2.00	20	19.7
h 3.00	19.4	19.4
h 4.00	19	19.1
h 5.00	19.3	18.8
h 6.00	19.6	18.8

Table 24: unpainted macadam temperatures

DBM P	T surf [°C]	T atm [°C]
h 7.00	18.4	17.3
h 8.00	19.8	17.9
h 9.00	21.9	19
h 10.00	25.3	21.6
h 11.00	28.4	24
h 12.00	30.1	25.1
h 13.00	30.7	25.7
h 14.00	30.5	25.8
h 15.00	30	25.6
h 16.00	29.1	25.3
h 17.00	27.9	24.9
h 18.00	26.5	24.2
h 19.00	24.8	23.4
h 20.00	23	22.3
h 21.00	22	21.5
h 22.00	21.3	20.8
h 23.00	20.6	20.2
h 0.00	20.1	19.7
h 1.00	19.7	19.3
h 2.00	19.3	18.9
h 3.00	18.9	18.6
h 4.00	18.6	18.3
h 5.00	18.5	18
h 6.00	19	18

Table 25: painted macadam temperatures

Comparing the results:

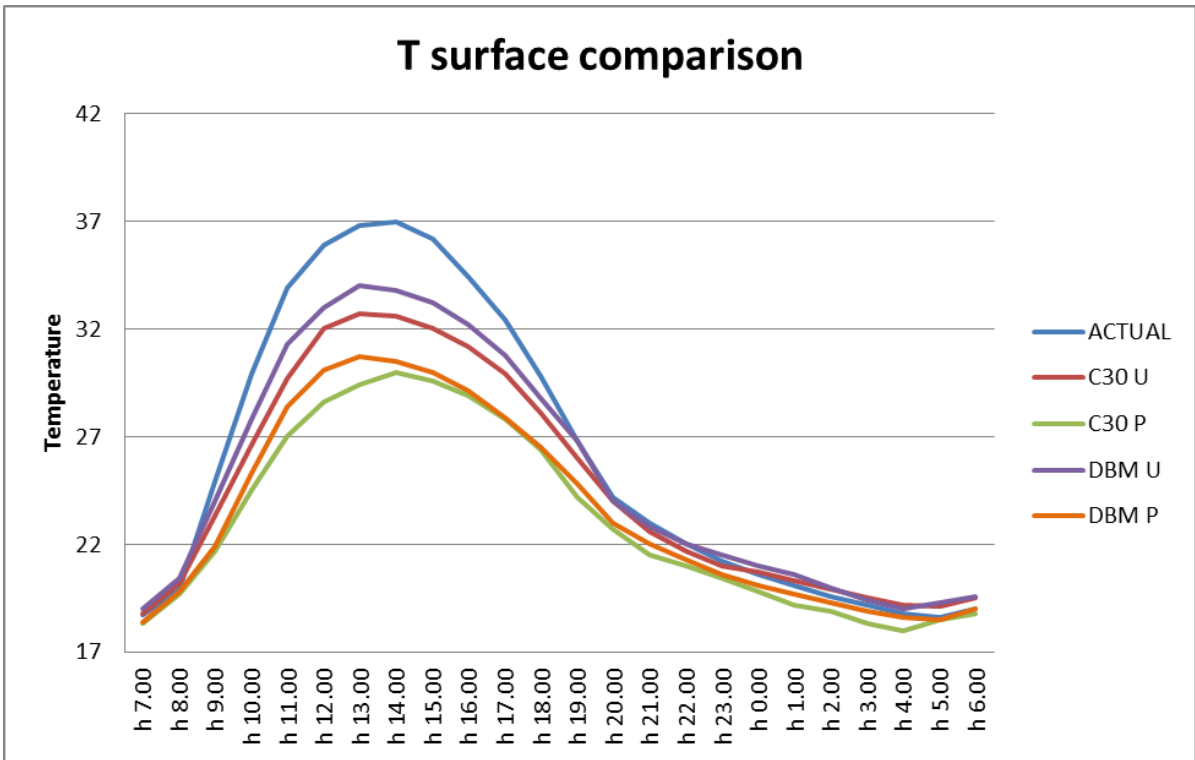


Figure 79: urban canyon surface temperatures

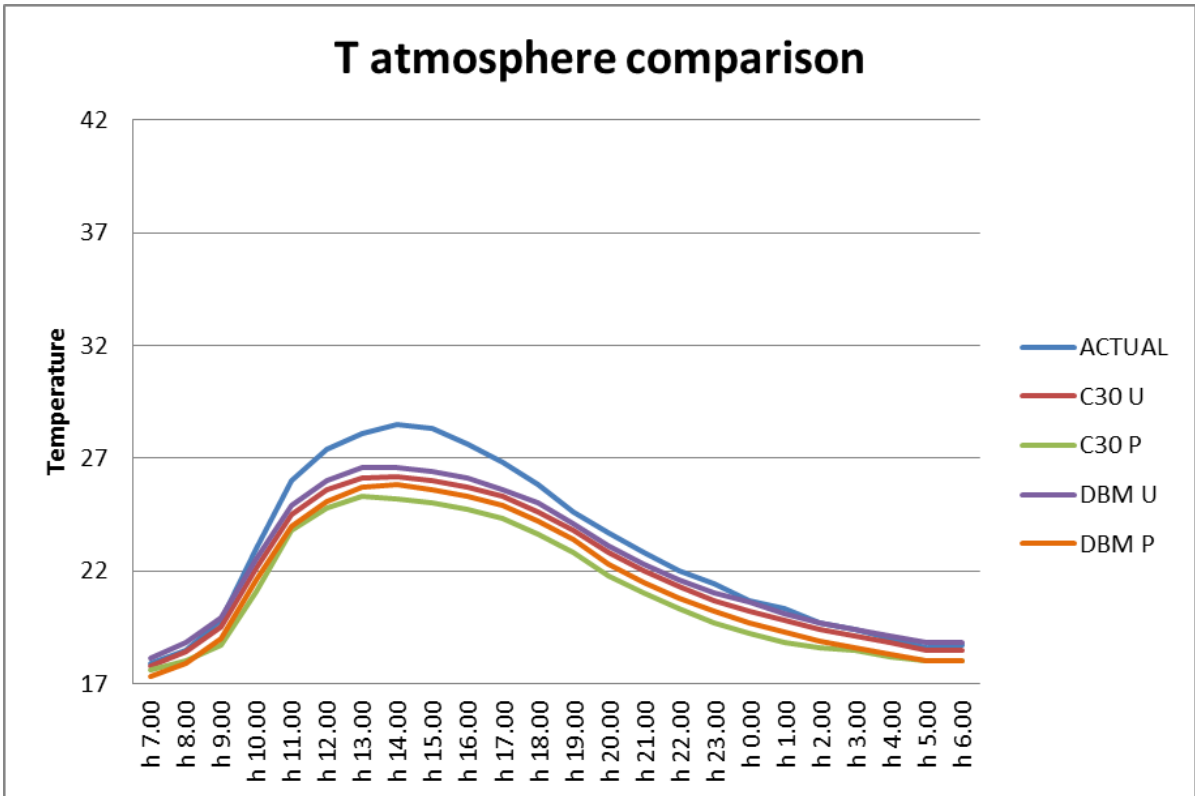


Figure 80: urban canyon atmospheric temperatures

From the displayed data it can be seen how all the materials substituted have shown an improvement compared to the real scenario (ACTUAL). In both the graphs, Goldsmith Road asphalt has the worst behaviour.

Regarding the surface comparison graph, temperature increases with a similar rate between all the surfaces. From 8:00 to 11:00 temperature increasing rates change, growing steeply, although with different slopes. In fact, the real surface (asphalt Goldsmith Road) increases of 14°C, DBM U of 10.9°C, C30 U of 9.5°C, DBM P of 8.6°C, C30 P of 7.3°C. After 11:00 temperature keeps growing, even tough with a smaller rate, until reaching the peak at 14:00. Then cooling phase begins with a steep drop in temperature until 20:00, when the slopes are reduced. At 20:00 cooling trends become similar, although shifted, until 4:00. After this point temperature begins to grow again.

Concrete C30 yellow painted presents the best performance, with a peak temperature of 30°C at 14:00, whilst real asphalt reaches a peak of 37°C (14:00). Temperature difference is 7°C. Considering the fact that concrete C30 painted also shows the lowest increasing rate during the heating up phase, it can be considered the best choice in this case. Also Dense Bitumen Macadam yellow painted shows a good thermal performance. It reaches a temperature peak of 30.7 °C at 13:00, just 0.7°C more than C30 P, and a 6.3°C difference with Goldsmith asphalt. Nevertheless, the DBM P heat up rate is faster than C30. Concrete C30 and Dense Bitumen Macadam unpainted present similar trends. Their reach respectively a peak of 32.7°C and 34°C, so 4.3°C and 3°C cooler than Goldsmith asphalt (tab.26). It can be noticed how the paint shifts the peak temperature from 13:00 to 14:00.

SURFACE T	peak [°C]	ΔT [°C]
ACTUAL	37	0
DBM UNP.	34	-3
C30 UNP.	32.7	-3.3
DBM PAINT.	30.7	-6.3
C30 PAINT.	30	-7

Table 26: differences in peak with actual material

As expected, the atmosphere temperature comparison graph shows a more uniform situation. All the curves are more flattened and close among them. Like the surface temperature trends, all the atmosphere temperature curves present an initial heating

phase, from 7:00 to 9:00. Subsequently, a steeper phase comes until 11:00. Cooling phases are quite regular, without any significant slope change.

The only curve evidently spaced from each other is the Goldsmith Road asphalt. It reaches a peak of 28.5°C at 14:00. The closest material is the Dense Bitumen Macadam unpainted, with a peak of 26.6°C and a difference of 1.9°C respect of the real asphalt. Temperature peak is reached at 14:00 for the Goldsmith asphalt and at 13:00 for all the others materials (tab.27). Comparing the two graphs, a clear correspondence can be observed. In fact, curves for both the situations are placed in the same mutual order, proving that surface temperature affects air temperature directly.

ATMOSPHERE T	peak [°C]	ΔT [°C]
ACTUAL	28.5	0
DBM UNP.	26.6	-1.9
C30 UNP.	26.2	-2.3
DBM PAINT.	25.8	-2.7
C30 PAINT.	25.3	-3.2

Table 27: differences in peak with actual material

4.1.5 Heat basin simulations

Heat basin scenario was recreated in the most simple way, in order to make easy to figure out the effects of the pavements changes. The geometry was conceived to be similar to the real situation of the Maudslay car parking (figg.81,82). Investigated surface was confined by buildings with different heights on each side, except for the lower one, where a 2 m tall wall was reproduced. Heights choose were 2 m, 5 m, 7 m and 12 m. Only the basin pavement was varied, leaving all the other parameters identical. Weather conditions are those of 21st of July 2014.

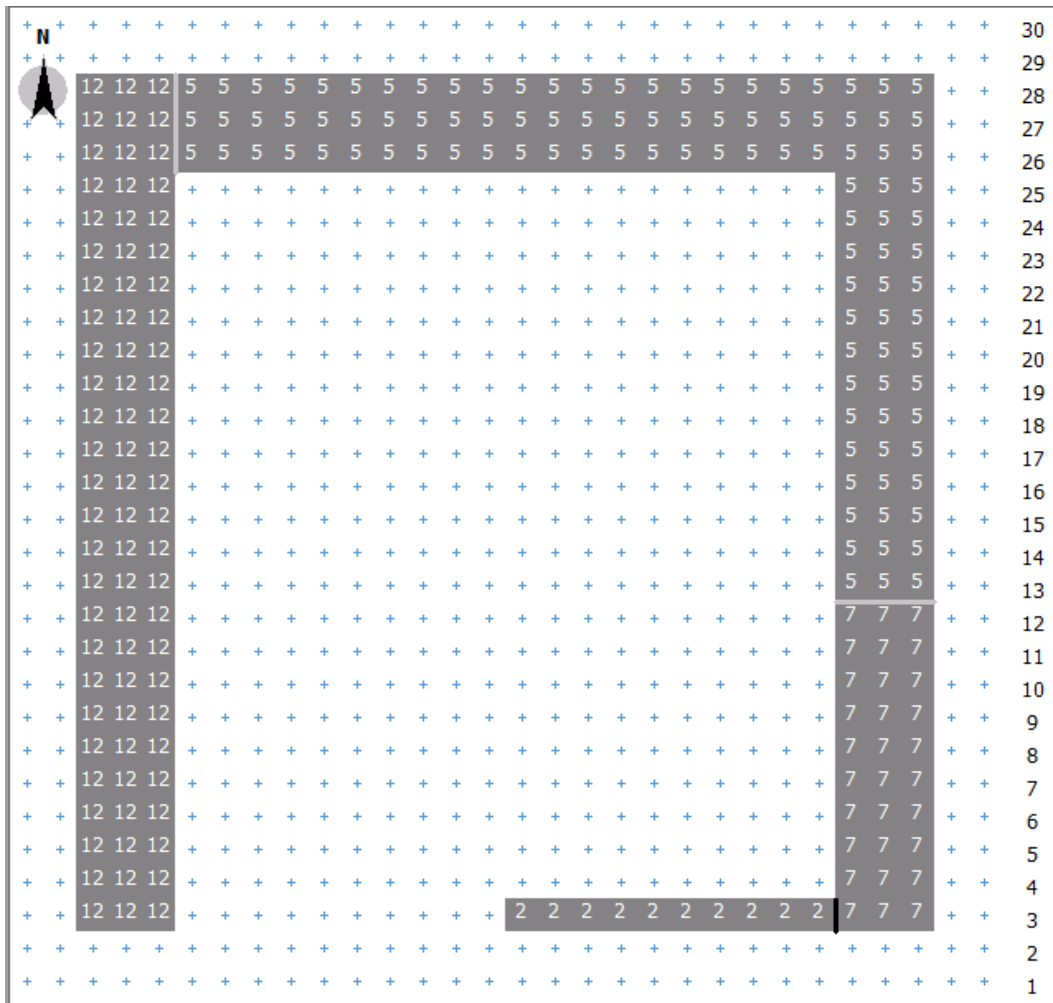


Figure 81: heat basin area

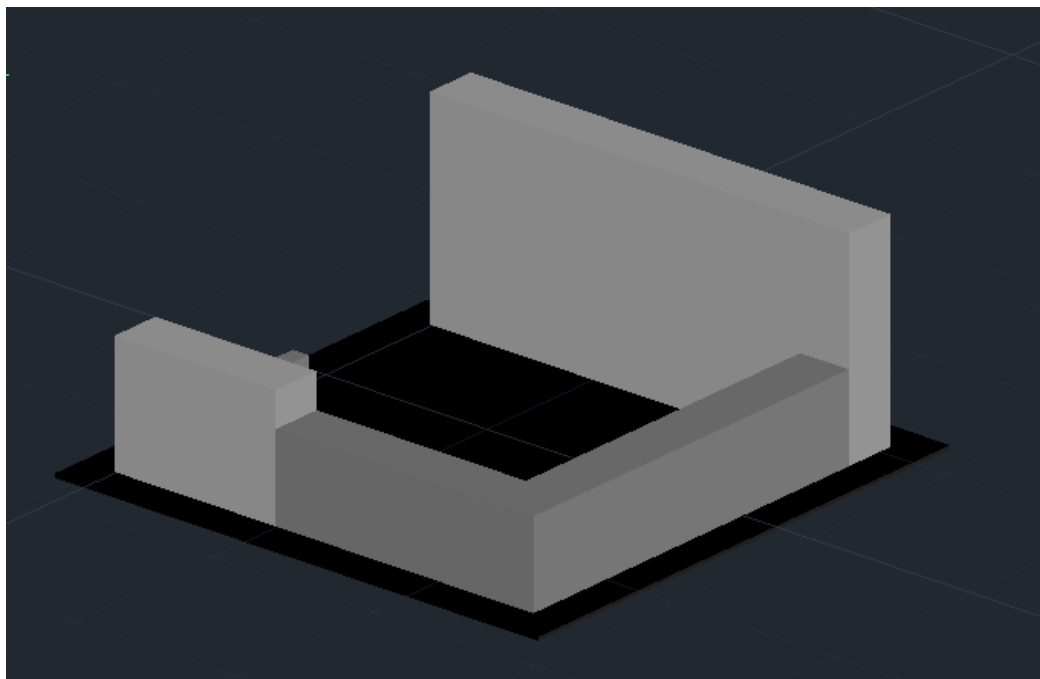


Figure 82: heat basin 3D geometry

Ten simulations were carried out by changing pavement materials:

- ACTUAL → measured asphalt Maudslay
- WHITE BRICK → tested white brick
- RED BRICK → tested red brick
- BLACK BRICK → tested black brick
- YELLOW BRICK → tested yellow brick
- DBM U → Dense Bitumen Macadam unpainted
- DBM P → Dense Bitumen Macadam yellow painted
- C30 U → concrete C30 unpainted
- C30 P → concrete C30 yellow painted
- GRANITE → measured granite sidewalk

Atmospheric temperatures were extracted at 1 m from the ground. This height was considered to be representative of the air level affecting the thermal comfort. Following are the simulations results (see Tables 28-37).

ACTUAL	T surf [°C]	T atm [°C]
h 7.00	21.3	18.9
h 8.00	23.9	19.7
h 9.00	26.6	20.9
h 10.00	30.5	24.3
h 11.00	34.7	27.9
h 12.00	38.4	30.2
h 13.00	40.3	31.8
h 14.00	39.6	32.1
h 15.00	38.1	31.7
h 16.00	35.9	31.2
h 17.00	33.7	30.7
h 18.00	31.9	30
h 19.00	30.3	29.2
h 20.00	28.5	28.2
h 21.00	27.3	27.3
h 22.00	26.4	26.5
h 23.00	25.7	25.8
h 0.00	25	25.1
h 1.00	24.4	24.5
h 2.00	23.9	24
h 3.00	23.5	23.5
h 4.00	23	23.1

h 5.00	22.8	22.7
h 6.00	23.5	22.6

Table 28: actual material temperatures

WHITE B	T surf [°C]	T atm [°C]
h 7.00	20.4	18
h 8.00	21.7	18.7
h 9.00	23.1	19.5
h 10.00	25.5	21.5
h 11.00	28.3	25.5
h 12.00	30.5	27.7
h 13.00	32.5	29
h 14.00	32.6	29.5
h 15.00	32.3	29.1
h 16.00	31.5	28.7
h 17.00	30.5	28.3
h 18.00	29.3	27.7
h 19.00	28.2	27.2
h 20.00	27.1	26.3
h 21.00	26.3	25.7
h 22.00	25.7	25
h 23.00	25.1	24.5
h 0.00	24.6	24
h 1.00	24.2	23.7
h 2.00	23.8	23.4
h 3.00	23.4	23
h 4.00	23	22.6
h 5.00	22.8	22.2
h 6.00	23.1	22.1

Table 29: white brick temperatures

RED B	T surf [°C]	T atm [°C]
h 7.00	21.3	18.8
h 8.00	23.6	19.6
h 9.00	26	20.8
h 10.00	29.6	23.7
h 11.00	33.5	27.3
h 12.00	37	29.6
h 13.00	39	31.2
h 14.00	38.5	31.5
h 15.00	37.2	31
h 16.00	35.3	30.5
h 17.00	33.4	30
h 18.00	31.8	29.3
h 19.00	30.3	28.7

h 20.00	28.6	27.7
h 21.00	27.6	26.8
h 22.00	26.7	26
h 23.00	26.1	25.4
h 0.00	25.4	24.7
h 1.00	24.9	24.1
h 2.00	24.4	23.6
h 3.00	24	23.1
h 4.00	23.6	22.7
h 5.00	23.4	22.3
h 6.00	23.9	22.2

Table 30: red brick temperatures

BLACK B	T surf [°C]	T atm [°C]
h 7.00	21.5	18.9
h 8.00	24.1	19.7
h 9.00	26.8	20.9
h 10.00	30.7	24.3
h 11.00	34.9	27.9
h 12.00	38.6	30.2
h 13.00	40.6	31.8
h 14.00	39.9	32.1
h 15.00	38.4	31.8
h 16.00	36.2	31.3
h 17.00	33.9	30.7
h 18.00	32.2	30
h 19.00	30.6	29.2
h 20.00	28.9	28.2
h 21.00	27.7	27.3
h 22.00	26.9	26.5
h 23.00	26.2	25.8
h 0.00	25.5	25.2
h 1.00	25	24.6
h 2.00	24.5	24
h 3.00	24	23.6
h 4.00	23.6	23.1
h 5.00	23.4	22.7
h 6.00	24.1	22.6

Table 31: black brick temperatures

YELLOW B	T surf [°C]	T atm [°C]
h 7.00	21	17.9
h 8.00	23.1	18.6
h 9.00	25.3	19.8
h 10.00	28.7	23.1

h 11.00	32.4	26.7
h 12.00	35.7	29
h 13.00	37.7	30.6
h 14.00	37.3	30.9
h 15.00	36.2	30.6
h 16.00	34.5	30.2
h 17.00	32.7	29.6
h 18.00	31.2	29
h 19.00	29.7	28.2
h 20.00	28.2	27.2
h 21.00	27.1	26.3
h 22.00	26.3	25.5
h 23.00	25.7	24.8
h 0.00	25.1	24.4
h 1.00	24.5	23.9
h 2.00	24.1	23.5
h 3.00	23.6	22.9
h 4.00	23.3	22.5
h 5.00	23	22.3
h 6.00	23.6	22

Table 32: yellow brick temperatures

DBM U	T surf [°C]	T atm [°C]
h 7.00	21.9	18.9
h 8.00	24.3	19.7
h 9.00	26.9	20.8
h 10.00	30.6	24.2
h 11.00	34.8	27.8
h 12.00	38.4	30.1
h 13.00	40.3	31.7
h 14.00	39.6	32
h 15.00	38.1	31.7
h 16.00	36.1	31.2
h 17.00	34	30.7
h 18.00	32.4	30
h 19.00	30.8	29.2
h 20.00	29	28.2
h 21.00	27.9	27.3
h 22.00	27	26.5
h 23.00	26.2	25.8
h 0.00	25.5	25.1
h 1.00	24.9	24.5
h 2.00	24.4	24
h 3.00	23.9	23.5

h 4.00	23.5	23.1
h 5.00	23.3	22.7
h 6.00	24	22.6

Table 33: unpainted macadam temperatures

DBM P	T surf [°C]	T atm [°C]
h 7.00	21.3	18.1
h 8.00	23.5	18.9
h 9.00	25.9	20
h 10.00	29.4	23.4
h 11.00	33.4	27
h 12.00	36.8	29.3
h 13.00	38.7	30.9
h 14.00	38.2	31.1
h 15.00	37	30.9
h 16.00	35.2	30.4
h 17.00	33.4	29.9
h 18.00	31.9	29.2
h 19.00	30.4	28.4
h 20.00	28.8	27.4
h 21.00	27.7	26.5
h 22.00	26.8	25.7
h 23.00	26.1	25
h 0.00	25.5	24.3
h 1.00	24.9	23.8
h 2.00	24.4	23.2
h 3.00	23.9	22.8
h 4.00	23.5	22.3
h 5.00	23.3	21.9
h 6.00	23.8	21.8

Table 34: painted macadam temperatures

C30 U	T surf [°C]	T atm [°C]
h 7.00	21.7	18.5
h 8.00	23.9	19.3
h 9.00	26.2	20.4
h 10.00	29.6	23.8
h 11.00	33.5	27.4
h 12.00	36.8	29.7
h 13.00	38.8	31.3
h 14.00	38.5	31.6
h 15.00	37.3	31.3
h 16.00	35.7	30.8
h 17.00	33.9	30.3

h 18.00	32.4	29.6
h 19.00	31	28.8
h 20.00	29.5	27.9
h 21.00	28.4	27
h 22.00	27.6	26.2
h 23.00	27	25.4
h 0.00	26.3	24.8
h 1.00	25.8	24.2
h 2.00	25.3	23.7
h 3.00	24.9	23.2
h 4.00	24.5	22.8
h 5.00	24.2	22.4
h 6.00	24.7	22.3

Table 35: unpainted concrete temperatures

C30 P	T surf [°C]	T atm [°C]
h 7.00	21	17.8
h 8.00	23.2	18.6
h 9.00	25.5	19.7
h 10.00	28.9	23.1
h 11.00	32.6	26.6
h 12.00	36	29
h 13.00	37.9	30.6
h 14.00	37.6	30.9
h 15.00	36.6	30.6
h 16.00	35	30.1
h 17.00	33.3	29.6
h 18.00	31.9	29
h 19.00	30.5	28.1
h 20.00	29	27.2
h 21.00	28	26.3
h 22.00	27.2	25.5
h 23.00	26.5	24.8
h 0.00	25.9	24.1
h 1.00	25.4	23.5
h 2.00	24.9	23
h 3.00	24.4	22.5
h 4.00	24	22.1
h 5.00	23.8	21.7
h 6.00	24.3	21.6

Table 36: painted concrete temperatures

GRANITE	T surf [°C]	T atm [°C]
h 7.00	21	17.6
h 8.00	22.8	18.3
h 9.00	24.6	19.4

h 10.00	27.4	22.7
h 11.00	30.5	26.3
h 12.00	33.4	28.6
h 13.00	35.4	30.2
h 14.00	35.4	30.5
h 15.00	34.8	30.2
h 16.00	33.6	29.8
h 17.00	32.2	29.3
h 18.00	30.9	28.7
h 19.00	29.8	27.9
h 20.00	28.5	26.9
h 21.00	27.6	26
h 22.00	26.9	25.2
h 23.00	26.3	24.5
h 0.00	25.8	23.9
h 1.00	25.3	23.3
h 2.00	24.9	22.8
h 3.00	24.5	22.3
h 4.00	24.1	21.8
h 5.00	23.8	21.5
h 6.00	24.2	21.3

Table 37: granite temperatures

Comparing the results:

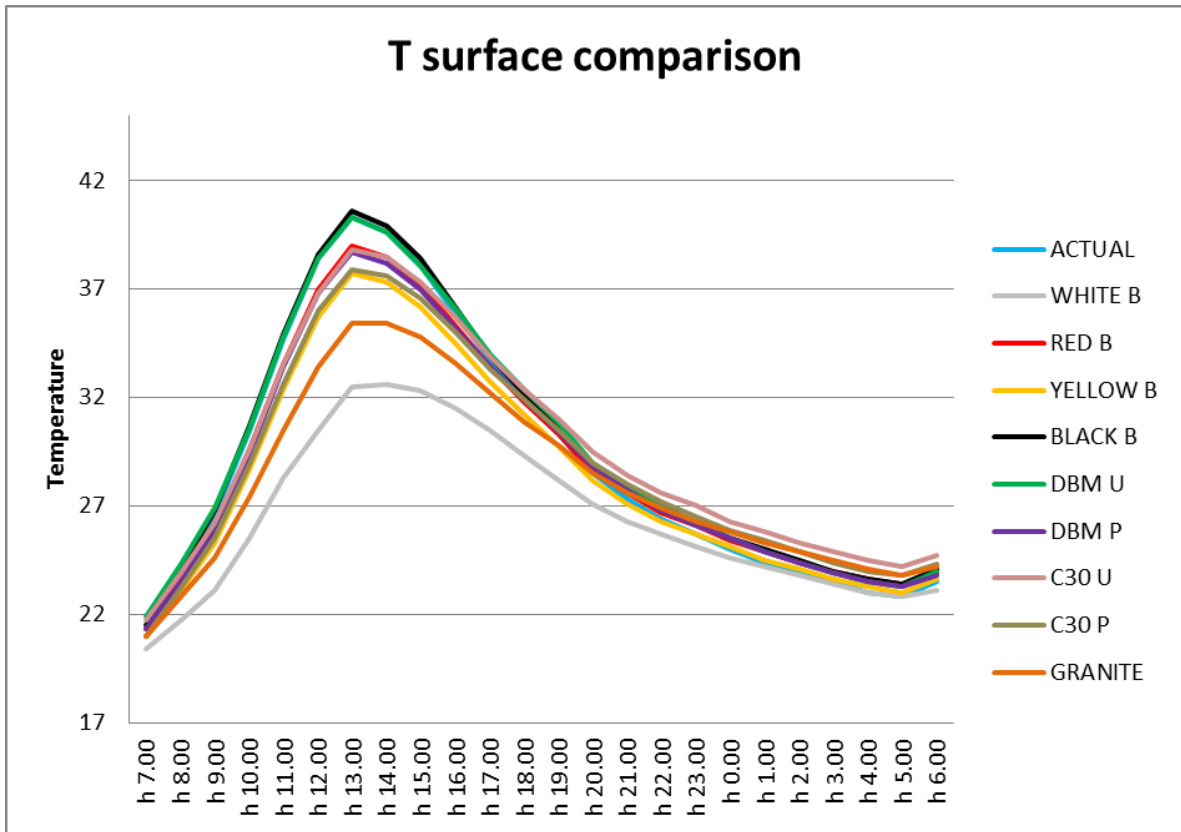


Figure 83: heat basin surface temperatures

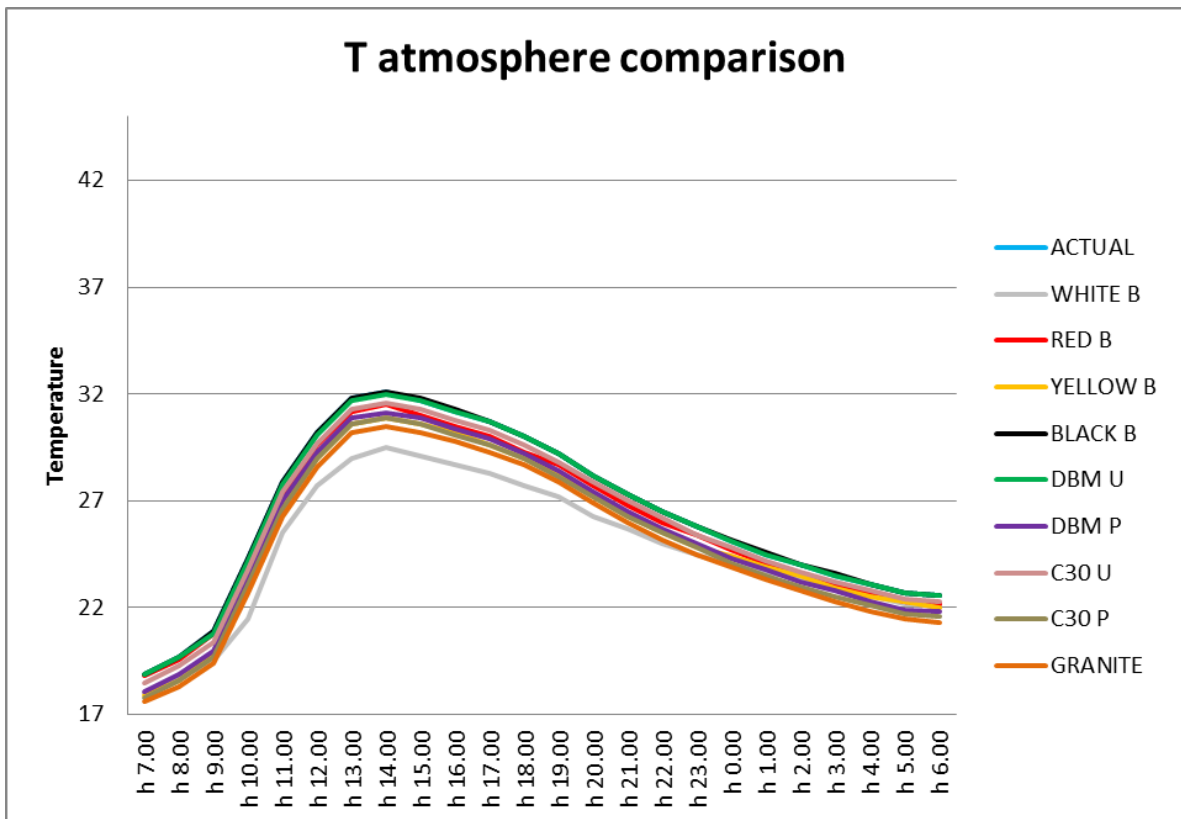


Figure 84: heat basin atmospheric temperatures

From the data displayed it can be seen how all the materials substituted have shown an improvement respect of the real scenario (ACTUAL). In both the graphs, Maudslay car parking asphalt has the worst behaviour.

Regarding the surface comparison graph (fig.83), temperature increases with a similar rate between all the surfaces. The worst material in terms of temperature performance is the black brick. It reaches a temperature peak of 40.6°C at 13:00. The actual material (Maudslay car parking asphalt) reaches a peak of 40.3°C at 13:00. It can be seen how white bricks and granite are the coolest materials. Their peaks are respectively of 32.6°C and 35.4°C, so 7.7°C and 4.9°C of difference with the actual material, proving their good thermal performance. They both could be employed as an effective solution against overheating given by UHI. The others trends have an intermediate performance between the real material and the granite, shown in table 38.

SURFACE T	peak [°C]	ΔT [°C]
BLACK BRICK	40.6	0.3
ACTUAL	40.3	0
DBM UNP.	40.3	0
RED BRICK	39	-1.3
C30 UNP.	38.8	-1.5
DBM PAINT.	38.7	-1.6
C30 PAINT.	37.9	-2.4
YELLOW BRICK	37.7	-2.6
GRANITE	35.4	-4.9
WHITE BRICK	32.6	-7.7

Table 38: differences in peak with actual material

Atmosphere comparison curves (fig.84) are really close among them. As previously verified, the worst performance is represented by the black brick surface, with a peak of 32.1°C at 14:00. The best cooling trend is the white brick surface, that reaches a peak of 29.5°C at 14:00: a difference of 2.6°C with Maudslay parking asphalt, that has the same peak temperature of the black brick (32.1°C at 14:00) (tab.39). Comparing the two graphs, a clear correspondence can be observed. In fact, curves for both the situations are placed in the same mutual order, proving that surface temperature affects air temperature directly.

ATMOSPHERE T	peak [°C]	ΔT [°C]
BLACK BRICK	32.1	0
ACTUAL	32.1	0
DBM UNP.	32	-0.1
C30 UNP.	31.6	-0.5
RED BRICK	31.5	-0.6
DBM PAINT.	31.1	-1
C30 PAINT.	30.9	-1.2
YELLOW BRICK	30.9	-1.2
GRANITE	30.5	-1.6
WHITE BRICK	29.5	-2.6

Table 39: difference in peak with actual material

Comparing the urban canyon and the heat basin, it can be seen how, in both surface and atmosphere results, the heat basin temperatures are higher than those of urban canyon. In particular, the warmest heat basin material (black brick) reached a peak of 40.6°C in surface temperature and a peak of 32.1°C in atmosphere temperature, whilst the warmest urban canyon material (actual Goldsmith Road asphalt) reached a peak of 37°C in surface temperature and a peak of 28.5°C in atmosphere temperature (fig.76). The two differences, amounting to 3.6°C, are likely due to the physical conformation of the scenarios. In fact, the heat basin operates like a big energy storage. Sunrays hit the horizontal surfaces and reflect them in every direction. There will be a part that buildings wall reflect back to the pavement, increasing the temperature. In addition also buildings store energy and emitting it: this infrared energy will be absorbed by the air and the surfaces. Finally buildings, acting like obstacles, prevent the natural wind circulation causing a delay in air and surfaces cooling process. On the contrary, urban canyon has a bigger air recirculation respect of the heat basin, thanks to the wind flow that cooling down the surfaces. Considering the surface graphs and assuming as reference point the temperature of 27°C, it can be noticed that all the canyon materials reach that point between 17:00 and 19:00, while all the heat basin materials do it between 20:00 and 23:00. Similarly to the surface, this fact is noticeable in the atmosphere graphs. Assuming as reference point the temperature of 22°C, is evident how in the canyon environment this point is reached between 20:00 and 22:00, while in the heat basin environment considerably later, even some materials never reach it (fig.85). This shift in time is one of the most important factors producing an Urban Heat Island, as it prevent the natural nocturnal air and surface cooling down.

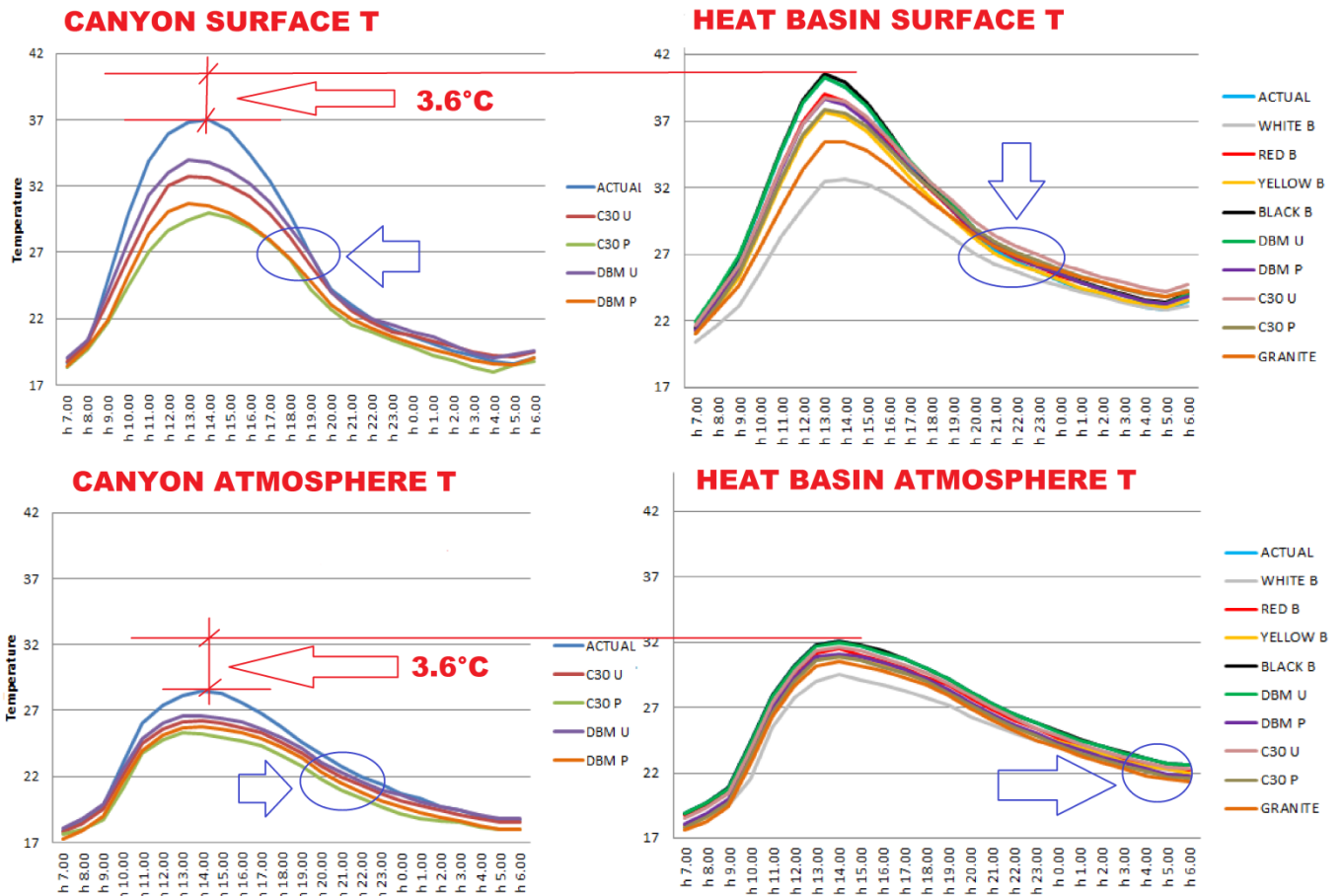


Figure 85: heat basin and urban canyon comparison

Taking in consideration the best material for the two situations, it is believed to be interesting a comparison between surface and atmosphere temperature trends.

Regarding the canyon scenario, the comparison on these parameters for the C30 painted is shown in figure 86. Considering the heat basin scenario, the same comparison is shown in figure 87 for the white brick.

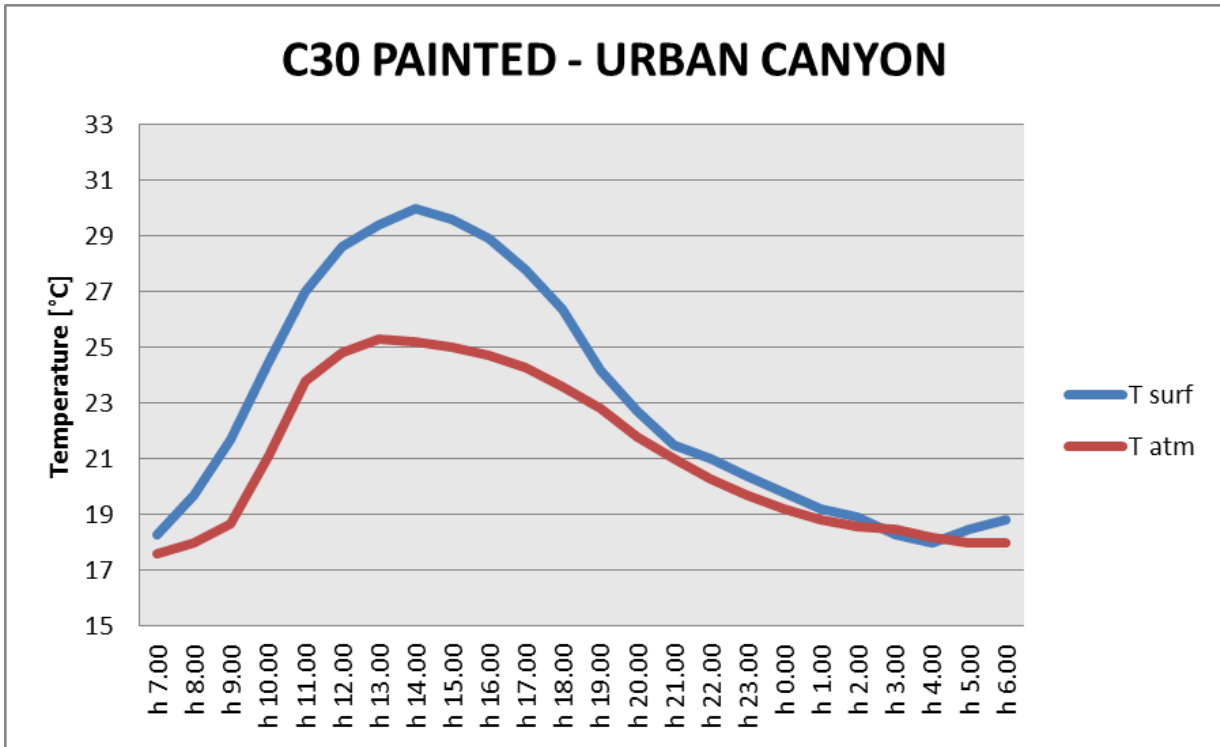


Figure 86: C30 P surface and atmosphere temperature comparison

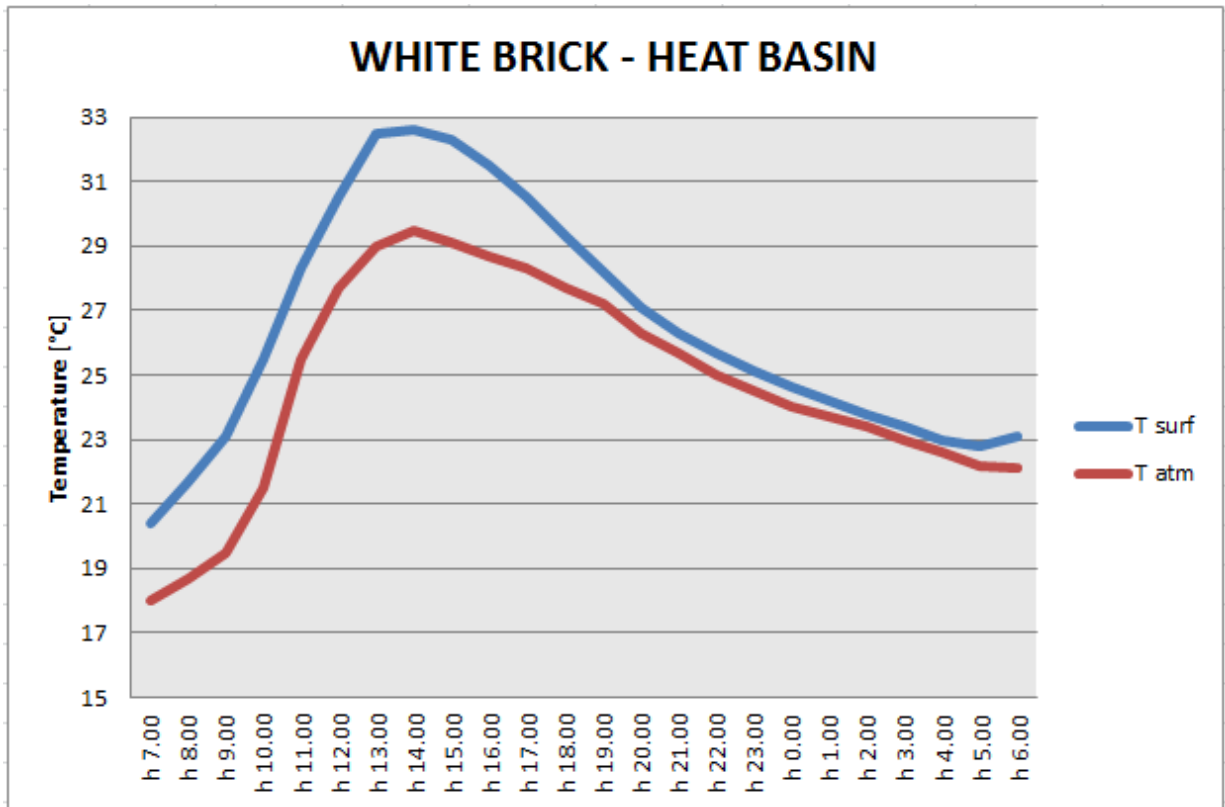
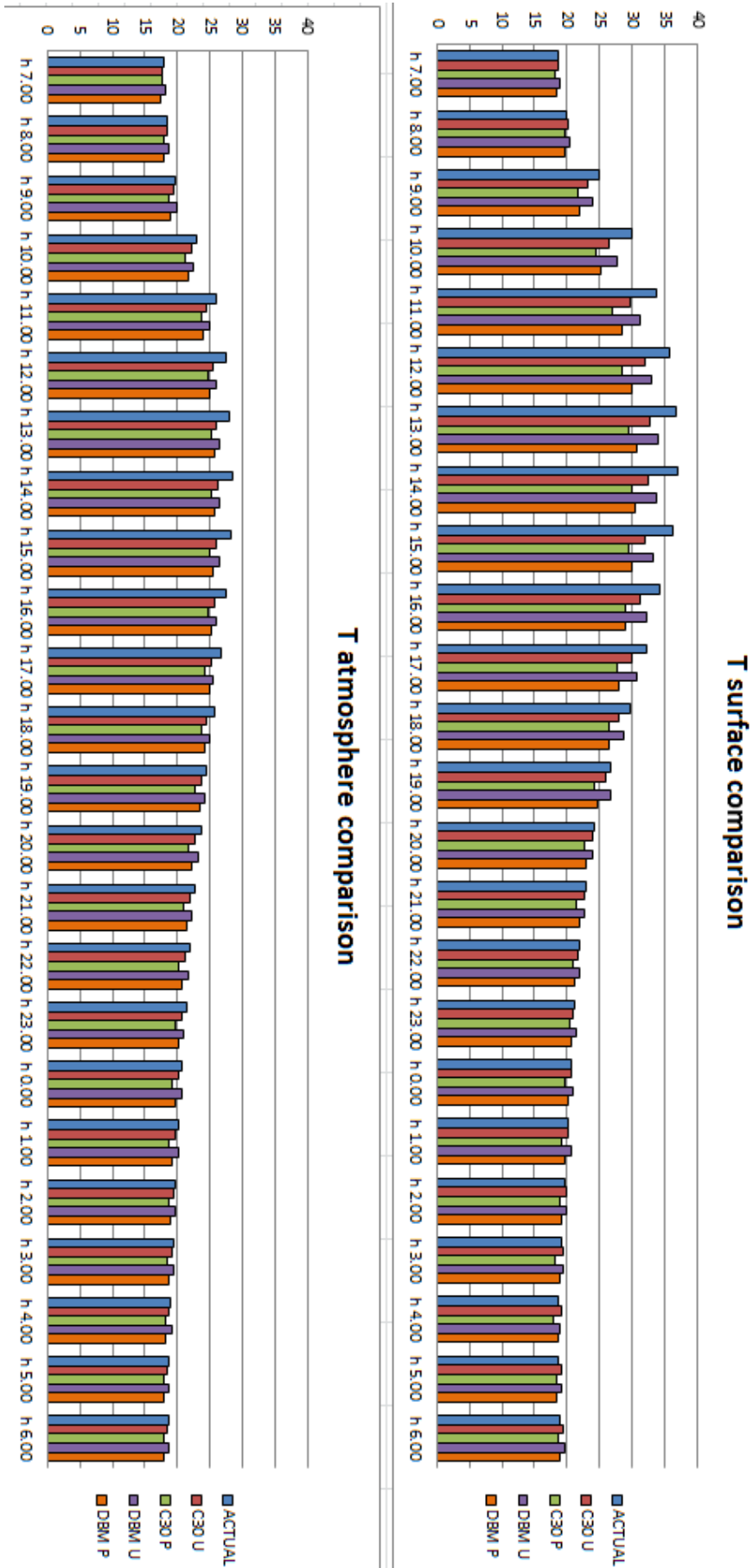


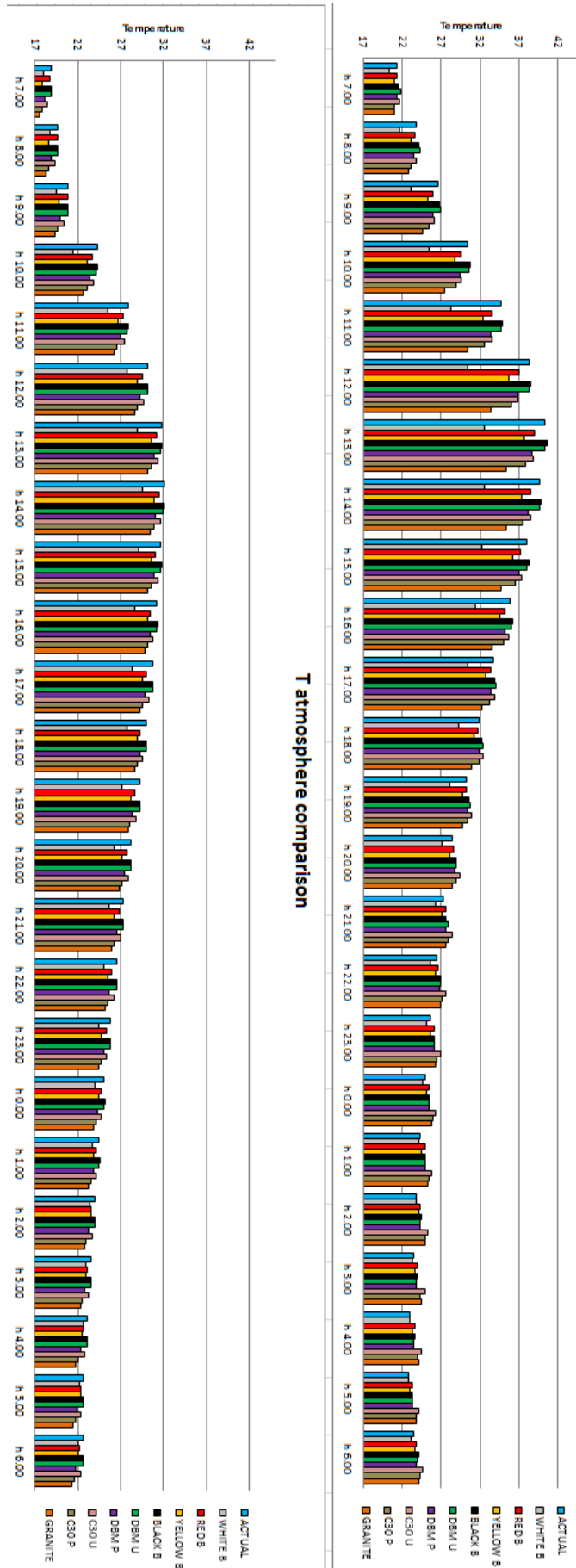
Figure 87: white brick surface and atmosphere comparison

The graphs show a bigger area between temperature and surface trends for the C30 painted, especially in the peak zone. In this point the maximum temperature difference is 4.7°C, while for the white brick the peak difference is 3.1°C. This fact could be due to bigger air recirculation, bringing cool air more frequently inside the canyon. On the contrary, in the heat basin air and surface temperatures tend to remain more similar. For both the scenarios, surface and atmosphere temperatures trends are close in the cooling down phase. This fact is significant because it means that the materials are good energy emitters, as they create a temperature balance between surfaces and air, storing a little part of heat and releasing the bigger part.

4.1.6 Annex 1: urban canyon simulations bar charts



4.1.7 Annex 2: urban heat basin simulations bar charts



CONCLUSIONS

The number of people living in cities is increasing, carrying all the effects related to urbanization. The urban heat island is certainly one these and it represents a concern capturing the attention of people worldwide. The phenomenon brings consequences in different sectors: it negatively affects sensitive subjects as children, elderly people and sick people; it increases the energy demand to cool down buildings; it gradually decreases the air and water quality. Besides, UHIs have been indirectly related to climate change due to their contribution to the greenhouse effect, and therefore, to global warming. A good mitigation strategy is to make a clever urban development planning, also acting on pavements and component materials.

Different urban surfacing materials have been tested, in order to evaluate their thermal performance in terms of Urban Heat Island.

The research was divided into three fundamental parts:

- Laboratory testing
- External work
- Simulation modelling

In the laboratory testing part, 4 concrete interblocks were analysed, respectively black, white, red and yellow coloured. Emissivity evaluations were carried out with two methods: the thermal camera manual's procedure and the thermocouples procedure. Results showed very similar emissivity values, proving the consistency and effectiveness of both methods. Only the white sample presented a 4% of difference. This discrepancy is likely due to the shiny paint on the surface that make the thermic photo acquisition more dependent on the little differences of the enlightenment conditions in the room. Considering the validity of both the procedures, it can be concluded that the choice has to be taken depending on the particular case. In an external situation can be more practical and effective to use the thermocouples: in this way the operator avoids wasting time in waiting that the same temperature between tape and surface is reached. In addition a thermocouple can be installed permanently on the surface recording the temperature trend with a data logger, making the measurements campaign more complete and accurate. On the other hand, in a controlled environment like a laboratory, thermal camera manual's method can result more indicate, as it avoid

thermocouples use and data logger set up. For both procedures, before beginning the data acquisition, is really important to check if the temperature difference between investigated surface and atmosphere is at least 20°C, otherwise the results can be inaccurate.

Focusing on the emissivity values, the two procedures worked out values ranging between 0.92 and 0.97. It can be seen how this parameter is really close among the 4 samples, and how it is big for the yellow one (0.96-0.97) compared to the red one (0.93-0.94). This fact is an indication of the little influence the colour has on the emissivity, in contrast to a maybe more obvious prediction of dependence between them. What can be deduced is that the component material and internal structure affect emissivity the most. Nonetheless, albedo had not been assessed. Probably the brick with the white shiny painted surface has a good overall thermal performance, making this pavement a good solution in mitigating UHI. For more information is recommended to consult Ricky Ashra's thesis work [53].

With the aim of getting a good understanding of the bricks thermal behaviour, heat releasing curves have been recorded. To do that, samples were heated for 2 hours and then left cooling down. Using the thermal camera and the thermocouples, bricks temperatures have been measured both on the surface and internally. From the resulting curves it can be seen how the black sample has had the worst thermal performance, the white one the best performance, the red and yellow ones very similar performance. This fact suggests that strong colours like black and white can influence the thermal behaviour significantly, while intermediate colours like red and yellow present pretty identical trends. Also the effect of shiny paint is clear: it increased the amount of reflected energy from the white brick, improving its thermal performance. These last statements on the colour can match the previous deductions: colour influences the overall thermal performance of surfaces, as well as the component material (e.g. concrete, asphalt). In order to get a complete and exhaustive knowledge of the investigated material, it is necessary to gather all the information derived from the emissivity and albedo measurements and from the temperature readings, and subsequently build up a description. None of these parameters can describe a material individually.

Another fact to take in consideration is the little deviation between the thermal camera and thermocouples surface temperature readings. The most likely reason of this is the disturbance given by the infrared lamp, unable to heat the bricks in a adequately

uniform way, thus the thermocouples reading are probably to be considered more correct. In the first 30' of the heating phase the difference between thermocouples and thermal camera measured temperature is not negligible. This gap is due to the too low samples surfaces temperature, that make the thermal camera readings wrong. The user manual call for a 20°C difference between surface and environment.

External work part consisted in investigating the existing pavements thermal parameters in order to analyse the actual situation and to use them in the modelling. Four surfaces were chosen: the asphalt Maudslay building car parking, the concrete bricks sidewalk, the granite sidewalk and the asphalt Goldsmith Road. Emissivity evaluation was conducted using the thermal camera. Results showed a typical situation with emissivities of 0.97 for the Maudslay building car parking asphalt, 0.91 for the sidewalk concrete bricks, 0.93 for the sidewalk granite, 0.98 for the Goldsmith Road asphalt. Albedo measurements were conducted using the sunshine pyranometer. Due to the traffic on the road and the pedestrian transit on the sidewalk, only the Maudslay car parking albedo was measured, getting 0.21: this is a typical value for an aged asphalt.

In addition, different experimentations related to the impact of some external factors on albedo measurements were conducted. In particular, the influence of yellow parking painting lines and the effects of the sonde height were assessed. This was investigated in two weather conditions: clear sky and haze. Changing the distance of the pyranometer from the lines it has been found an albedo increase of 12.8%. Regarding the sonde height, it influences albedo as well: the more is the distance between sonde and ground the more is the disturbance in albedo measurement. Also weather conditions affect albedo: with the haze pyranometer underestimated albedo, with clear sky measurements were more accurate. These kind of information could be useful if there is the necessity of assessing albedo in different conditions respect of those recommended by the standard ASTM E1918-06.

Thermal camera was used also to collect surfaces temperatures during a day measurements campaign.

The third part of this research consisted in creating different urban scenarios in order to mitigate the UHI effect. ENVI-met software was used to simulate different configurations where existing pavements were substituted with the tested bricks and other materials. Due to lacks of data regarding buildings thermal parameters and

materials component sub-base layers, the calibration phase has not worked as expected. It was decided to compare two usual urban scenarios: a urban canyon and a heat basin. The two scenarios were built up with a geometry similar to Maudslay car parking for the heat basin and to Goldsmith Road for the urban canyon. Then, setting the real weather conditions of measurements day campaign (21st July 2014), different simulations were carried out. For each of them, the surfacing material was changed. Materials used were the existing asphalt, all the investigated bricks, a painted and unpainted concrete, a painted and unpainted dense bitumen macadam and a granite for the heat basin, while the existing asphalt, a painted and unpainted concrete and a painted and unpainted dense bitumen macadam for the urban canyon.

The painted concrete was the cooler material for the urban canyon, with a peak surface temperature 7°C cooler than the existing Goldsmith Road asphalt, that resulted the warmest (30°C against 37°C). Also the DBM yellow painted showed a good thermal performance, reaching a 6.3°C difference with Goldsmith asphalt (30.7°C against 37°C). Nevertheless, the DBM heat up rate was faster than concrete. As Di Maria proved in her thesis work [34], this is a common feature for asphalts. Atmosphere temperature curves resulted in the same mutual order of the surface temperature curves, proving that surface temperature affects directly air temperature.

Regarding the heat basin scenario, the coolest material was the white brick, with a peak surface temperature 7.7°C cooler than the existing Maudslay building asphalt (32.6°C against 40.3°C). Also the granite had a good thermal performance, reaching a 4.9°C temperature difference with real Maudslay asphalt (35.4°C against 40.3°C). In this case, the warmest material was the black brick, resulting 0.3°C warmer than Maudslay asphalt (40.6°C against 40.3°C). As for the urban canyon trends, atmosphere curves mutual order confirmed the air temperature dependence on the surface temperature.

The heat basin resulted to be warmer than urban canyon. This could be a valid indication in designing urban spaces. Obviously, most of times is impossible to avoid these geometries, but more efforts could be made in this direction, for example by changing pavement materials, especially in situations where the existing urban scenario is being modified.

Concrete white painted interblocks seem to be a good solution in improving urban environment, although it is inappropriate for trafficked roads . The material could be employed to pave car parks, sidewalks, pedestrian roads, bike roads and so on. The

laboratory testing on it has been confirmed by software simulations, as in each situations it resulted the coolest. Also granite showed a good thermal behaviour (fig.79). In addition, interblocks can bring many other benefits to the urban environment (Ashra thesis work [53]). For these reasons they can be adopted in mitigating Urban Heat Island.

The other tested brick showed intermediate performances, except for the black one that resulted as the worst material in heat basin simulations. Yellow or red bricks could be adopted when the white paint is susceptible to create glare problems.

Yellow paint has demonstrated its ability in improving the thermal behaviour of some paving materials. In fact, painted materials used in this experimentation resulted cooler than the same unpainted materials (fig.88). This fact is confirmed by Di Maria in her thesis work [34]. In addition painted surfaces presented higher albedos than unpainted. Also yellow paint can help in mitigating UHI.

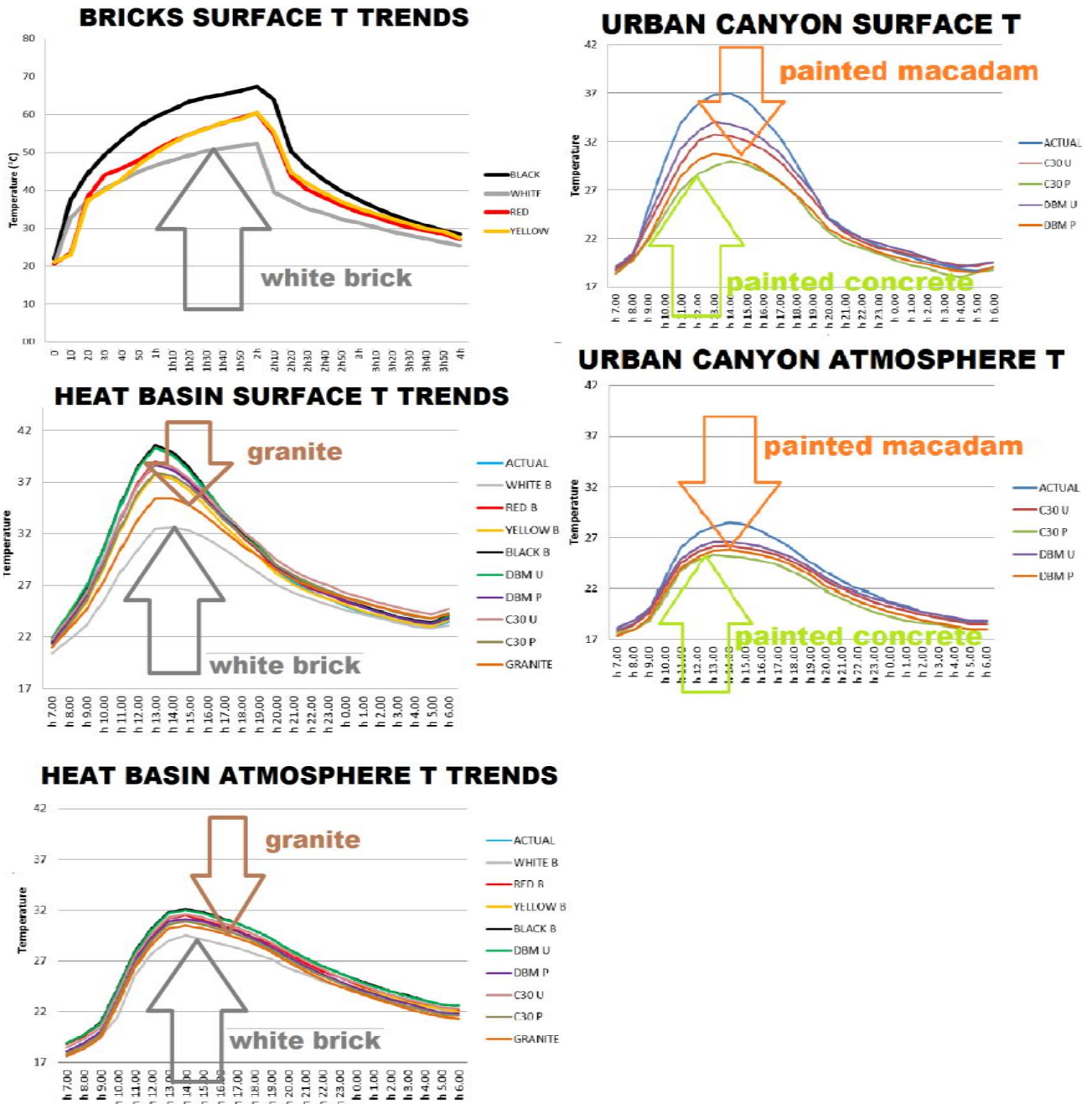


Figure 88: white brick, granite and painted materials T trends

ENVI-met software is a powerful tool. It is able to reproduce urban scenarios reliably and to work out large amounts of data. Nonetheless, it requires a quantity of input information in order to reproduce the real situation through the calibration phase. In this case, input data was not enough to calibrate the model. Despite that, the software resulted a valuable tool in modelling comparable scenarios, and can be considered a good urban planning instrument in Urban Heat Island mitigation.

ACKNOWLEDGEMENTS

The Author would like to thank his family Mariella, Pietro, Ilaria, Edoardo and dogs for all the support provided during these years at university.

A special thanks goes to Ingg. Cesare Sangiorgi, Valentina Di Maria and to Dr. Mujib Rahman for their guidance during the Erasmus experience, the research and the writing of the dissertation.

Another big thanks goes to the Author's friends of Mogliano and Bologna, in memory of all the great times they had together.

Last but not least, the Author would like to thank Enrica for the aid and the presence.

BIBLIOGRAPHY

1. **Geneva International Energy Agency.** *World Energy Outlook 2008-2009*.
2. **Climate Protection Partnership Division.** “*Reducing Urban Heat Islands: Compendium of Strategies - UHI basics*”. United States Environmental Protection Agency - EPA. 2008.
3. **Oke, T.R. in: Thompson, R.D. and Perry, A. (eds).** “*Urban Climates and Global Environmental Change*”. Applied Climatology: Principles and Practices. 1997, pp. 273-287.
4. **Oke, T.R.** “*Boundary Layer Climates*”. New York, Routledge : s.n., 1987.
5. **User:TheNewPhobia.** Urban Heat Island (Celsius). *Wikipedia Commons*. [Online] [http://commons.wikimedia.org/wiki/File:Urban_heat_island_\(Celsius\).png](http://commons.wikimedia.org/wiki/File:Urban_heat_island_(Celsius).png).
6. **Oke, T.R.** “*The Energetic Basis of Urban Heat Island*”. Quarterly Journal of the Royal Meteorological Society. 1982, 108, pp. 1-24.
7. **Mirzaei, P.A. and Haghghat, F.** “*Approaches to study urban heat island - abilities and limitations*”. Building and Environment. 2010, 45 (10), pp. 2192-2201.
8. **Santamouris, M.** “*Heat island research in Europe - the state of the art*”. Journal Advances Building Energy Research. 2007, 1, pp. 123-150.
9. **Mihalakakou, P., et al., et al.** “*Application of neural networks to the simulation of the heat island over Athens, Greece, using synoptic types as a predictor*”. Journal of Applied Meteorology. 2002, 41, pp. 519-527.
10. **Mihalakakou, P., et al., et al.** “*Simulation of the urban heat island phenomenon in Mediterranean climates*”. Journal of Pure and Applied Geophysics. 2004, 161, pp. 429-451.
11. **Livada, I., et al., et al.** “*Determination of places in the great Athens area where the heat island effect is observed*”. Theoretical and Applied Climatology. 71, pp. 219-230.
12. **Voogt, J.A. and Oke, T.R.** “*Thermal Remote Sensing of Urban Areas*”. Remote Sensing of Environment. 2003, 86, pp. 370-384.
13. **Roth, M., Oke, T.R. and Emery, W.J.** “*Satellite-derived Urban Heat Islands from Three Coastal Cities and the Utilization of Such Data in Urban Climatology*”. Int. J. Remote Sensing. 1989, 10, pp. 1699-1720.
14. **Berdahl, P. and Bretz, S.** “*Preliminary Survey of the Solar Reflectance of Cool Roofing Materials*”. Energy and Buildings. 1997, 25, pp. 149-158.

15. **Pérez, A.C.** “*Cinq exemples de terrains de jeux synthétiques et de températures associées par une image thermique Landsat 5*”. Westmount Park, Westmount, Canada : s.n., 2007. Discussion publique sur des terrains synthétiques.
16. **Zayat, Marcos, Garcia-Parejoab, Pilar and Levy, David.** “*Preventing UV-light damage of light sensitive materials using a highly protective UV-absorbing coating*”. s.l. : Chemical Society Reviews. 2006.
17. **Goode, P. R. and al, et.** “*Earthshine Observations of the Earth's Reflectance*”. 2001, Geophysical Research Letters 28, pp. 1671-1674.
18. **Insitute, APTI - Air Pollution Training.** Urban Heat Island Wind Circulations. <http://www.shodor.org/>. [Online]
19. **FLIRcorporation.** FLIR B200 thermocamera user manual.
20. **RAYTEKcompany.** Noncontact Infrared Temperature Measurement. www.raytek.com. [Online]
21. **Moccia, Lauren Paul.** “Climate Change In Urban Areas F.A.Q.” (Moccia Mix). <http://www.terry.ubc.ca/>. [Online]
22. **Berkeley Lab.** <http://newscenter.lbl.gov/2011/11/03/cool-roofs-really-can-be-cool/>. [Online]
23. **Cambridge Systematics, Inc.** *Cool Pavement Report - EPA Cool Pavement Study - Task 5*. 2005.
24. **EPA.** “*Reducing Urban Heat Islands: Compendium of Strategies: Cool Pavements*”. 2008.
25. **Levinson, R., H. Akbari, S. Konopacki, and S. Bretz.** “*Inclusion of Cool Roofs in Nonresidential Title 24 Prescriptive Requirements*”. Lawrence Berkeley National Laboratory, Berkeley, CA. : s.n., 2002.
26. **Tran, N., B. Powell, H. Marks, R. West, and A. Kvasnak.** “*Strategies for Design and Construction of High-Reflectance Asphalt Pavements*” . s.l. : Under review for the 2009 Transportation Research Board Annual Meeting , 2008.
27. **FHWA.** <http://www.fhwa.dot.gov/pavement/concrete/pubs/07025/>. *Federal Highway Administration*. [Online]
28. **Gilbert Arizona.** <http://www.gilbertaz.gov/departments/development-services/planning-development/urban-heat-island>. [Online]
29. **Pavement Interactive.** <http://www.pavementinteractive.org/article/cool-pavementgeneral/>. [Online]

30. **Santamouris, M., Synnefa, A. and Karlessi, T.** “Using advanced cool materials in the urban built environment to mitigate heat islands and improve thermal comfort conditions”. 2011, pp. 3085-3102.
31. **FLIR.** THERMAL IMAGING GUIDEBOOK FOR BUILDING AND RENEWABLE ENERGY APPLICATIONS. [Online]
32. **Iddynamics.**
http://www.iddynamics.com/how_a_thermal_imaging_camera_works1.html.
www.iddynamics.com. [Online]
33. **FLIR.** <http://www.flir.com/cs/emea/it/view/?id=41530>. [Online]
34. **Di Maria, Valentina.** *Master Thesis: "Thermal Response From Different Paved Surfaces"*. Università di Bologna, Facoltà di Ingegneria. 2013.
35. **Wikipedia, contributors.** "Pyranometer". *Wikipedia, the free encyclopedia*. [Online]
36. **AT DELTA-T DEVICES.** <http://www.delta-t.co.uk/product-display.asp?id=SPN1%20Product&div=Meteorology%20and%20Solar>.
<http://www.delta-t.co.uk/>. [Online]
37. **InstrumentationToolBox.**
<http://www.instrumentationtoolbox.com/2011/01/sensors-used-in-industrial.html#axzz3P6fjOm97>. www.intrumentationtoolbox.com. [Online]
38. **ExtechInstruments.** *Model 445815 Humidity Alert II User's Guide*.
39. **WunderUnderground.** <http://www.wunderground.com/cgi-bin/findweather/hdfForecast?query=52.962%2C-1.159&sp=IENGLAND359&MR=1>.
www.wunderground.com. [Online]
40. **Google.** Google Maps. [Online]
41. **ENVI-met.com.** <http://www.envi-met.info/hg2e/doku.php?id=root:start>. *The Hitchhiker's Guide to ENVI-met*. [Online]
42. **M. Zinzi, E. Carnielo, G. Fasano.** “Determinazione delle proprietà termofisiche di materiali ad elevata riflettanza solare per applicazioni a scala urbana: limiti e potenzialità”. ENEA, Università degli Studi Roma Tre. 2012.
43. **Aldo Fanchiotti, Emiliano Carnielo.** “Impatto di cool material sulla mitigazione dell'isola di calore urbana e sui livelli di comfort termico negli edifici”. ENEA, Università degli Studi Roma Tre. 2011.
44. **Bisson, Marta.** *TESI SPECIALISTICA: "Simulazione del microclima urbano di Milano mediante il software ENVI-met"*. Facoltà di Ingegneria, Ingegneria Edile-

Architettura, Corso di Laurea Specialistica in Ingegneria Edile, Politecnico di Milano.
Milano : s.n., A.A. 2009-2010.

45. **Sebastian Huttner, Michael Bruse, Paul Dostal.** “*Using ENVI-met to simulate the impact of global warming on the microclimate*”. Geographisches Institut (Environmental Modelling Group), Johannes-Gutenberg-University of Mainz, Germany.

46. **Micheal Bruse.** “*Modelling and strategies for improved urban climates*”. Department of Geography, University of Bochum, Bochum D44780 Germany.

47. **Esther Lahme, Michael Bruse.** “*Microclimatic effects of a small urban park in a densely build up area: measurements and model simulations*”. Department of Geography, University of Bochum, Bochum, Germany.

48. **Nunez, M; T. R. Oke.** “*The Energy Balance of an Urban Canyon*”. Journal of Applied Meteorology **16**: 11–19. 1977.

49. **Dr. ir. Christof Gromke.** PhD research: “*Vegetation and urban air quality: CFD evaluation of vegetation effects on pollutant dispersion*” . Eindhoven University of Technology. 2012-2014.

50. **CasaToday.it.** <http://www.casatoday.it/parcheggio-in-cortile-un-diritto-per-tutti/> [online]

51. **Interlocking Concrete Pavement Institute.** www.icpi.org [online]

52. **Behlen Building Systems.** <http://www.behlenbuildingsystems.com/BuildingGreen.htm> [online]

53. **Ashra, Ricky.** Thesis work: “*Analysing The Thermal Response Of Permeable Paving Surfaces In Relation To The Urban Heat Island Effect*”. Nottingham Trent University, Architecture, Design and the Built Environment Academic School. 2014.